Multi-detector thermal field-flow fractionation (ThFFF) as a characterization technique for complex polymer self-assemblies

by

Upenyu Lucky Muza

Thesis presented in partial fulfilment of the degree of

Master of Science (Polymer Science)

at

Stellenbosch University

Supervisor: Professor Harald Pasch

March 2017

Declaration

By submitting this thesis electronically, I declare that the entirety of the work contained therein is my own, original work, that I am the sole author thereof (save to the extent explicitly otherwise stated), that reproduction and publication thereof by Stellenbosch University will not infringe any third party rights and that I have not previously in its entirety or in part submitted it for obtaining any qualification.

Upenyu Lucky Muza   March 2017

Abstract

Amphiphilic block copolymer micelles have found a niche in pharmaceutical, electronics, environmental, cosmetics and hygiene industries. These micelles, whether in the pure or mixed micelle form, often exist as multiple morphologies (spherical, cylindrical, worm or vesicular) in equilibrium with each other. However none of the current techniques can successfully separate and characterize these multiple morphologies with regards to size, molar mass, chemical composition and their respective distributions, in a single measurement. Thermal field-flow fractionation (ThFFF) is shown to be capable of separating and characterizing pure micelles prepared from two types of polystyrene - polyethylene oxide block copolymers (PS-PEO), of different PS block sizes but similar PEO block sizes. Moreover, multiple micelle morphologies induced by the addition of 1 mM LiBr, as well as multiple mixed micelles prepared from various binary blending protocols of the two PS-b-PEO copolymers were successfully characterized. In addition, ThFFF is shown to be capable of monitoring the dynamics of formation of the mixed micelles.

Opsomming

Amfifiliese blok ko-polimere het n nismark in verskeie farmaseutiese, elektroniese, kosmetiese, higiëniese asook in die omgewings industrië gevind. Miselles, suiwer of gemeng, bestaan gewoonlik in ewewig met verskeie morfologië soos bv. silindries, spheries of wurm. Tans is daar geen enkele analitiese tegniek wat hierdie verskeie morfologië kan skei in terme van groote, molekulêre massa en chemiese samestelling, of hul verspreidings, in n enkele analiese nie. Dit word gewys dat termiese veldvloeifraksionering (ThFFF) miselles, wat bestaan uit polistireen-blok-poli(etileenoksied) (PS-PEO) ko-polimere met verskeie PS blok lengtes maar selfde PEO blok lengtes, kan skei. Dit word ook gewys dat verkseie morfologië

word gevorm in 1 milimolar litium bromide en dat hierdie morfologië, asook gemengde miselles wat berei is deur verskillende tegnieke, deur ThFFF gekarakteriseer kan word. Dit word ook gewys dat ThFFF gebruik kan word om die vormings dynamika van miselles te monitor.

Acknowledgements

Firstly, I would like to express my sincerest gratitude to my supervisor, Prof. Harald Pasch, for the opportunity to study in this group and for the financial support. I am forever indebted for his invaluable guidance and mentoring.

I would also like to thank all the members of our researcher group, namely Dr G. Greyling and A. Ndiripo, as well as all the staff members at the Department of Chemistry and Polymer science for the unwavering support I received.

Special thanks goes to my family for their support and sacrifices throughout my studies.

Most importantly I give thanks and praise to the Almighty for His grace and mercies.

Contents

Table of figures

Table of tables

List of symbols and abbreviations

ABC	Amphiphilic block copolymer
ACN	Acetonitrile
AF4	Asymmetric flow field-flow fractionation
A_2	Second virial coefficient
C	Concentration of analyte
C_o	Concentration of analyte at the accumulation wall
CCD	Chemical composition distribution
CMC	Critical micelle concentration
CMT	Critical micelle temperature
D	Diffusion coefficient
dc/dx	Change in concentration over the mean layer thickness
DCP	Diblock copolymer
D_h	Diameter of molecule/particle
DLS	Dynamic light scattering
dn/dc	Specific refractive index increment
D_T	Thermal diffusion coefficient
dT/dx	Temperature gradient between hot and cold wall, (also see ΔT)

F	Force
f	Coefficient of friction
FFF	Field-flow fractionation
FlFFF	Flow field-flow fractionation
G	Gravitational force
^{1}H-NMR	Proton nuclear magnetic resonance spectroscopy
J	Net flux of energy
K	Boltzmann constant
K*	Optical constant
L	Distance from the accumulation wall
MALLS	Multi-angle laser light scattering
MMD	Molecular mass distribution
M'	Effective mass
M_w	Molar mass/ molecular weight
N_a	Avogadro's number
NMR	Nuclear magnetic resonance spectroscopy
P(θ)	Particle scattering function
PS	Polystyrene

PSD   Particle size distribution

PS - PEO   Polystyrene - polyethylene oxide block copolymer

Q   Scattering vector

R   Retention ratio

$R(\theta)$ Rayleigh ratio

R_g Radius of gyration

R_g/R_h Shape factor

R_h Hydrodynamic radius

RI   Refractive index

S   Soret coefficient

SEC   Size exclusion chromatography

SEM   Scanning electron microscopy

STEM   Scanning transmission electron microscopy

T   Temperature

T_c Cold wall temperature

t_o Void time

t_r Retention time

ΔT Applied temperature gradient

THF	Tetrahydrofuran
ThFFF	Thermal field-flow fractionation
TEM	Transmission electron microscopy
U	Field-induced migration
UV	Ultraviolet
W	Channel thickness
Z	Aggregation number

1 Introduction

1.1 Background

Block copolymers (BCPs) consist of two or more different types of polymer chains covalently bonded together. The different polymer chains often have different polarities and solvent interactions, with one segment being hydrophobic and the other being hydrophilic, hence the molecule is referred to as amphiphilic. The amphiphilic BCPs can self-assemble to form spherical, cylindrical or vesicular micelles as a function of various molecular and solution factors.[1–3] Molecular factors include the hydrophobic-to-hydrophilic chain ratio, the molecular weight (M_w) and the polymer architecture.[3,4] Solution factors include solvent composition, polymer concentration, pH, temperature, and additives such as salts and homopolymers.[4,5] Solution factors offer ease and flexibility in designing specific micellar structures relative to the complex and tedious synthesis approach based on molecular factors.

The self-assembly of BCPs has found applications in industries such as pharmaceutical, food, oil recovery, cosmetics, electronics and nanotechnology.[1,3,6,7] The self-assembly behaviour of amphiphilic BCPs in solution to form micelles has been extensively studied and is well understood.[3,8–10] Most recently it has been noted that unique properties can be achieved by blending pure micelles to form mixed micelles.[11–13] The concept of mixed micelles enables the design of new and superior properties via simple blending protocols, thereby avoiding the complex polymerization of suitable BCPs. As such, a growing interest has been directed towards the blending of micelles.[12,14]

The characterisation of micelles in general is critical as it relates to properties useful for industrial applications.[15] The morphology, size and molar mass are fundamental to the resultant properties and functionalities.[16] However, the characterization of these micelles is

extremely challenging because of the interdependence of properties such as molar mass (M_w), chemical composition (CC) and structural distributions.[17]

Micelles are generally characterised using a number of techniques such as size exclusion chromatography (SEC), proton nuclear magnetic resonance spectroscopy (H^1-NMR), transmission electron microscopy (TEM), scanning electron microscopy (SEM), fluorescence techniques, small angle neutron scattering (SANS) and small angle x-ray scattering (SAXS).[3,18] ^{1}H-NMR and fluorescence microscopy have been used to investigate corona composition and average M_w of micelles. TEM and SEM can be used to investigate micellar size and morphology; however the measured size is not the accurate solution size, since the analysis is performed on a dried sample. With the exception of SEC, all the other techniques yield no information regarding molar mass distribution (MMD) and chemical composition distribution (CCD). However, in SEC micelles very frequently disassemble and adsorb on the SEC column.[19] In addition SEC only gives indicative molar mass (M_w) since its determination is based on a relative calibration. Moreover, it is challenging to prepare micelle standards for the calibration.

Field-flow fractionation (FFF) has recently evolved as a competitive alternative method for the characterization of micelles because of the channel-based separation, which offers less harsh conditions for the analysis of the fragile micelles. Unlike in SEC, sub-techniques of FFF such as asymmetrical flow FFF (AF4) and thermal FFF (ThFFF) can be used to measure the absolute M_w when coupled to a multi-angle laser light scattering (MALLS) detector.[20,21] FFF is the only technique to date that has been shown to be suitable for the characterization of micelles with respect to molar mass, chemical composition, particle size, morphology and their respective distributions.[22,23]

Micelle characterization by FFF has largely been carried out via AF4,[21,24] with only two reports being currently available on the characterization of micelles using ThFFF.[22,23] However, separations by AF4 are only size-based and AF4 uses a partially permeable membrane which can interact with the micelles and result in sample loss. As such, ThFFF becomes an interesting alternative with the capability of separating micelles according to both size and chemical composition. Moreover, sample losses are insignificant due to the absence of a membrane.

The characterization of micelles prepared from BCPs of the same homologous series, but of different molar masses of the core blocks and similar masses for the corona blocks, has been studied before.[8] However, no separation and quantification with regards to molar mass and chemical composition has been performed. In instances where the core blocks are highly hydrophobic, the micelle cores will exist in a collapsed state. Therefore different core block sizes could result in different core densities of the micelles. Moreover, micelles seldom exist in a single morphology, but often as multiple morphologies in equilibrium. Micelle blending and salt additives have been reported to enhance the evolution of multiple morphologies.[7,25–27] In addition to micelle blending stimulating the evolution of multiple morphologies, it can also give rise to new micellar structures with unique properties. However, most current techniques can only characterize the micelle blends before formation or after formation, but cannot monitor the process and provide information on the kinetics of formation.

In this thesis, multi-detector ThFFF shall be used to try and address the challenges and gaps in knowledge concerning the characterization of micelles with regard to the issues raised in this section.

1.2 Aim

This study will focus on multi-detector thermal field-flow fractionation (ThFFF) as a characterization technique for micelles prepared from polystyrene-block-polyethylene oxide (PS-b-PEO). The aim is to investigate morphology-based separations of PS-b-PEO micelles in acetonitrile (ACN) and provide detailed information on size, molar mass, chemical composition, morphology and their respective distributions. Additional investigations shall be on the characterization of various binary blends of these PS-b-PEO BCPs to form mixed micelles, and the monitoring of the dynamics of formation. Ultimately, the evolution and separation of multiple morphologies shall be investigated for both pure and mixed micelles.

1.3 Objectives

1. Prepare pure micelles from two different PS-PEO BCPs by the co-solvent method.

2. Prepare mixed micelles by the co-solvent method using various binary blending protocols of the two PS-PEO BCPs.

3. Determine critical micelle concentration (CMC) and critical micelle temperature (CMT).

4. Modify the ionic strength of the pure micelles with LiBr and investigate the morphological evolution of the micelles.

5. Separate the micelles using multi-detector ThFFF.

6. Determine the molecular weight (M_w), aggregation number (Z) and shape factor (R_g/R_h).

7. Determine diffusion, thermal diffusion and Soret coefficients.

8. Tentatively investigate the effect of the core density on micellar properties.

1.4   Layout of thesis

Chapter 1

The main concepts around BCPs, micelles and ThFFF are introduced. The associated analytical challenges and the probable solutions are discussed. Thereafter, the scope of the study is defined by outlining the aims and objectives.

Chapter 2

The relevant theoretical and historical background concerning FFF, ThFFF and self-assemblies are discussed in detail, as guided by the aims and objectives.

Chapter 3

Chapter 3 outlines the experimental procedures and instrument parameters utilised in the characterization of the pure and mixed micelles of PS-b-PEO via ThFFF.

Chapter 4

This chapter contains discussions on the results of the characterization of the pure and mixed micelles.

Chapter 5

Chapter 5 outlines the conclusions as derived from overall thesis discussions. Relevant recommendations as well as probable future works are included.

1.5   References

(1)   Blanazs, A.; Armes, S. P.; Ryan, A. J. *Macromol. Rapid Commun.* **2009**, *30* (4–5), 267–277.

(2)   Owen, S. C.; Chan, D. P. Y.; Shoichet, M. S. *Nano Today* **2012**, *7* (1), 53–65.

(3)   Riess, G. *Prog. Polym. Sci.* **2003**, *28* (7), 1107–1170.

(4)   P. Alexandridis, B. L. *Amphiphilic Block Copolymers: Self-Assembly and Applications*; Elsevier: Amsterdam, 2000.

(5)   Oranli, L.; Bahadur, P.; Riess, G. *Can. J. Chem.* **1985**, *63* (10), 2691–2696.

(6)   Tseng, Y. C.; Darling, S. B. *Polymers (Basel).* **2010**, *2* (4), 470–489.

(7)   Yang, J. *Curr. Opin. Colloid Interface Sci.* **2002**, *7* (5–6), 276–281.

(8)   Pioge, S.; Fontaine, L.; Gaillard, C.; Nicol, E.; Pascual, S. *Macromolecules* **2009**, *42* (12), 4262–4272.

(9)   Discher, D. E.; Eisenberg, A. *Science* **2002**, *297* (5583), 967–973.

(10)   Bronstein, L. M.; Chernyshov, D. M.; Timofeeva, G. I.; Dubrovina, L. V.; Valetsky, P. M.; Khokhlov, A. R. *Langmuir* **1999**, *15* (19), 6195–6200.

(11)   Ebrahim Attia, A. B.; Ong, Z. Y.; Hedrick, J. L.; Lee, P. P.; Ee, P. L. R.; Hammond, P. T.; Yang, Y. Y. *Curr. Opin. Colloid Interface Sci.* **2011**, *16* (3), 182–194.

(12)   Huang, L.; Somasundaran, P. *Langmuir* **1997**, *13* (25), 6683–6688.

(13)   Clint, J. H. *J. Chem. Soc. Faraday Trans. 1* **1975**, *71*, 1327.

(14)   Zhang, Y.; Lam, Y. M. *J. Nanosci. Nanotechnol.* **2006**, *6* (12), 3877–3881.

(15)   Schimpf, M. E.; Caldwell, K.; Giddings, J. C. *Field-Flow Fractionation Handbook*; John Wiley & Sons: New York, USA, 2000; Vol. 4.

(16)   Barnhill, S. a.; Bell, N. C.; Patterson, J. P.; Olds, D. P.; Gianneschi, N. C. *Macromolecules* **2015**, *48* (4), 1152–1161.

(17)   Philipsen, H. J. *J. Chromatogr. A* **2004**, *1037* (1–2), 329–350.

(18)   Ahmad, F.; Baloch, M. K.; Jamil, M.; Jeon, Y. J. *J. Appl. Polym. Sci.* **2010**, *118* (7), 1704–1712.

(19)   Horst, S.; Klingler, J.; Rossmanith, P.; Frechen, T.; Gerst, M.; Feldthusen, J.; Muller, A. H. E. *J. Chromatogr.* **2000**, No. 33, 1734–1740.

(20)   Runyon, J. R.; Williams, S. K. R. *J. Chromatogr. A* **2011**, *1218* (38), 6774–6779.

(21)   Moon, M. H. *J. Sep. Sci.* **2010**, *33* (22), 3519–3529.

(22)   Greyling, G.; Pasch, H. *Macromolecules* **2016**, *49*, 1882−1889.

(23)   Greyling, G.; Pasch, H. *J. Chromatogr. A* **2015**, *1414*, 163–172.

(24)   Glantz, M.; Hakansson, A.; Mansson, H. L.; Paulsson, M.; Nilsson, L. *Langmuir* **2010**, *26* (15), 12585–12591.

(25)   Berret, J.-F. *Mol. Gels* **2005**, 235–275.

(26)   Das, N. C.; Cao, H.; Kaiser, H.; Warren, G. T.; Gladden, J. R.; Sokol, P. E. *Langmuir* **2012**, *28* (33), 11962–11968.

(27)   Bhargava, P.; Zheng, J. X.; Quirk, R. P.; Cheng, S. Z. D. *J. Polym. Sci. Part B Polym. Phys.* **2006**, *44* (24), 3605–3611.

2   Literature Review

2.1   Introduction to FFF

Field-flow fractionation (FFF) is a channel-based separation technique that was introduced in 1966 by Calvin Giddings.[1] Separation is achieved via a field-induced differential displacement of the analyte inside a channel. The channel-based approach enables the analysis of sensitive and fragile analytes. As such, FFF has found a niche in the separation of complex macromolecules, aggregates, micro-organisms, colloids and particles.[2]

2.2   Basic principles of FFF

The FFF system comprises of a spacer positioned between two walls (thereby generating a channel), with one of the walls acting as the accumulation wall and the other the depletion wall. A carrier solvent is pumped through the channel and the large aspect ratio of the channel ensures a parabolic flow profile. Separation is initiated by an external field applied at right angles to the flow. The external field drives the analyte molecules away from the depletion wall towards the accumulation wall, which generates a concentration gradient. A schematic representation of a FFF system and the associated mass movement created by the external field is shown in Figure 2.1 below.
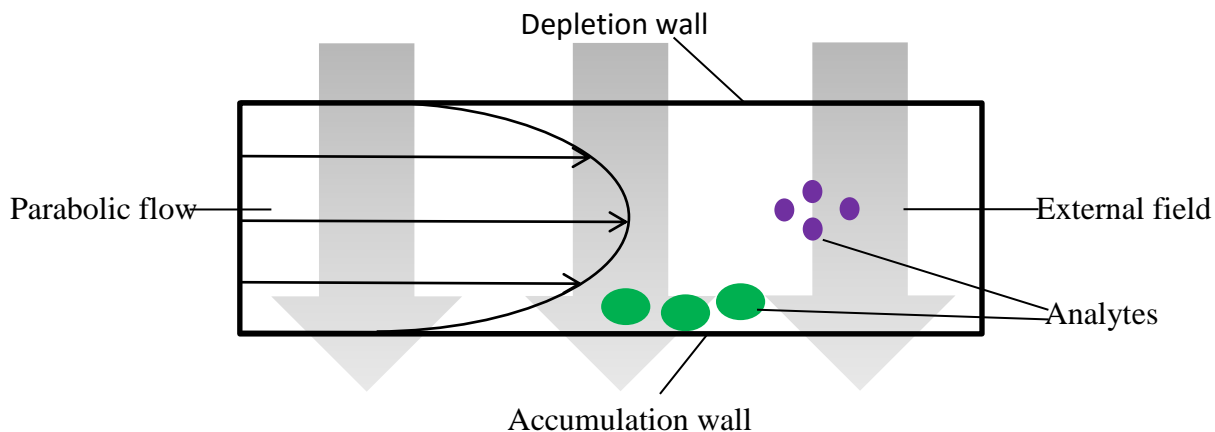
Figure 2.1.   Schematic for FFF separation mechanism.

The concentration gradient sets up a counteracting mass transfer movement (diffusion) of the analyte molecules away from the accumulation wall. Eventually, these two antagonistic mass movement forces establish a state of equilibrium with different analytes being positioned in different laminar flow streams formed within the channel. Laminar flow streams inherently have different velocities and the differential displacement of analyte molecules in different flow streams is the basis of their separation.

Separation in FFF can be related to an array of physicochemical properties such as size, thermal diffusion, chemical composition, charge, density, mass and magnetic susceptibility. This makes FFF highly versatile with numerous sub-techniques and broad applications.

2.3   Advantages of FFF

The major advantages of FFF over traditional column-based techniques can be related to the channel-based separation. The channel is void of any packing material and therefore shear degradation of the analyte is significantly reduced and sensitive molecules such as micelles and emulsions can be analysed.[1]

9

Another advantage is that FFF has a larger separation range from 0.001-100µm.[1] Therefore larger sized molecules, otherwise impossible to analyse by size exclusion chromatography (SEC), can be separated. Overall, complex mixtures of suspended particles, gels and soluble polymers can be analysed in a single measurement.[1,2]

2.4 FFF modes of operation

The FFF mode of operation predicts the order of elution based on size for a particular analyte and is an effect of the interaction of the hydrodynamic forces at play in the channel.[1] In FFF there are three main modes of operation; 1) normal mode, 2) steric mode, and 3) hyperlayer mode. These modes of operation shall be explained further in the following sections.

2.4.1 Normal mode

The normal mode is the most common mode of elution and mainly applies to molecules in the sub-micrometer range.[1,3] Smaller particles elute first due to a higher diffusion rate away from the accumulation wall and into faster moving flow streams.[1] The normal mode is illustrated in Figure **2.2** below.
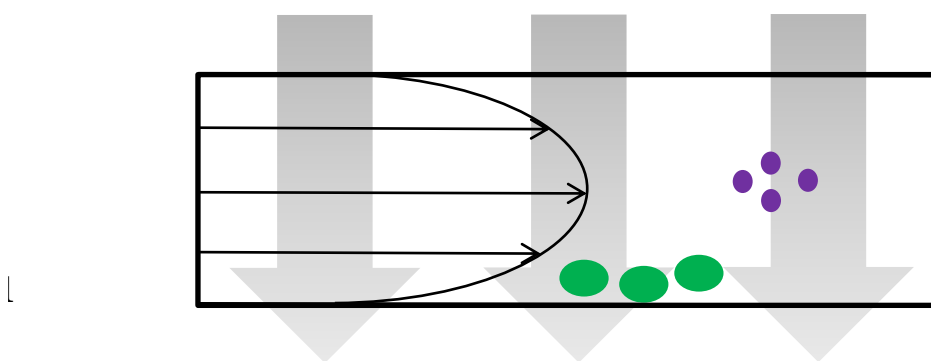
Figure 2.2.   Schematic for FFF normal mode of elution.

2.4.2   Steric mode

When larger particles above 1 µm are pressed to the accumulation wall by a strong driving force, their diffusion away from the accumulation is insignificant relative to their size. In this instance, the distance of the particle centre of mass away from the accumulation wall determines the order of elution. Particles with larger size and thus greater distance from the accumulation wall protrude into high velocity flow stream of the parabolic flow profile.[1] As such, the larger particles are dragged more rapidly along the accumulation wall and elute first. The schematic for the steric mode of elution is shown in Figure 2.3 below.
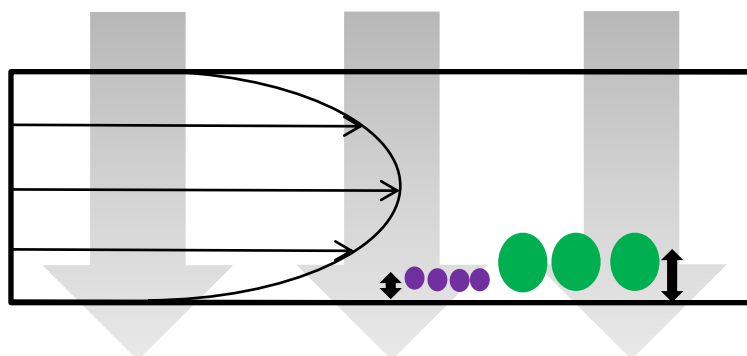
Figure 2.3.   Schematic for FFF steric mode of elution.

2.4.3   Hyperlayer mode

In a special case for large particles above 1 µm, where the driving force is not strong enough to press analytes to the accumulation wall, or there are strong lift forces, the particles are tossed up and elevated away from the accumulation wall. Larger particles are elevated higher than the smaller particles and thus elute first.[1] Generally this retention behaviour is referred to as the steric/hyperlayer mode as it is difficult to distinguish between the two modes. A schematic for the hyperlayer mode is shown in Figure 2.4 below.
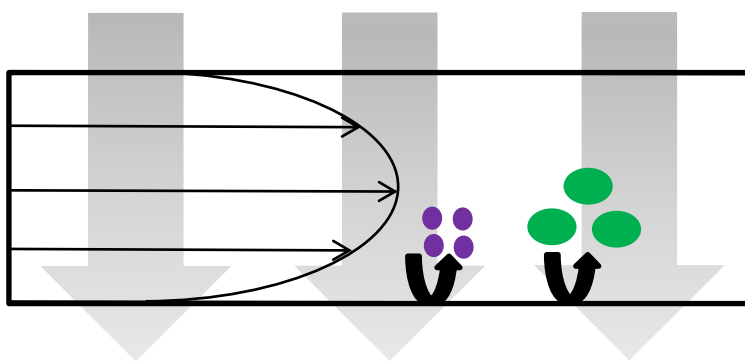
Figure 2.4.   Schematic for FFF hyperlayer mode of elution.

These modes of elution are applicable to all FFF sub-techniques. The next section will focus on the various FFF sub-techniques available.

2.5   FFF sub-techniques

As a general rule, the nomenclature for FFF sub-techniques is based on the particular external field involved. Empirically, all possible external fields are applicable to FFF provided the field interacts with a physicochemical property of the analyte, thereby effecting mass movement to the accumulation wall.[1,4,5]

The ideal field should have the following three properties in order to be highly effective:

(1) Adequate field strength to drive the analyte into highly localized regions of the parabolic flow velocity profile;

(2) Sufficient selectivity to insure different components are driven to different parts of the flow velocity profile and thus separate; and

(3) Ease of implementation for practical and economical application.

Currently, only Thermal (ThFFF), Asymmetrical Flow (AF4) and Sedimentation (SdFFF) FFF have been successfully commercialised and have made a significant scientific impact.

2.5.1   Sedimentation FFF (SdFFF)

SdFFF utilizes a sedimentation field to separate according to effective mass (true mass minus buoyant mass) which equates to variance in size and density.[1,3] The channel encircles a spinning centrifuge basket that exerts differential acceleration on different particles. SdFFF has the advantage of a larger analyte separation size range (0.05 – 100 µm) and relatively short analysis times (1 - 5 minutes). However, the technique involves complex and expensive instrumentation.

2.5.2   Flow FFF (FlFFF)

Separation in FlFFF is achieved by a cross-flow that is pumped through the channel walls, perpendicular to the streamline flow within the channel. FlFFF is the most frequently used FFF sub-technique because its working principle is universally applicable to all analytes. The current size range for analytes separated by FlFFF is 0.001-50 µm. Compared to other sub-techniques, FlFFF requires a lot of solvent and generally operates under aqueous conditions. The FlFFF setup is simple but requires different pump heads to supply the different flow streams required. The main disadvantage arises from the instability of the semi-permeable membrane that acts as the accumulation wall. FlFFF has different variants namely the original symmetric channel with two permeable walls and the most commonly used asymmetric (AsFlFFF/ AF4) channel with one non-permeable wall.

2.5.3   Thermal FFF (ThFFF)

A temperature gradient is applied across a thin ribbon-like channel between two metallic plates, with one plate being maintained at high temperature and the other kept cold (room temperature). Therefore, a thermal gradient is established which sets up the thermal diffusion motion of analytes towards the cold wall that acts as the accumulation wall. The

13

accumulation of analyte molecules at the cold wall generates a concentration gradient which forces the analytes to diffuse back into the channel.[1,6] Normal diffusion is a function of analyte size in solution and thermal diffusion is a function of the chemical composition of the solvent and analyte. Therefore ThFFF can be used to separate analytes according to size and chemical composition in one measurement analogous to two-dimensional SEC (2D-SEC).

2.6   ThFFF separation mechanism

This thesis is based on ThFFF as a fractionation technique and as such an in-depth focus will be directed towards the theoretical background of the separation mechanism involved in ThFFF. Figure 2.5 below shows a schematic illustration of the ThFFF separation mechanism.

Hot wall

Cold/ accumulation wall
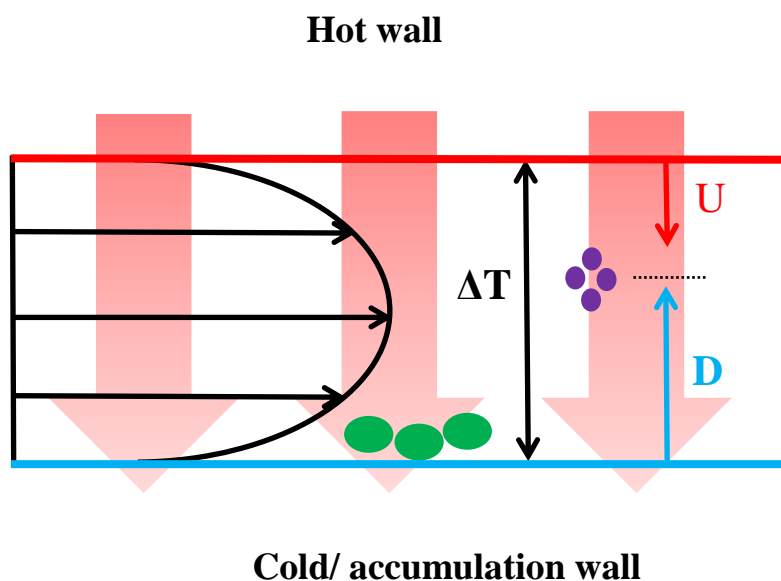
Figure 2.5.   Schematic for ThFFF separation mechanism.

The thermal gradient field drives analytes towards the cold wall with a thermophoretic velocity U. In turn, the accumulation of analyte molecules at the cold wall generates a concentration gradient which counteracts the thermophoretic motion with a diffusive motion. The net flux of material in the direction of the cold wall is given by Equation 2.1.[1]

$$J = Uc - D\,\frac{dc}{dx} \qquad\qquad \textbf{2.1}$$

The first term on the right hand side of the equation represents the flux due to the thermophoretic mass movement and the second term represents the flux related to the normal diffusion. At steady state conditions the two terms balance and the overall flux is zero (Equation 2.2).

$$Uc = D\,\frac{dc}{dx} \qquad\qquad \textbf{2.2}$$

The thermophoretic velocity (U) generated when a uniform thermal gradient exists between two metal plates, can be estimated from Equation 2.3, where D_T and D are the thermal and normal diffusion coefficients, respectively. $\Delta T/W$ is the thermal gradient across a channel with a thickness W, and γ is the thermal expansion coefficient of the solvent.

$$U = D\left[\gamma + \frac{D_T}{D}\right]\frac{\Delta T}{W} \qquad\qquad \textbf{2.3}$$

However γ is negligible and can be ignored since $D_T / D \gg \gamma$.

$$U = D\left[\frac{D_T}{D}\right]\frac{\Delta T}{W} \qquad\qquad \textbf{2.4}$$

The ratio between the distance of the analyte from the cold wall (L) and the total distance between the two walls (W) is given by a dimensionless parameter λ, where $\lambda = L/W$. The external force F exerted on the analyte is related to λ by the expression in Equation 2.5:

$$\lambda = \frac{kT}{FW} \qquad\qquad \textbf{2.5}$$

The force acting on the analyte can be calculated from Equation 2.6.

$$F = kT\left[\frac{D_T}{D}\right]\frac{\Delta T}{W} \qquad\qquad \textbf{2.6}$$

From Equations 2.6 and 2.5, it can be deduced that;

$$\lambda = \frac{D}{D_T\,\Delta T} \qquad\qquad \textbf{2.7}$$

D can be calculated from the Einstein-Stokes law (Equation 2.8); where η is the solvent viscosity, and D_h is the polymer hydrodynamic diameter.

$$D = \frac{kT}{3\pi\eta D_h} \qquad\qquad \textbf{2.8}$$

The relationship between λ and retention can be approximated from the expression below, where R is the retention parameter.

$$R = 6\lambda \left[coth \left(\frac{1}{2\lambda}\right) - 2\lambda \right] \quad \textbf{2.9}$$

Equation 2.9 can be simplified to give Equation 2.10, by ignoring the term in the parenthesis because of its relatively small value which makes it insignificant at high retention, which is normally checked during the optimisation stage.

$$R \approx 6\lambda \qquad\qquad\qquad \textbf{2.10}$$

Alternatively, R can be expressed simply as a ratio of the peak maxima of the unretained and retained peaks, as shown in Equation 2.11.

$$R = \frac{t_0}{t_r} \qquad\qquad\qquad \textbf{2.11}$$

Therefore Equations 2.7, 2.10 and 2.11 above can be rearranged to give the simplified expression for D_T (Equation 2.12).

$$D_T = \frac{6Dt_r}{\Delta t_0} \qquad\qquad\qquad \textbf{2.12}$$

The interplay of D and D_T gives rise to a parameter called the Soret coefficient (S),[7,8] As defined by Equation 2.13. A variation of S values enables a simultaneous separation of molecules with respect to their differences in both M_w and chemical composition. Molecules with larger S values are retained more relative to molecules with smaller values.[1]

$$S = \frac{D_T}{D} \qquad\qquad\qquad \textbf{2.13}$$

16

Thermal diffusion (D_T) is the fundamental physicochemical property in ThFFF and as such the next section shall be dedicated to the historical background of D_T in the characterization of polymers.

2.7   Thermal diffusion

Thermal diffusion is a known function of chemical composition, thus can be used to address some of the analytical challenges related to surface chemistry, microstructure and architecture of complex polymers.[5,9,10]   Therefore, it is fundamental to understand the nature of thermal diffusion.

By the late 19th century, several theories had been postulated to try and explain thermal diffusion in liquids. In 1981, Borchard and de Gennes postulated that polymers and their constituent monomers possess the same thermophoretic velocity in a given constant thermal gradient.[11] As such the associated D_T should be independent of molar mass. This resonated with findings by Schimpf and Giddings in 1987, which showed D_T to be fundamentally independent of both molar mass and the type of branching.[12] Schimpf and Giddings managed to demonstrate using their newly developed separation technique, ThFFF, that none of the theories at present could distinctly explain thermal diffusion.[9,12] However, the advent of ThFFF in collaboration with advanced analytical technologies has created a better framework to try and explain thermal diffusion.[5,9,10,12,13] None the less, thermal diffusion remains a vaguely understood phenomenon, despite all the remarkable progress.[7,14]

In the following section, the role of thermal diffusion and normal diffusion (or size) in the characterization of polymers by ThFFF is discussed.

2.8 Characterization of polymers by ThFFF

A broad range of copolymers have been separated via ThFFF and D_T was found to be highly dependent on the peripheral monomers, in cases where radial segregation of polymer chains is experienced.[5] This highlights the dependency of D_T on surface chemistry and independence of molar mass. Similarly, retention for PS-b-PEO in tetrahydrofuran (THF) was found to be comparable to the retention of the corresponding PS homopolymer regardless of the overall molar mass of the BCP.[15] PS-b-PEO was assumed to undergo radial segregation in THF, with the PS block dominating the surface chemistry. As such, the elution of the BCPs was observed to be similar to that of the corresponding PS homopolymers.

ThFFF has been used to separate latex particles with similar sizes but different chemical surface chemistries.[16] The results show that size is not the only parameter affecting retention but rather a combination of size and chemical composition. This functionality gives ThFFF an advantage over conventional techniques like SEC and HPLC which distinctly separate according to either size or chemical composition, respectively.

With regards to complex polymeric self-assemblies such as micelles, multi-detector ThFFF has been shown to be capable of separating micelles as a function of corona composition.[18] The multidetector approach has managed to provide detailed information on size, molar mass, chemical composition, and the respective distributions in a single measurement. Also, ThFFF has no semi-permeable membrane, therefore no sample loss is experienced, as with AF4.

More importantly, only spherical micelles have been successfully separated by ThFFF,[18] and therefore the characterisation of multiple morphologies remains an unexplored area of interest. Different micelle morphologies (such as spheres, vesicles and worms) can exist in pure state or in equilibrium with each other, depending on the polymer and solvent system.

However, there is currently no technique capable of separating and characterising these morphologies, while also determining the PSD, CCD and MMD.

This thesis seeks to characterise multiple micellar morphologies prepared from PS-b-PEO. Therefore, the next segment will briefly outline the materials background.

2.9   Amphiphilic block copolymers (ABCs)

The advent of smart materials technology has heightened the demand for cheaper but suitable polymeric material designs. At present, material design seldom involves the synthesis of distinctly novel polymers but rather the precise blending and alloying of existing polymers to yield new unique materials.[19,20,21] Amphiphilic block copolymers (ABCs) have been a successful result of the latter. ABCs consist of two distinctively different polymeric segments, one being hydrophilic and the other hydrophobic, attached together by a covalent bond.

2.10 Self-assembly of amphiphilic block copolymers
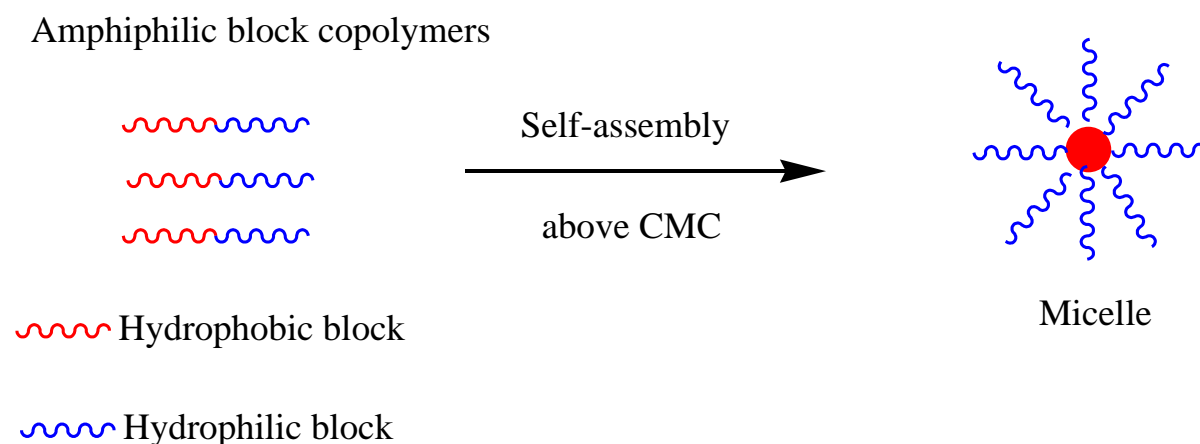
Figure 2.6.   Schematic for the self-assembly of amphiphilic block copolymers.

The two dissimilar segments of ABCs characteristically adopt different affinities for a particular solvent and consequently self-assemble in solution, analogous to low molecular weight surfactants as shown in Figure 2.6 above.[21–24] The self-assembly occurs as the polymer and solvent system attempts to lower the free energy, by maximizing favourable interactions of the polymer with the solvent and minimizing unfavourable interactions; within the constraints imposed by the polymer chain's architecture.[25,24] Various microphase morphologies such as micelles and vesicles emanate from such self-assembly.[23]

The field concerning the self-assembly of ABCs is of crucial industrial and scientific significance.[26] ABCs in general have been one of the strong candidates for potential applications in pharmaceutical and environmental technologies, cosmetic and detergent formulations, and templates for the production of nanostructured materials including cylinders, spheres, lamellae and gyroids.[27,28] The next section will briefly outline the synthesis of PS-b-PEO.

2.11 PS-b-PEO synthesis

Commercially available PS-b-PEO is mainly synthesised via living ionic polymerization. PS-b-PEO is typically prepared in a solution of tetrahydrofuran (THF) at -78 °C using cumyl potassium as the initiator. Styrene monomers are initially polymerized to give PS chains. On complete polymerization of the styrene monomers, the reaction solution is kept between room temperature and 40 °C.

The PS chains are still active and can react further, and are thus commonly referred to as "living". A specific amount of PEO monomers is subsequently added. The PEO monomers polymerise onto the living polystyrene (PS) chains. Upon complete polymerization of the ethylene oxides, termination and isolation proceed, respectively. The isolation step involves

precipitation of the end product in a non-solvent. Once the ABC product has been prepared it can be used to prepare micellar structures via an appropriate micellization process, as shall be discussed in the next section.

2.12 Micellization

Micellization describes the self-assembly or aggregation behaviour of surfactant or BCP molecules above certain concentration and temperature conditions. The driving force for the micellization of amphiphilic BCP in both aqueous and non-aqueous solutions is the solvent selectivity for different blocks. Moreover, the variation in organic solvents leads to a diversity in the association behaviour.[30]

Polymer chains in the micelles experience two types of forces that oppose the self-assembly. The first force is due to the chains opposing the confinement as a result of the chain transfer from solution to form micelles. Secondly, the micelle chains also experience electrostatic repulsion due to their similar polarity. These two forces counter micellization by surging the Gibbs free energy (ΔG) of the micelle and solvent system, and opposing chain transfer.[31] Micellization depends on the overall balance between the self-assembly and the counter forces. The ultimate goal is to minimize the Gibbs free energy. Equation 2.14 shows the classic expression for ΔG, where ΔH is change in enthalpy, T is temperature and ΔS represents change in entropy.

$$\Delta G = \Delta H - T \Delta S \qquad 2.14$$

In both aqueous and non-aqueous solutions, micellization of block copolymers is strongly dependent on chemical composition, block length ratio,[32] the total molecular weight and the chain architecture.[33]

Two distinct methods are generally used to prepare micelles, namely;

1. co-solvent method

2. direct dissolution.

The first method involves dissolving the BCP in a 'good' solvent for both blocks. A selective solvent for just one block is gradually added. The final step involves evaporating the initial good solvent from the system. In the second method, the BCPs undergo direct dissolution in a selective solvent. The micellar solution undergoes thermal treatment and eventually ultrasonic agitation. However, micelle formation by direct dissolution in a selective solvent is generally not ideal.

After micelle preparation, it is imperative to define the thermodynamic stability of the micelles. The critical micelle concentration (CMC) and critical micelle temperature (CMT) parameters determine the thermodynamic stability of the micelles, as shall be explained in the next section.

2.13 Critical micellization parameters

The CMC is defined as the polymer concentration, above which the formation of micelles occurs. The associated CMT is defined as the transition temperature, above or below (in organic solvents, usually below) which the formation of associated structures becomes appreciable.

A larger hydrophobic block makes the BCP less soluble and more likely to self-assemble at lower concentrations to form micelles. As a result, the CMC is lowered by increasing the size of the hydrophobic block.[34,35] A lower CMC means that micelles can form at lower concentrations, which is ideal for stable micelles.[22] A lower CMT entails that the enthalpy of formation of the micelles is lower, and thus achievable with minimum energy requirements.

22

Unimers (non-assembled BCP chains) are much smaller than micelles and therefore the two polymeric species record a significant difference in intensities for fluorescence, absorbance, emittance and light scattering. The CMC can be determined from a plot of the referred intensities as a function of the sample concentration. Fluorescence spectrometry has a lower sample concentration detection limit relative to absorption spectrometry, and is therefore more ideal for measuring very low CMCs. Alternatively DLS offers a more flexible and user friendly approach by measuring diffusion or the associated size as a function of both concentration and temperature.[36] Therefore both CMC and CMT can easily be determined.

2.14 Evolution of multiple morphologies

The effect of salt on both low M_w surfactants and BCP micelles has been comprehensively reported.[37] Anionic and cationic micelles in aqueous solution have been reported to increase in size due to the reduced repulsion effect induced by the salt on the corona chains.[38] Furthermore, the effectiveness of a particular salt is dependent on the hydrophobic chain length.[37]

Salts have been reported to decrease the surface tension in aqueous micelle solutions, thereby effectively reducing the CMC by more than a factor of 10.[39] Furthermore, tetrabutyl ammonium bromide salt (TBAB) has been reported to induce micellar growth to form long flexible worm-like micelles.[22,38,40] Salt induced worm-like micelles have been reported to exist in equilibrium with spherical micelles.[38] For this study LiBr salt was selected. The salt induced evolution of the worm-like micelles shall be explained as follows.

A system of spherical micelles can undergo one dimensional growth to form rod-like and eventually worm-like micelles. Spherical to worm-like micelle transition is influenced by the concentration, ionic strength and temperature of the system. Above a critical concentration,

the worm-like micelles entangle and develop into a network of flexible worm-like structures with viscoelastic properties analogous to polymers in solution.[38] The viscoelastic property gives the network of worm-like micelles remarkable rheological properties.[41]

Worm-like micelles have been reported to have enhanced drug solubility compared to spherical micelles.[42] Furthermore these micellar structures have relatively large compartments for drug delivery.

2.15 Mixed micelles

Two or more pure micelles can be blended to form new micellar species with unique properties. The unique properties of the mixed micelle are dependent on the pure component species.[43,44] The formation of mixed micelles is a complex process governed by thermodynamic and kinetic parameters, which in turn are a function of the component BCPs structure, M_w and composition.[43,44] The size of mixed micelles has been reported to be dependent on the component pure micelles.[37]

The idea of mixed micelles is to circumvent a tedious synthesis process of specific BCPs or surfactants in order to prepare desired micellar structures.[21] A lot of research interest has been directed at various micelle blends. However, studies have been largely confined to the determination of the CMC, CMT, morphology and size.[37,45,46] Very few reports are available on the kinetics of formation, CCD, MMD and PSD of mixed micelles.[18]

The kinetics involved in the reassembly of unimers from different micelles to form mixed micelles are very challenging to observe experimentally. Most classical techniques such as SANS and SAXS have been limited to characterising mixed micelles either before or after formation. Microscopy has been used to monitor the structural evolution of mixed micelles,[47] but only morphology and size related analysis can be carried out. Xie et al. used SEC-

24

MALLS to investigate the complexation between PAA and PEO in the formation of mixed micelles between PMMA-b-PEO and PS-b-PAA.[48] However, such a setup is prone to column-based limitations and the separation can only be related to molar mass. Apart from multidetector ThFFF, no other technique has been able to simultaneously provide detailed information on size, morphology, chemical composition, structural evolution and kinetics of formation of mixed micelles.[18]

Although mixed micelles have been successfully characterized by ThFFF,[18] no studies have been carried out via ThFFF with regards to multiple mixed micelles prepared from varying mass compositions of the component BCPs. Theoretical models predict the structural properties of mixed micelles to be dependent on the composition ratios of the component BCP mixtures.[43,49] Therefore, ThFFF can be used as an advanced monitoring technique to establish the impact of each component in mixed micelle formation.

2.16 References

(1)   Schimpf, M. E.; Caldwell, K.; Giddings, J. C. *Field-Flow Fractionation Handbook*; John Wiley & Sons: New York, USA, 2000; Vol. 4.

(2)   Ratanathanawongs Williams, S. K.; Lee, D. *J. Sep. Sci.* **2006**, *29* (12), 1720–1732.

(3)   Messaud, F.; Sanderson, R. D.; Runyon, J. R.; Otte, T.; Pasch, H.; Williams, S. K. R. *Prog. Polym. Sci.* **2009**, *34* (4), 351–368.

(4)   Giddings, J. C. *Science* **1993**, *260* (5113), 1456–1465.

(5)   Schimpf, M. E.; Giddings, J. C. *J. Polym. Sci. Part B Polym. Phys.* **1990**, *28* (13), 2673–2680.

(6)   Runyon, J. R.; Williams, S. K. R. *J. Chromatogr. A* **2011**, *1218* (38), 6774–6779.

(7)   Chan, J.; Popov, J. J.; Kolisnek-Kehl, S.; Leaist, D. G. *J. Solution Chem.* **2003**, *32* (3), 197–214.

(8)   Leroyer, Y.; Wurger, A. *J. Chem. Phys.* **2011**, *135* (5).

(9)   Schimpf, M. E.; Giddings, J. C. *J. Polym. Sci. Part B Polym. Phys.* **1989**, *27* (6), 1317–1332.

(10)   Vanasten, C.; Stegeman, G.; Kok, W. T.; Tijssen, R.; Poppe, H. *Anal. Chem.* **1994**, *66* (19), 3073–3080.

(11)   Borchard, F.; de Gennes, P.-G. *C. R. Hebd. Seances Acad. Sci.* **1981**, *293*, 1025.

(12)   Schimpf, M. E.; Giddings, J. C. *Macromolecules* **1987**, *20* (7), 1561–1563.

(13)   Cho, K.-H.; Park, Y. H.; Jeon, S. J.; Kim, W.-S.; Lee, D. W. *J. Liq. Chromatogr. Relat. Technol.* **1997**, *20* (16–17), 2741–2756.

(14)   Rauch, J.; Ko, W. *Macromolecules* **2005**, *38*, 3571–3573.

(15)   Ngaza, N.; Brand, M.; Pasch, H. *Macromol. Chem. Phys.* **2015**, 1355–1364.

(16)   Ratanathanawongs Williams, S. K.; Shiundu, P. M.; Giddings, J. C. *Colloids Surfaces A Physicochem. Eng. Asp.* **1995**, *105*, 243–250.

(17)   Greyling, G.; Pasch, H. *Macromol. Rapid Commun.* **2014**, *35* (21), 1846–1851.

(18)   Greyling, G.; Pasch, H. *Macromolecules* **2016**, *49*, 1882−1889.

(19)   Schacher, F. H.; Rupar, P.; Manners, I. *Angew. Chemie - Int. Ed.* **2012**, *51* (32), 7898–7921.

(20)   Pasch, H.; Trathnigg, B. *HPLC of Polymers*; Springer: New York; 1998.

(21)   Wright, D. B.; Patterson, J. P.; Pitto-Barry, A.; Lu, A.; Kirby, N.; Gianneschi, N. C.; Chassenieux, C.; Colombani, O.; OReilly, R. K. *Macromolecules* **2015**, *48* (18), 6516–6522.

(22)   P. Alexandridis, B. L. *Amphiphilic Block Copolymers: Self-Assembly and Applications*; Elsevier: Amsterdam, 2000.

(23)   Linse, P. *Modelling of the self-assembly of block copolymers in selective solvent*; Woodhead Publishing Limited: Cambridge, UK, 2000.

(24)   Blanazs, A.; Armes, S. P.; Ryan, A. J. *Macromol. Rapid Commun.* **2009**, *30* (4–5), 267–277.

(25)   Martinez, A. P.; Cui, Z.; Hire, C.; Seery, T. a. P.; Adamson, D. H. *Macromolecules* **2015**, *48* (13), 4250–4255.

(26)   Tseng, Y. C.; Darling, S. B. *Polymers (Basel).* **2010**, *2* (4), 470–489.

(27)   Ibrahim, K.; Salminen, A.; Holappa, S.; Kataja, K.; Lampinen, H.; Löfgren, B.; Laine, J.; Seppälä, J. *J. Appl. Polym. Sci.* **2006**, *102* (5), 4304–4313.

(28)   Discher, D. E.; Eisenberg, A. *Science* **2002**, *297* (5583), 967–973.

(29)   Hadjichristidis, N.; Pispas, S.; Floudas, G. *Block copolymers: synthetic strategies, physical properties and applications.*; John Wiley & Sons Ltd, Chichester, UK, 2002.

(30)   Liu, T.; Liu, L.-Z.; Chu, B. *Formation of Amphiphilic Block Copolymer Micelles in Nonaqueous Solution.*; Woodhead Publishing Limited: Cambridge, UK, 2000.

(31)   Riess, G. *Prog. Polym. Sci.* **2003**, *28* (7), 1107–1170.

(32)   Bronstein, L. M.; Chernyshov, D. M.; Timofeeva, G. I.; Dubrovina, L. V.; Valetsky, P. M.; Khokhlov, A. R. *Langmuir* **1999**, *15* (19), 6195–6200.

(33)   Chu, B.; Zhou, Z. In *Nonionic Surfactants: Polyoxyalkylene Block Copolymers*; 1996; pp 67–143.

(34)   Sandoval, R. W.; Williams, D. E.; Kim, J.; Roth, C. B.; Torkelson, J. M. *J. Polym. Sci. Part B Polym. Phys.* **2008**, *46*, 2672–2682.

(35)   Li, X.; Mya, K. Y.; Ni, X.; He, C.; Leong, K. W.; Li, J. *J. Phys. Chem. B* **2006**, *110*, 5920–5926.

(36)   Malvern Instruments Zetasizer Nano application note. Surfactant micelle characterization using dynamic light scattering www.malvern.com.

(37)   Aswal, V. K. *Chem. Phys. Lett.* **2003**, *371* (3–4), 371–377.

(38)   Shrestha, R. G.; Aramaki, K. *J. Nepal Chem. Soc.* **2009**, *23*, 65–73.

(39)   Mata, J.; Varade, D.; Ghosh, G.; Bahadur, P. *Colloids Surfaces A Physicochem. Eng. Asp.* **2004**, *245* (1–3), 69–73.

(40)   Khaled A, Aame, Raja S, G. N. *Block Copolymers in Nanoscience*; Massimo Lazzari, Guojun Liu, S. L., Ed.; John Wiley & Sons: New York, USA, 2007.

(41)   Berret, J.-F. *Mol. Gels* **2005**, 235–275.

(42)   Cai, S.; Vijayan, K.; Cheng, D.; Lima, E. M.; Discher, D. E. *Pharm. Res.* **2007**, *24* (11), 2099–2109.

(43)   Huang, L.; Somasundaran, P. *Langmuir* **1997**, *13* (25), 6683–6688.

(44)   Whitmore, M. D.; Noolandi, J. *Macromolecules* **1985**, *18* (4), 657–665.

(45)   Clint, J. H. *J. Chem. Soc. Faraday Trans. 1* **1975**, *71*, 1327.

(46)   Jain, S.; Bates, F. S. *Macromolecules* **2004**, *37* (4), 1511–1523.

(47)   Ebrahim Attia, A. B.; Ong, Z. Y.; Hedrick, J. L.; Lee, P. P.; Ee, P. L. R.; Hammond, P. T.; Yang, Y. Y. *Curr. Opin. Colloid Interface Sci.* **2011**, *16* (3), 182–194.

(48)   Xie, D.; Xu, K.; Bai, R.; Zhang, G. *J. Phys. Chem. B* **2007**, *111* (4), 778–781.

(49)   Zhang, Y.; Lam, Y. M. *J. Nanosci. Nanotechnol.* **2006**, *6* (12), 3877–3881.

3   Experimental Procedures

3.1   Chemicals and materials

Polystyrene-polyethylene oxide block copolymer (PS - PEO) standards were purchased from Polymer Source (Dorval, Canada). Acetonitrile (99.9%), tetrahydrofuran (99.9%) and lithium bromide (99%) were supplied by Sigma Aldrich (Missouri, United States) and used as received.
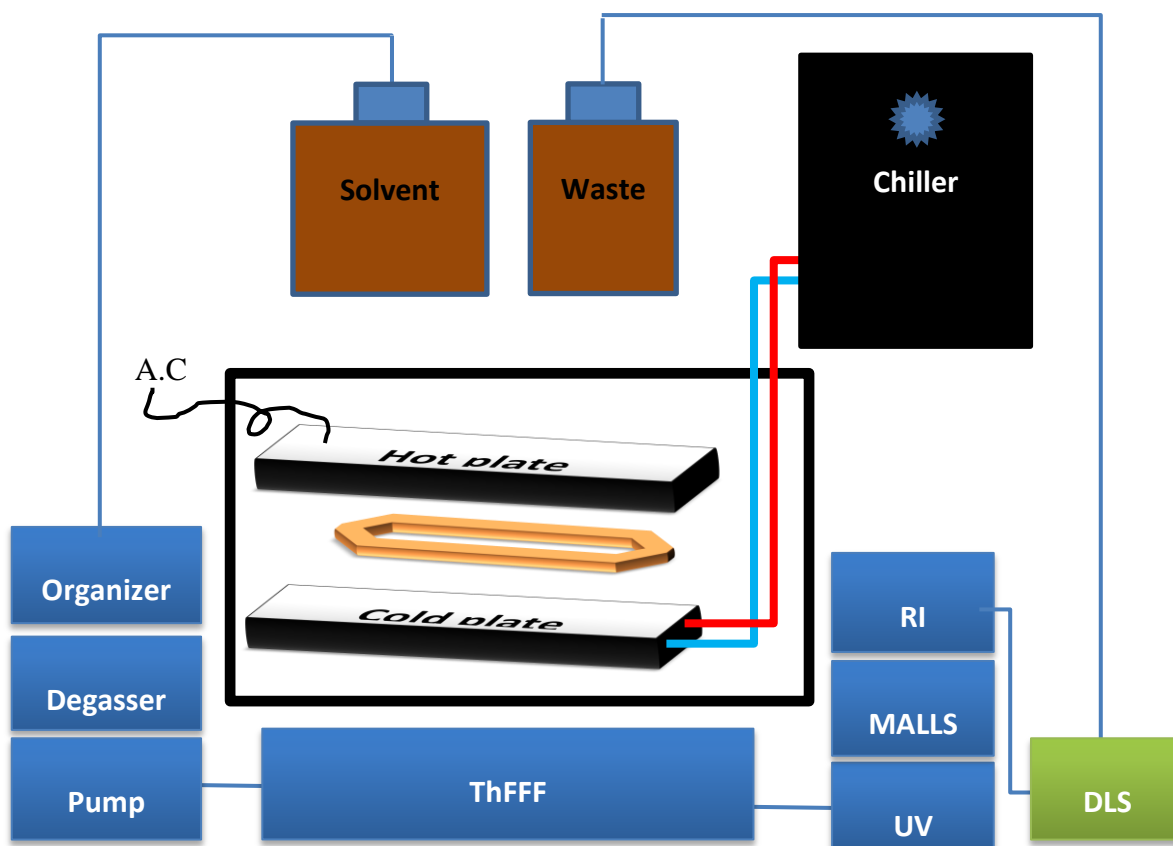
3.2   Instrumentation

The ThFFF system (TF2000, Postnova Analytics, Landsberg, Germany) was coupled online to UV (PN 3212 at 254 nm, Postnova Analytics), MALLS (PN 3070, Postnova Analytics), dRI (PN 3150, Postnova Analytics) and DLS detectors (Zen 1600, Malvern Instruments, Worcestershire, UK). The TF2000 channel had a tip-to-tip length of 45.6 cm, breadth of 2 cm, thickness of 127 μm and void volume of 1.14 mL.

3.3   ThFFF analysis conditions

Fractionation was induced by various temperature gradients from ≈25 – 40 °C, while the cold wall was maintained between ≈20 – 24 °C by an external chiller (Unichiller, Monitoring and Control Laboratories, South Africa), depending on the temperature gradient applied. 100 μL of sample were manually injected into a 100 μL capillary sample loop, and each analysis was performed in triplicate. The carrier solvent was pumped by an isocratic pump (PN 1130, Postnova Analytics) at a flow rate of 0.2 mL/min unless otherwise stated. The normal mode of elution was observed for all separations. A schematic illustration of the ThFFF instrumentation setup at Stellenbosch University is shown in Figure 3.1 below.

Figure 3.1.   Schematic illustration of the ThFFF instrumentation setup.

3.4   STEM imaging

The TEM micrographs were acquired using the Field Emission Scanning Electron Microscope (Zeiss MERLIN, Oberkochen, Germany). Prior to loading the samples into the microscope, the sample solution was dropped onto carbon-coated copper TEM grids. After evaporation of the solution, the TEM grid was loaded into the 12-place STEM sample holder and fastened into place with a copper ring and screw.

A Zeiss five-diode Scanning Transmission Electron Detector (Zeiss STEMA Detector) and Zeiss Smart SEM software were used to generate the STEM images. Beam conditions during analysis on the Zeiss MERLIN FE-SEM were a 20 kV accelerating voltage, 250 pA probe

current and a working distance of approximately 4mm. Images were acquired in bright field mode with the S1 diode activated.

3.5   Micelle preparation

The micelles were prepared by the co-solvent method[1,2] by first dissolving ≈4 mg of the block copolymers (BCPs) in 0.3 mL tetrahydrofuran (THF) as the good solvent. The BCP solution was placed in a hot water bath and acetonitrile (ACN) was slowly added dropwise as the selective solvent for PEO. THF was gradually evaporated out and the micelle solution made up to 4 mL via the dropwise addition of ACN.

3.6   Detectors

The MALLS, UV, RI, DLS were successfully coupled to the ThFFF system.[3,4,5,6] The multi-detector approach enables a simultaneous online determination of M_w and molecular mass distributions (MMD) by MALLS, particle size and particle size distribution (PSD) as well as the diffusion and thermal diffusion coefficients of the eluting polymers by DLS. The UV and RI are complimentary detectors which enable dual concentration detection via multi-detector ThFFF. The detectors shall be discussed individually in detail in the next subsections.

3.6.1   DLS

Light scattering can be used to determine the diffusion coefficient (D) and the hydrodynamic radius (R_h) of polymers in solution. DLS in particular can be used to determine the Z-average diameter, which is the mean hydrodynamic diameter, and the polydispersity index, which is an estimate of the width of the size distribution. Unimers are much smaller than micelles and therefore have a lower scattering intensity. As a result light scattering intensity at the CMC

31

increases drastically due to the presence of the larger micelles. Therefore, a change in light scattering intensity can be used to determine the CMC.[8]

3.6.2   UV detector

The UV detector consists of an ultraviolet light source, a flow cell and light sensor. The detector measures the absorbance of monochromatic light of fixed wavelength in the UV or visible wavelength spectrum. The detector relates absorbance to sample concentration based on the Beer-Lambert law. Suitable analytes for UV detection typically include unsaturated bonds, aromatic groups and functional groups containing heteroatoms, which contain π and σ nonbonding orbitals into which electrons are promoted to absorb the incident energy. Solvents that absorb UV radiation in the same region as the sample are not suitable for UV detection.

3.6.3   dRI detector

Unlike the UV detector, the dRI detector is a universal concentration sensitive detector. The dRI detector consists of flow and reference cells. The dRI detector measures the difference in the refractive index of a sample in the flow cell and pure solvent in the reference, in order to measure the sample concentration. Importantly, the dRI response is dependent on both the polymer concentration and chemical composition.

3.6.4   MALLS

Multi-angle laser light scattering (MALLS) is a static light scattering technique for absolute M_w measurements, which requires input of the differential refractive index increment (dn/dc) values for the polymer and solvent system. Theory of the dn/dc is discussed further in the next subsection.

3.6.4.1 Differential refractive index increment (dn/dc)

The dn/dc is an important parameter for light scattering and refers to the rate of change of the refractive index with the concentration for a particular sample at a given temperature, wavelength, and solvent.[9] Accurate dn/dc values are required for accurate molar mass determination,[9] because M_w determined by light scattering is dependent on the square of dn/dc,[10,11] therefore a small error greatly affects the results.[12] Equation 3.14 below relates M_w to dn/dc;[10,11]

$$\frac{K^* \, C}{R(\theta)} = \frac{1}{M_w \, P(\theta)} + 2 \, A_2 \, C \qquad 3.14$$

Where: M_w is the weight average molecular weight; $P(\theta)$ is the scattering function which accounts for angular dependence for finite-sized molecules, $R(\theta)$ is the Rayleigh scattering intensity at an angle θ, C is the sample concentration and A_2 is the second virial coefficient which accounts for solvent/solute interaction and K^* is given by Equation 15:

$$K^* = \frac{4 \, \Pi^2 \, n_0{}^2 \, (dn/dc)^2}{N_A \, \lambda_0^4} \qquad 3.15$$

Where: N_A is the Avogadro number; λ_0 is the incident wavelength in vacuum and n_o is the solvent refractive index at λ_0.[10,11] M_w is given by the intercept of a plot of K^* C / Rθ versus $\sin^2(\theta/2)$, and the radius of gyration is determined from the slope.

The dn/dc values from literature can be used but it is important that experimental conditions such as mobile phase, temperature, and wavelength are identical, when carrying out the measurements.[13] A more accurate approach is to measure the dn/dc on-line using the dRI detector.[9]

3.7 Detector calibration

Polystyrene (PS) was used as the calibration standard for the RI and MALLS detectors. 2 mg/mL of PS 64 000 g/mol was dissolved in THF and injected into the 100 µL sample loop at ThFFF conditions of 60 °C ΔT and 0.3 mL/min flow rate. Polystyrene 64 000 g/mol is ideal because it is an isotropic scattering molecule, therefore, the intensity of the scattered light is independent of the angle. Furthermore the dn/dc value for PS is readily available in literature for convenience.[13] The dRI was calibrated first in accordance with the Postnova Manual,[14] and the detector coefficient was determined to be $1.359E^{-1}$. The dRI detector coefficient was used in the calibration of the MALLS 90° angle and the other angles were calibrated relative to the 90° angle via a normalization process.[14]

3.8 References

(1)   Pioge, S.; Fontaine, L.; Gaillard, C.; Nicol, E.; Pascual, S. *Macromolecules* **2009**, *42* (12), 4262–4272.

(2)   Cai, S.; Vijayan, K.; Cheng, D.; Lima, E. M.; Discher, D. E. *Pharm. Res.* **2007**, *24* (11), 2099–2109.

(3)   Greyling, G.; Pasch, H. *Macromolecules* **2016**, *49*, 1882−1889.

(4)   Messaud, F.; Sanderson, R. D.; Runyon, J. R.; Otte, T.; Pasch, H.; Williams, S. K. R. *Prog. Polym. Sci.* **2009**, *34* (4), 351–368.

(5)   Ngaza, N.; Brand, M.; Pasch, H. *Macromol. Chem. Phys.* **2015**, 1355–1364.

(6)   Greyling, G.; Pasch, H. *Macromol. Rapid Commun.* **2014**, *35* (21), 1846–1851.

(7)   Li, X.; Mya, K. Y.; Ni, X.; He, C.; Leong, K. W.; Li, J. *J. Phys. Chem. B* **2006**, *110*, 5920–5926.

(8)   Sutherland, E.; Mercer, S. M.; Everist, M.; Leaist, D. G. *J. Chem. Eng. Data* **2009**, *54* (2), 272–278.

(9)   Held, D. *The Column*; Polymer Standards Service: Mainz, 2008; Vol. 10.

(10)   Roessner, D. Jocks, T. *G.I.T. Lab. J.* **2008**, 40–42.

(11)   Ogendal, L. *Light Scattering Demystified Theory and Practice*; University of Copenhagen, 2013.

(12)   Itakura, M.; Sato, K.; Lusenkova, M. A.; Matsuyama, S.; Shimada, K.; Saito, T.; Kinugasa, S. *J. Appl. Polym. Sci.* **2004**, *94* (3), 1101–1106.

(13)   Brandup, J.; Immergut, E.; Grulke, E. *Polymer handbook*; Interscience: New York, USA, 1999.

(14)   Postnova Analytics. Software Manual TF2000 Series Thermal FFF: Landsberg am Lech pp 1–93.

4   Results and Discussion

4.1   Introduction

This study is focused on pure micelles and micelle blends prepared from two types of PS-b-PEO block copolymers (BCPs), namely PS (40 000)-PEO (28 000) and PS (102 000)-PEO (33 000) as shown in Table 4.1 below. These BCPs are code named PS_{385}-PEO_{636} and PS_{981}-PEO_{773}, respectively. Both have comparable PEO block lengths but different sized PS blocks. In general PS is hydrophobic and PEO is hydrophilic, therefore, the hydrophobicity for the PS_{981}-PEO_{773} BCP in solution is expected to be higher owing to the larger PS block.

Table 4.1.   PS-PEO BCP samples, M_w, dispersity and degree of polymerization (DP).

| Copolymer	M_w (g/mol)		Dispersity	DP
	PS	PEO		
PS_{385}-PEO_{636}	40 000	28 000	1.05	385:636
PS_{981}-PEO_{773}	102 000	34 000	1.02	981:773

The two block copolymers were separately dissolved in THF, thereafter micelles were prepared by introducing acetonitrile (ACN) and simultaneously evaporating THF. This process is termed the co-solvent method for micelle preparation. THF is a good solvent for both blocks but ACN is a selective solvent for PEO, therefore, the micelles should have PEO coronas and PS cores. The difference in size of the core forming PS block therefore means that the prepared micelles should also have different core densities, with PS_{981}-PEO_{773} micelles expected to have the larger value. After the preparation process, the next step was to

36

validate the presence of micelles using scanning transmission electron microscopy (STEM) and dynamic light scattering (DLS).

4.2   Micelle characterisation by STEM and offline DLS

4.2.1   STEM

A few drops of the prepared micelles were placed on carbon grits then left to evaporate at ambient conditions prior to STEM imaging. STEM micrographs for the two pure micelles are shown in Figures 4.1. Large aggregate structures (>50 nm) with spherical morphologies can be seen for both pure micelles. Similar spherical morphologies have been observed by Eisenberg and Zhang for pure micelles prepared from BCPs with core blocks larger than the corona blocks,[1] as in this case.
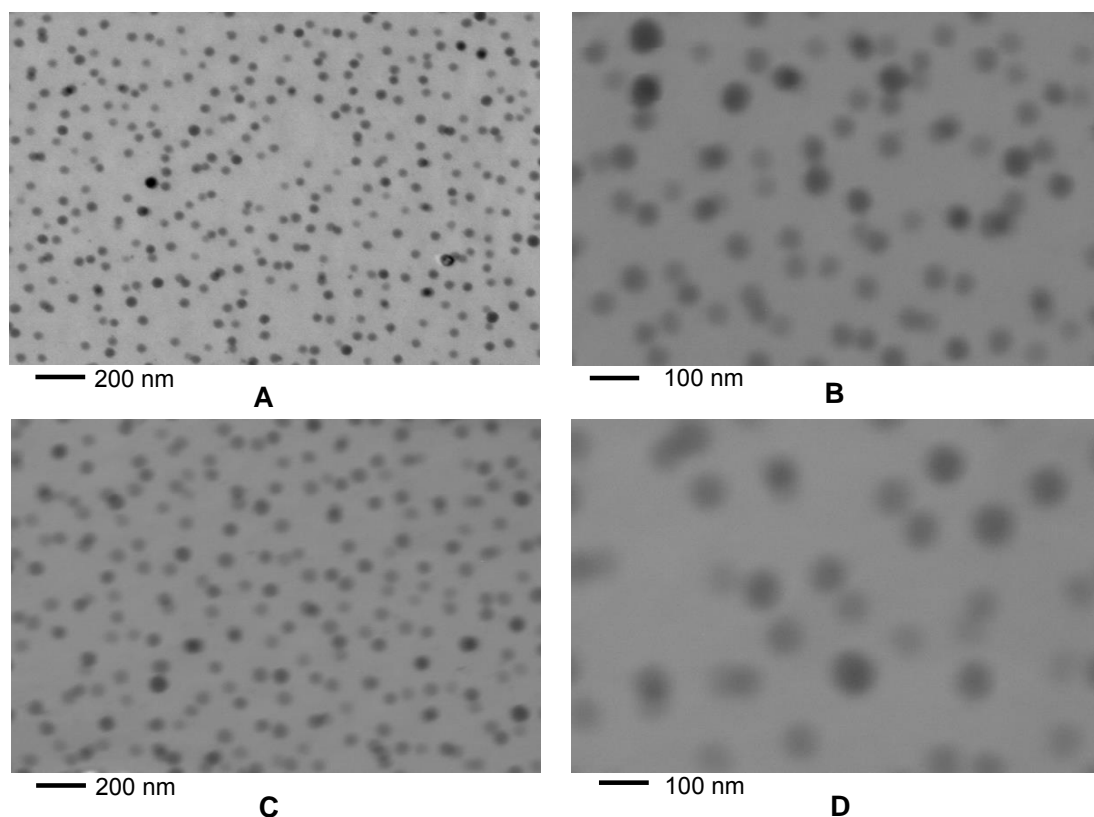
Figure 4.1.   STEM images for the pure micelles; PS_{385}-PEO_{636} (A and B) and PS_{981}-PEO_{773} (C and D).

37

Additionally, different mixed micelles were prepared by the same method using various binary blending ratios of PS_{385}-PEO_{636} and PS_{981}-PEO_{773} BCPs as illustrated in Table 4.2 below. The code names for the mixed micelles and the mass % of the component BCPs are also shown in Table 4.2. The idea of micelle blending is to prepare new micellar structures with unique properties, without the need to undergo the rigorous and complex synthetic process for appropriate amphiphilic BCPs.

Table 4.2.   Binary blending protocols for mixed micelles.

Copolymer	Mixing ratio		PS_{385}-PEO_{636} mass %	PS_{981}-PEO_{773} mass %
	PS_{385}-PEO_{636}	PS_{981}-PEO_{773}		
S3M	3	1	75	25
SM	2	2	50	50
S1M	1	3	25	75

Figure 4.2 shows that mixed micelles are all spherical, which means that both mixed and pure micelles have similar morphologies. Therefore, the blending protocol had no impact on morphology, although various blending protocols can be used to induce morphological transformation. Bates and co-workers observed morphological transformations induced by various binary blends of PEO-PB BCPs in preparing mixed micelles.[2,3]

200 nm

A

100 nm

B

150 nm

C
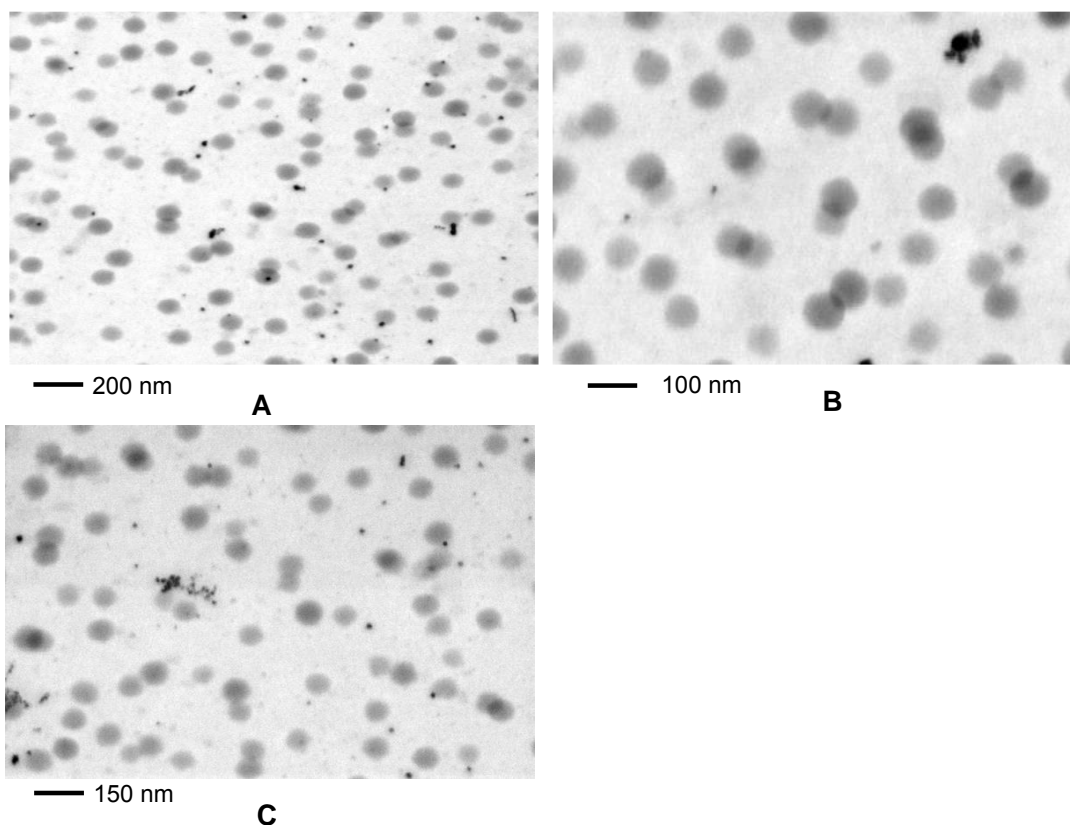
Figure 4.2.   STEM images for the mixed micelles; S3M (A), SM (B) and S1M (C).

In general, other factors such as molar mass, block ratios and the solvent system need to be considered for the transformations to occur.

Although STEM is regularly used to characterise micelles, it cannot accurately measure actual size in solution since sample evaporation is a prerequisite prior to analysis. Consequently offline DLS was performed on the micelles in solution.

4.2.2   DLS

Figure 4.3 below shows the superimposed DLS size distribution graphs for the pure and mixed micelles. All the graphs confirm the presence of large sized species (60-100 nm) with a unimodal size distribution.
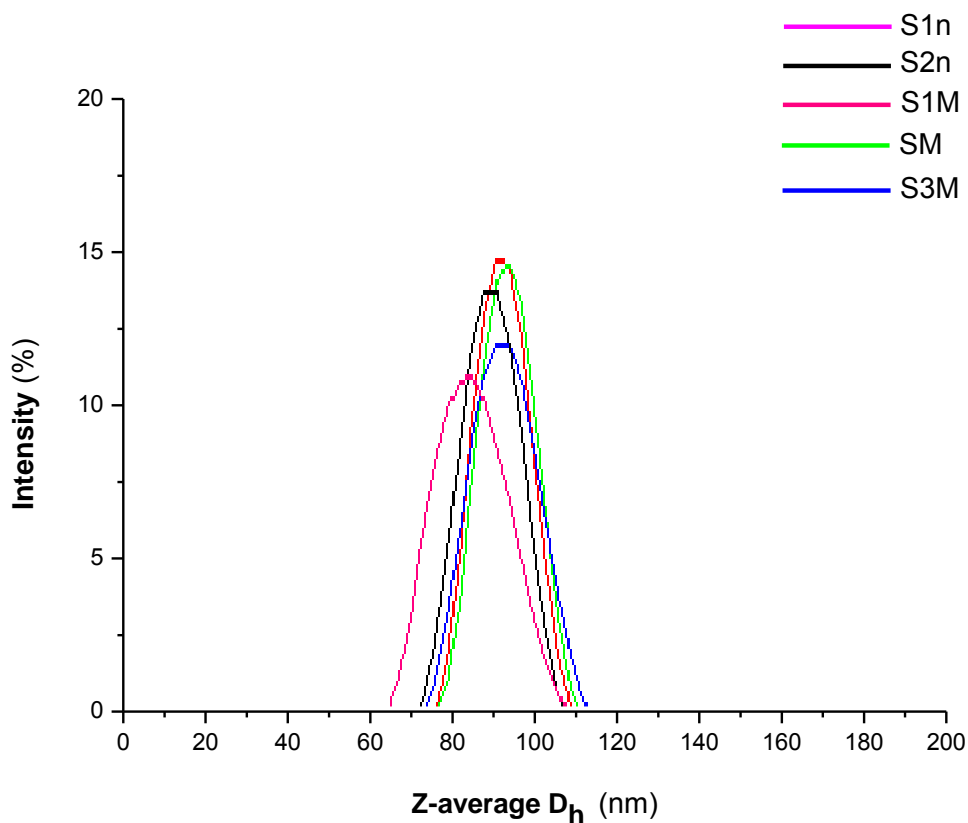
Figure 4.3.   Superimposed DLS size distribution graphs for the pure and mixed micelles at 25 ºC.

The size values from DLS measurements are shown in Table 4.3 below. Interesting to note is that all mixed micelles have larger hydrodynamic diameter (D_h) values relative to the pure micelles. This might be due to enhanced aggregation as a result of complexation interactions between the two different PS-PEO unimers.

Table 4.3.   Offline DLS measurements for D_h and D for the pure and mixed micelles.

Micelle	D_h (nm)	D x 10^{-7} (cm^2/s)
PS$_{385}$-PEO$_{636}$	63.0 ± 0.3	2.02 ± 0.10
S3M	94.3 ± 0.1	1.35 ± 0.10
SM	99.8 ± 0.5	1.27 ± 0.10
S1M	93.3 ± 0.1	1.36 ± 0.10
PS$_{981}$-PEO$_{773}$	81.3 ± 0.1	1.56 ± 0.10

Contrary to morphology, size appears to be dependent on binary blending protocols used to prepare mixed micelles, and this dependency appears to be nonlinear as seen in Figure 4.4. Nonetheless, mixed micelles with unique sizes are shown to be easily designed by simply altering relative amounts of the component unimers.[3] The 50:50 mass % binary blend (SM) is shown to be ideal for optimum size growth (Figure 4.4). This is possibly due to the 1:1 ratio having a reduced probability of either BCP acting as a limiting component, as compared to 1:3 or 3:1 for S1M and S3M, respectively, in which one component is always in excess.
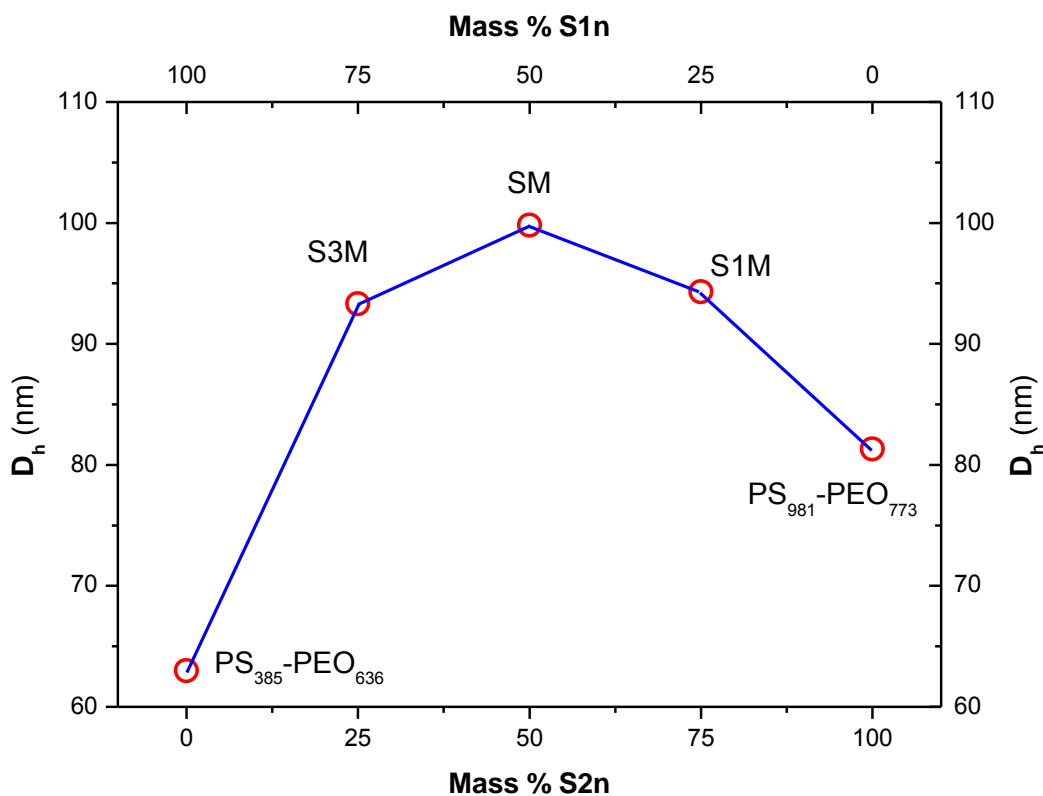
Figure 4.4. D_h as a function of block copolymer mass % composition for pure and mixed micelles.

DLS can be used further to determine critical micelle concentration (CMC) and critical micelle temperature (CMT) by measuring size as a function of concentration and temperature, respectively.[4] CMC and CMT are important parameters that can be used to explain the thermodynamic stability of the micelles. Furthermore, concentration and temperature limits for stable micelles can be defined in order to establish ideal ThFFF analysis conditions.

Table 4.4 below shows the respective CMC and CMT values determined from size measurements obtained via DLS. For pure micelles, CMC for the $PS_{981}-PEO_{773}$ micelles is lower than $PS_{385}-PEO_{636}$, as expected.[1,5,6] Therefore, micellization occurs at lower concentrations for the $PS_{981}-PEO_{773}$ BCPs. This is due to the higher hydrophobicity of the $PS_{981}-PEO_{773}$ BCPs owing to the larger hydrophobic PS blocks, which stimulates aggregation

at lower unimer concentration, as opposed to remaining in solution. Furthermore, the larger PS block implies a lower solubility, which results in enhanced aggregation tendencies at much lower concentration in solution. Overall, the lower CMC value for PS_{981}-PEO_{773} micelles points to greater thermodynamic stability.[7]

Table 4.4.   Critical micelle concentration (CMC) and critical micelle temperature (CMT) for pure and mixed micelles.

Mixed micelle	CMC (mg/mL)	CMT (^{o}C)
PS_{385}-PEO_{636}	0.21	21
PS_{981}-PEO_{773}	0.10	20
S3M	0.11	20
SM	0.10	19
S1M	0.12	20

Figures 4.5-4.9 below illustrate plots of size as a function of concentration, from which CMC can be determined. Micelles exist at concentrations equal to or above the CMC. A direct proportionality between size and concentration is observed for concentrations equal to, or above CMC, as expected.[6,8,9] This is due to more unimers being available in solution for micellization and micelle growth. Below the CMC, the concentration of free unimers in solution is high. These free unimers should have much smaller sizes compared to micelles, however, larger sizes are observed, which is unexpected. The explanation can be drawn from the high general hydrophobicity for these particular unimers, which enables them to form
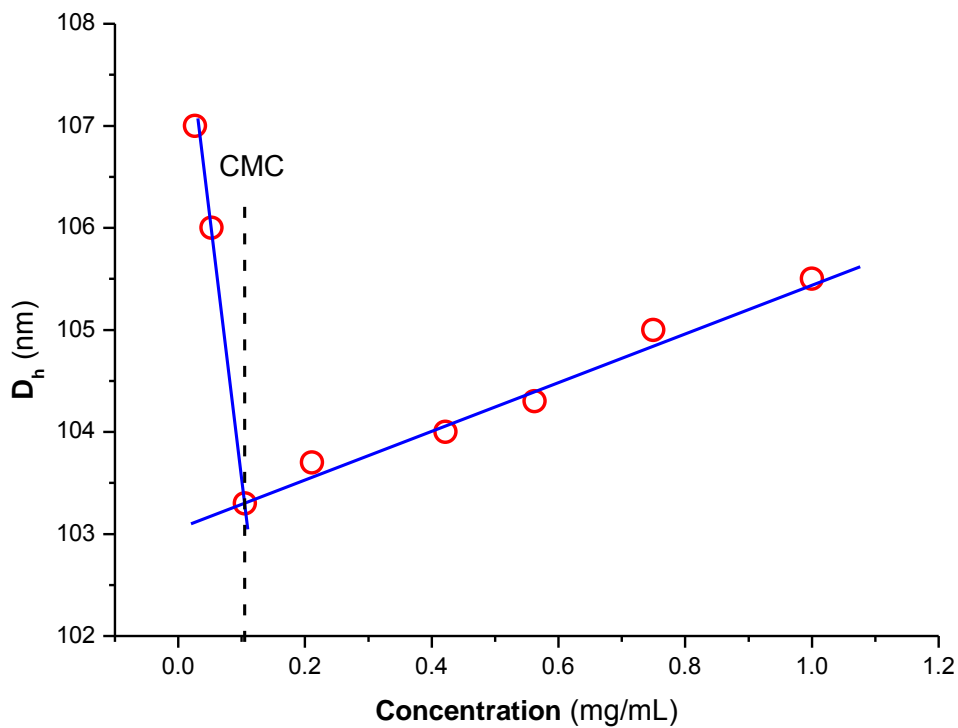
large non-structured aggregates below this CMC. The light scattering intensity for the large non-structured aggregates is expected to be high, which explains the observed size increase below CMC.
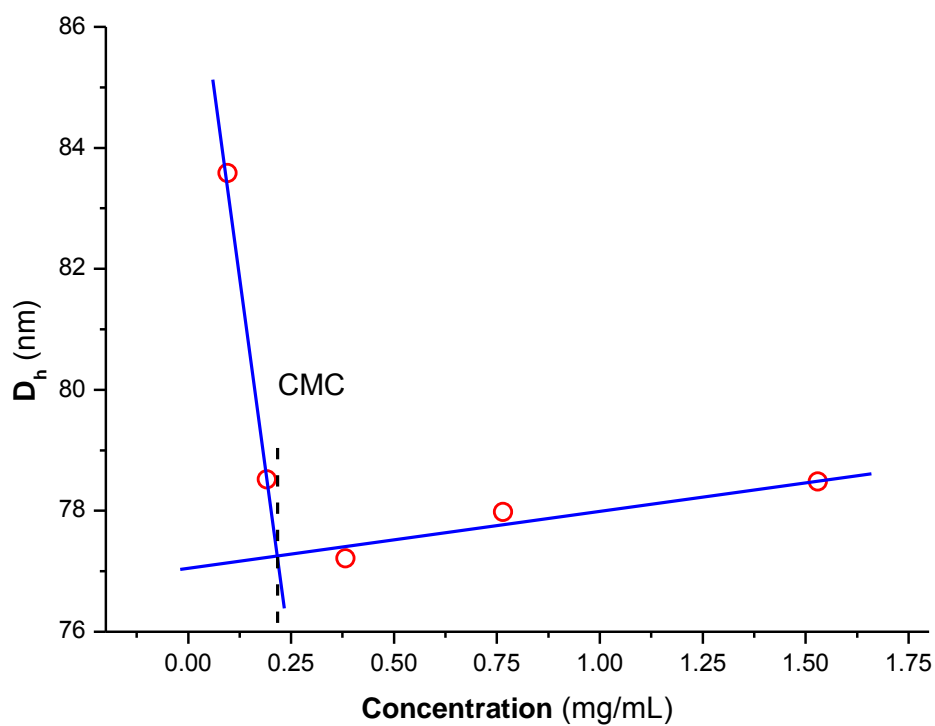
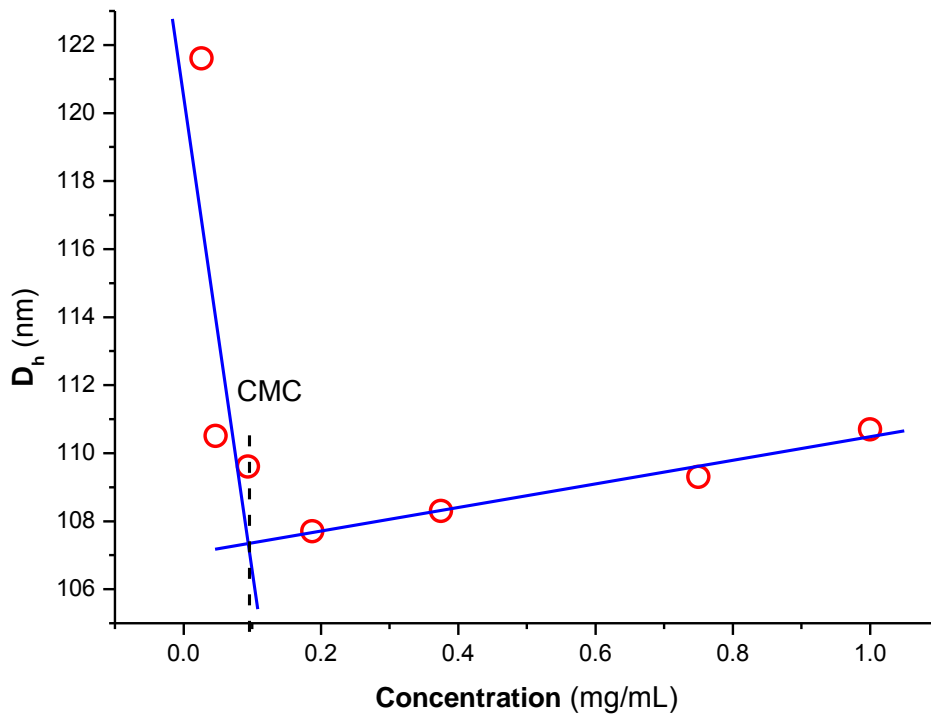**Figure 4.5.**   CMC determination for PS_{385}-PEO_{636} micelles.
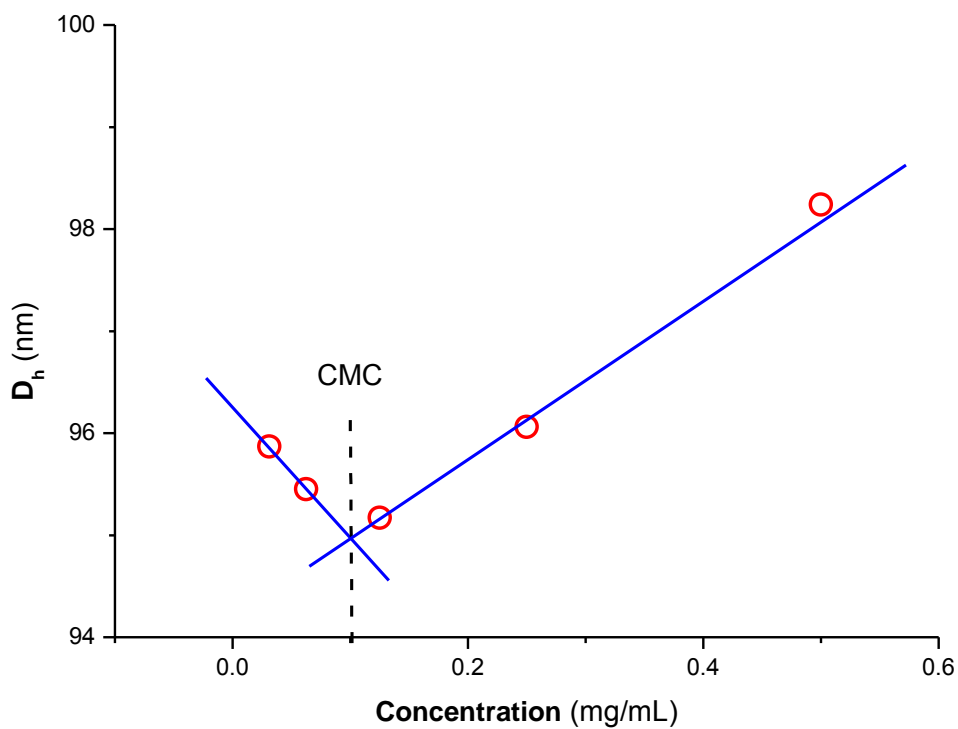
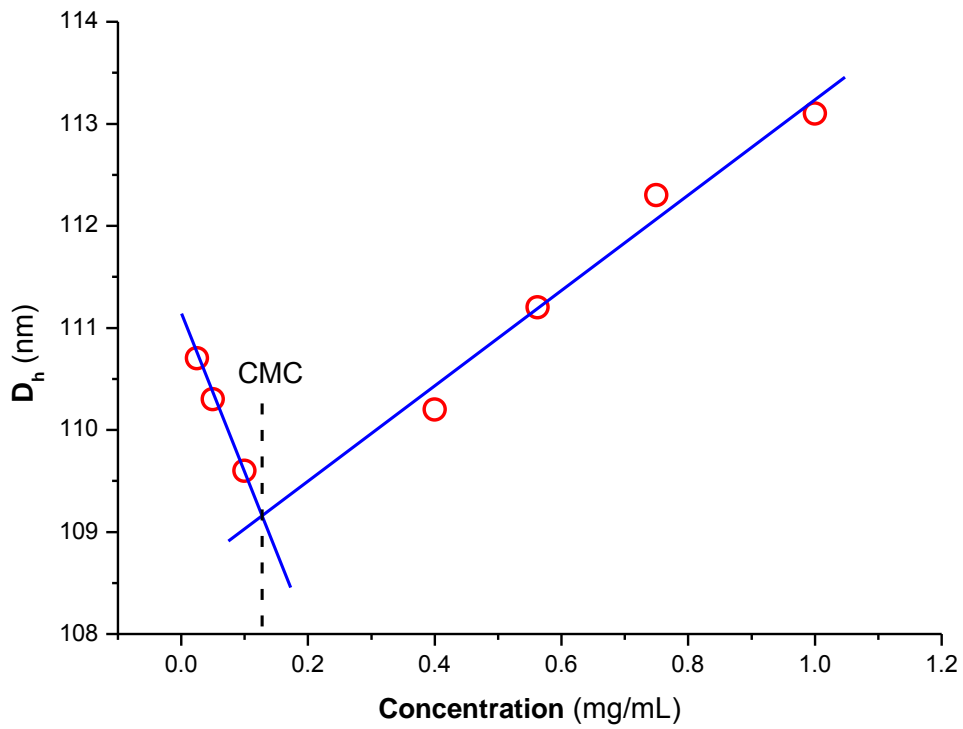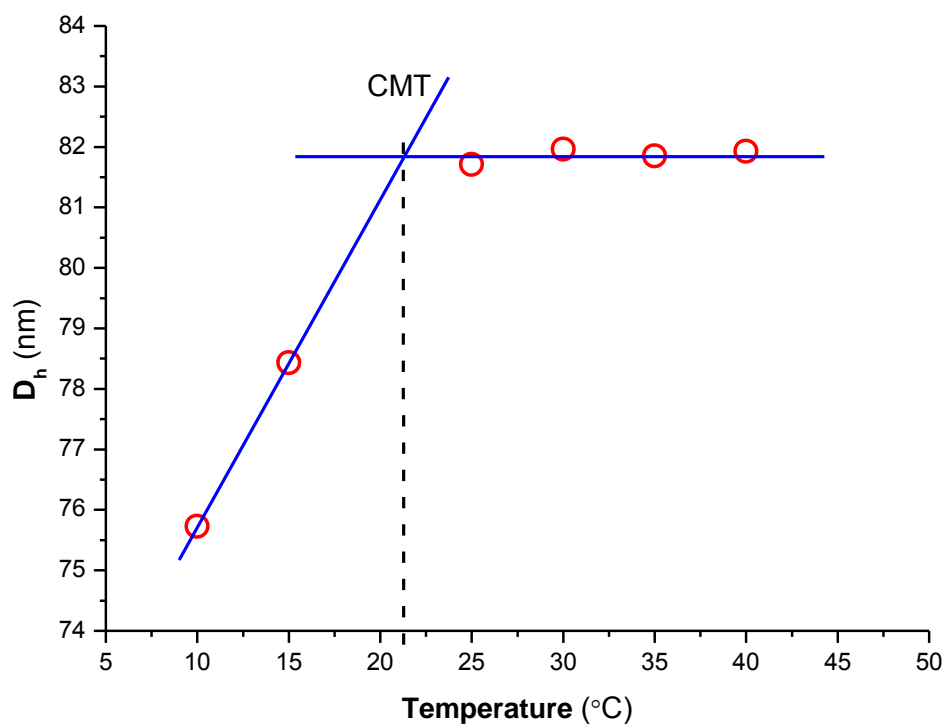**Figure 4.6.**   CMC determination for PS_{981}-PEO_{773} micelles.

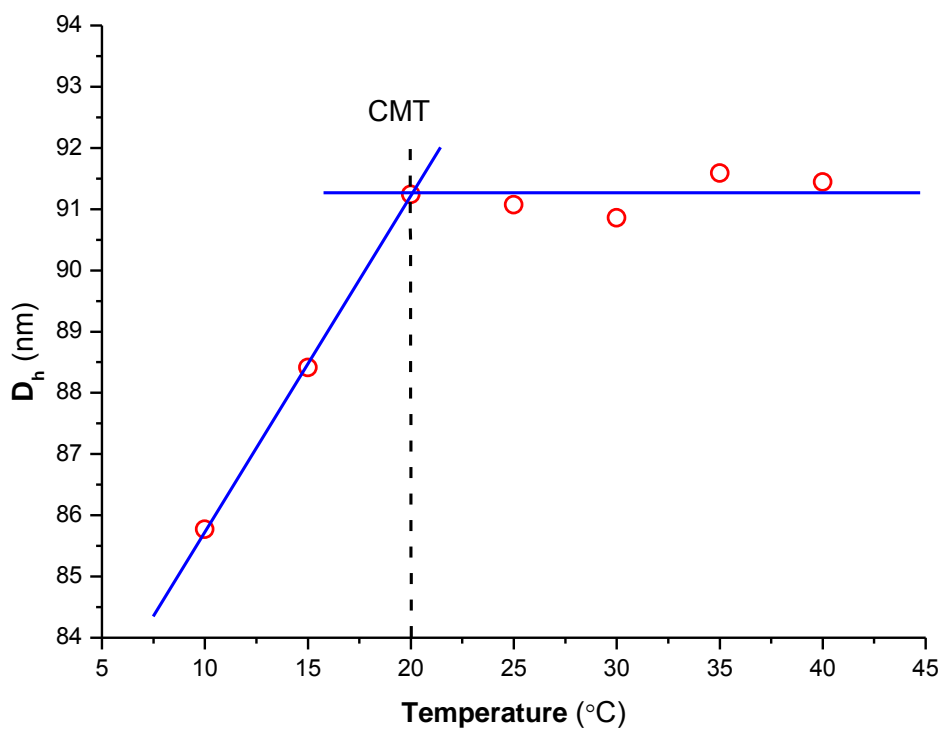**Figure 4.7.**   CMC determination for S3M mixed micelles.

Figure 4.8.   CMC determination for SM mixed micelles.
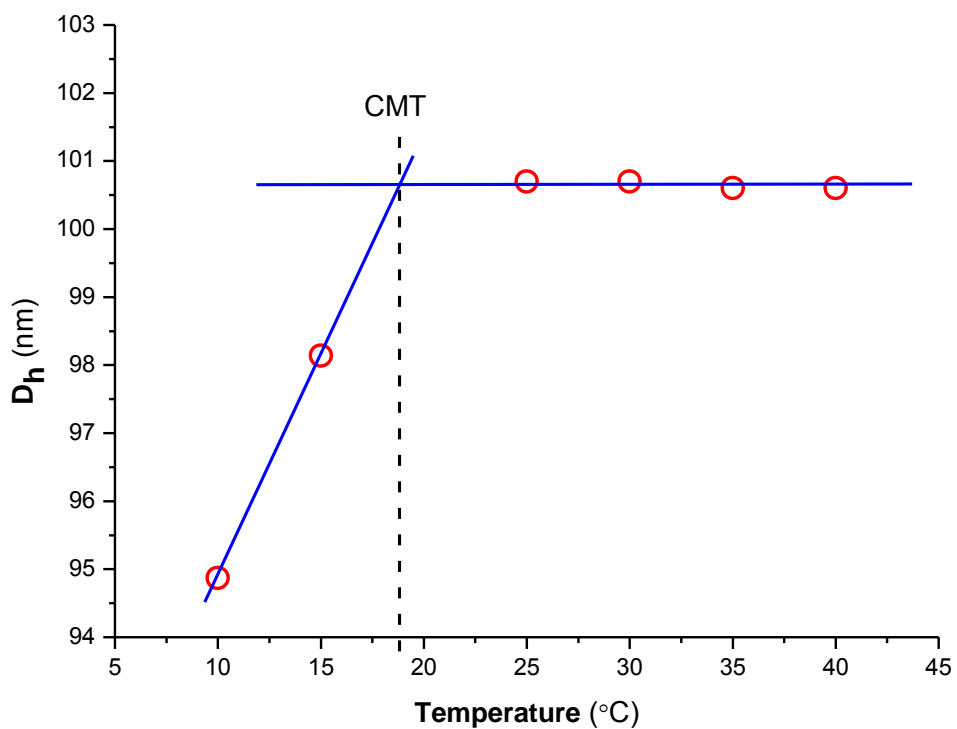

Figure 4.9.   CMC determination for S1M mixed micelles.

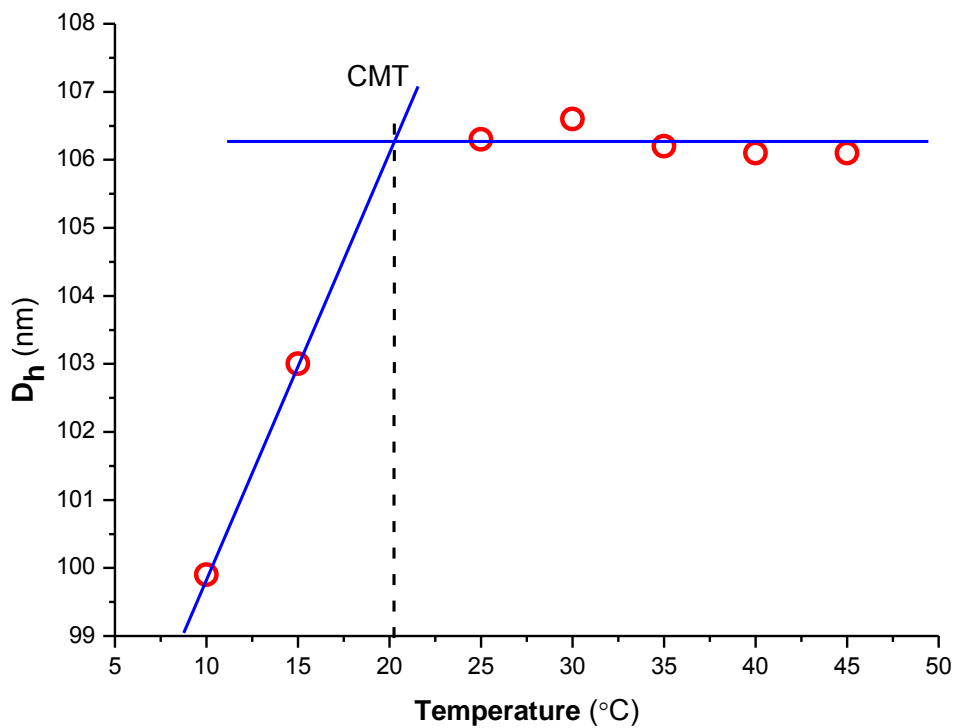**Figure 4.10.**   CMT determination for PS$_{385}$-PEO$_{636}$ micelles.
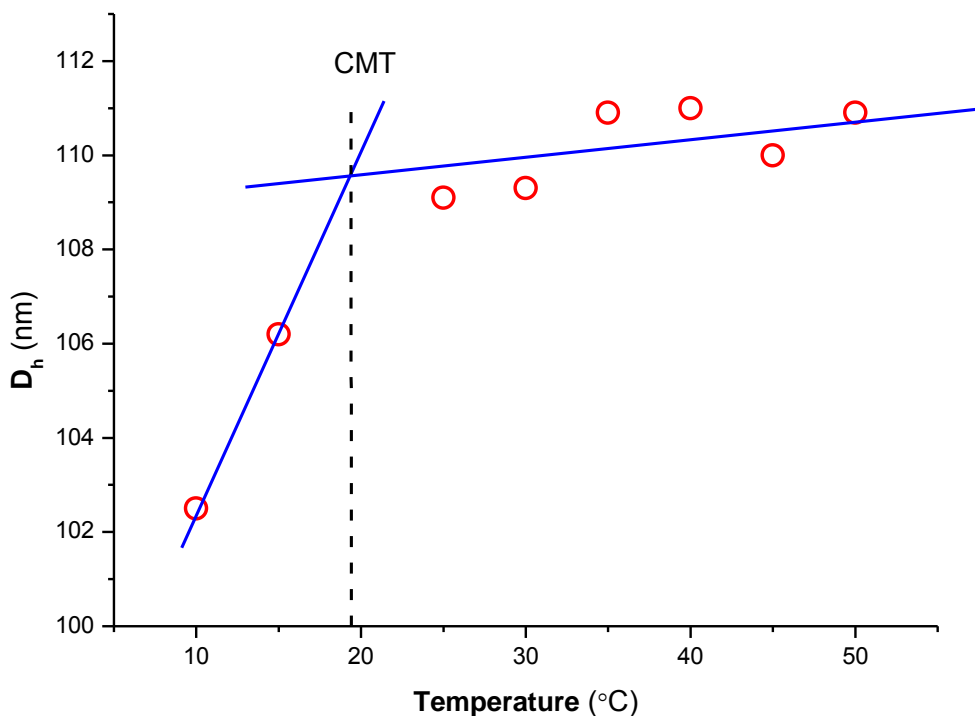

Figure 4.11.   CMT determination for PS$_{981}$-PEO$_{773}$ micelles.

Figure 4.12. CMT determination for S3M mixed micelles.

Figure 4.13. CMT determination for SM mixed micelles.

48

Figure 4.14.   CMT determination for S1M mixed micelles.

Figures 4.10-4.14 illustrate size as a function of temperature for micelles at their CMC, from which the CMT can be determined. Below CMT, size is shown to increase with temperature as expected. This is because temperature improves solubility and entropy of the unimers which enhances aggregation and promotes micelle growth. At the CMT, maximum entropy is achieved which equals to enthalpy of formation for micelles, and any further temperature increase has no significant effect on size.

4.3   ThFFF analysis of the micelles

4.3.1   Pure micelles

After determining CMC and CMT values for each sample, suitable sample concentrations and temperature gradients were selected, and the pure and mixed micelles were characterised

by ThFFF with regard to their molecular properties. Table 4.5 below summarises the separation and analysis for PS_{385}-PEO_{636} micelles.

Table 4.5. Cold wall temperature (T_C), retention time (t_r), hydrodynamic diameter (D_h), diffusion coefficient (D), thermal diffusion coefficient (D_T), Soret coefficient (S), aggregation number (Z), and shape factor (R_g/R_h) for PS_{385}-PEO_{636} micelles determined by ThFFF at various temperature gradients (ΔT).

| $T_{C, \Delta}$ (°C)	t_r (min)	Z	D_h (nm)	D x 10^{-7} (cm^2/s)	D_T x 10^{-8} (cm^2/s/K)	S x 10^{-1} (1/K)	R_g/R_h
22, 25	17.9 ± 0.7	341± 18	60.1 ± 0.1	2.11 ± 0.00	0.76 ± 0.01	0.38 ± 0.01	0.75
22, 30	20.4 ± 0.2	327 ±10	59.5 ± 0.7	2.13 ± 0.03	0.86 ± 0.01	0.40 ± 0.01	0.86
23, 35	22.9 ± 0.4	331 ±12	61.2 ± 0.8	2.07 ± 0.01	0.93 ± 0.01	0.45 ± 0.01	0.72
24, 40	25.6 ± 0.1	333 ±16	60.0 ± 1.0	2.11 ± 0.02	1.04 ± 0.01	0.49 ± 0.01	0.80

Figures 4.15-4.18 below show the UV, RI, MALLS and DLS fractograms for PS_{385}-PEO_{636} micelles at various ΔT. All these detectors record noise-like peaks near t_0. This can be attributed to the elution of unimers, which are expected to constitute the bulk of the unretained species. As for the retained species eluting between 15 and 40 min, the R_g/R_h values (0.75 - 0.86) for all temperature gradients infer spherical micelles to be the predominant morphology. In general, R_g/R_h values ranging between 0.7-0.9, 1.0-1.2 and 1.3-1.6 represent spherical, worm and vesicle micelles respectively.[1,8] Therefore, the micelles do not undergo any temperature induced morphological transitions. It can be drawn from this morphological consistency that the micelles are thermally stable for all thermal gradients under investigation, as expected.

From the various fractograms it can be seen, that PS_{385}-PEO_{636} micelles show an increase in retention as a function of the temperature gradient. This increase is expected due to the obvious increase in fractionation potential as a function of the temperature gradient. With regards to Z and D_h values, these show similarities, which is a further indication that the micelles are thermodynamically stable for the temperature gradients under investigation.

Similar single distributions are observed at various ΔT confirming single and stable micellar species. In general, temperature induced unimer interactions are substantial above the glass transition temperature (t_g) of the core.[10] However the related PS block molar mass has a high glass transition temperature (≈80 °C),[11,12] which is way above the maximum ThFFF temperatures involved, and PS is also highly insoluble in acetonitrile. Therefore the micelles are expected to have collapsed cores and thus be very compact.
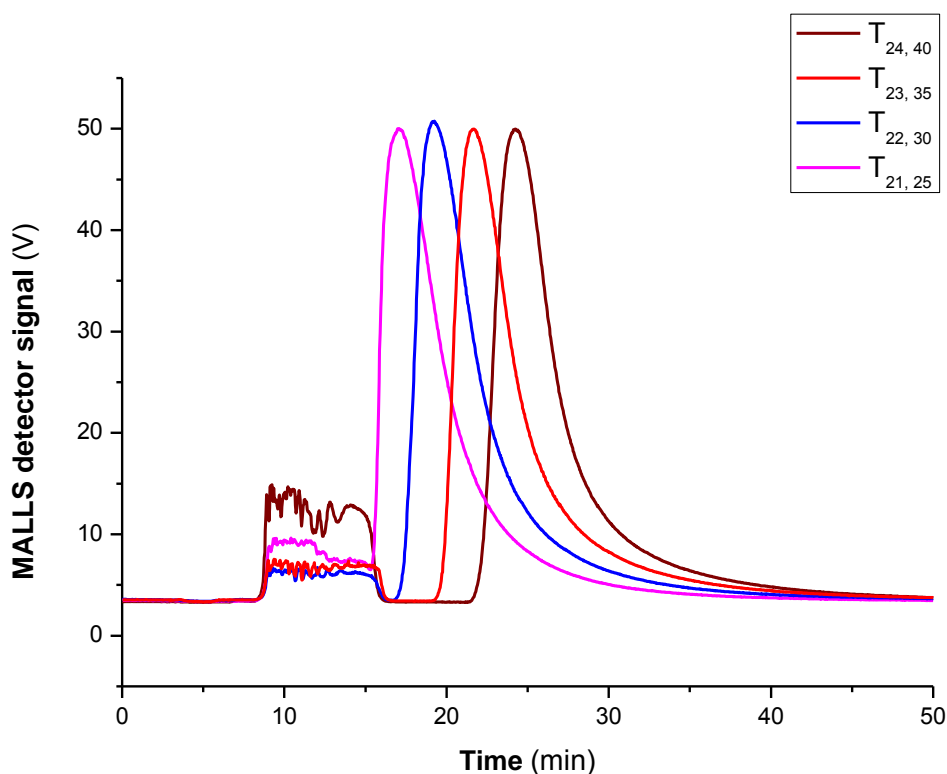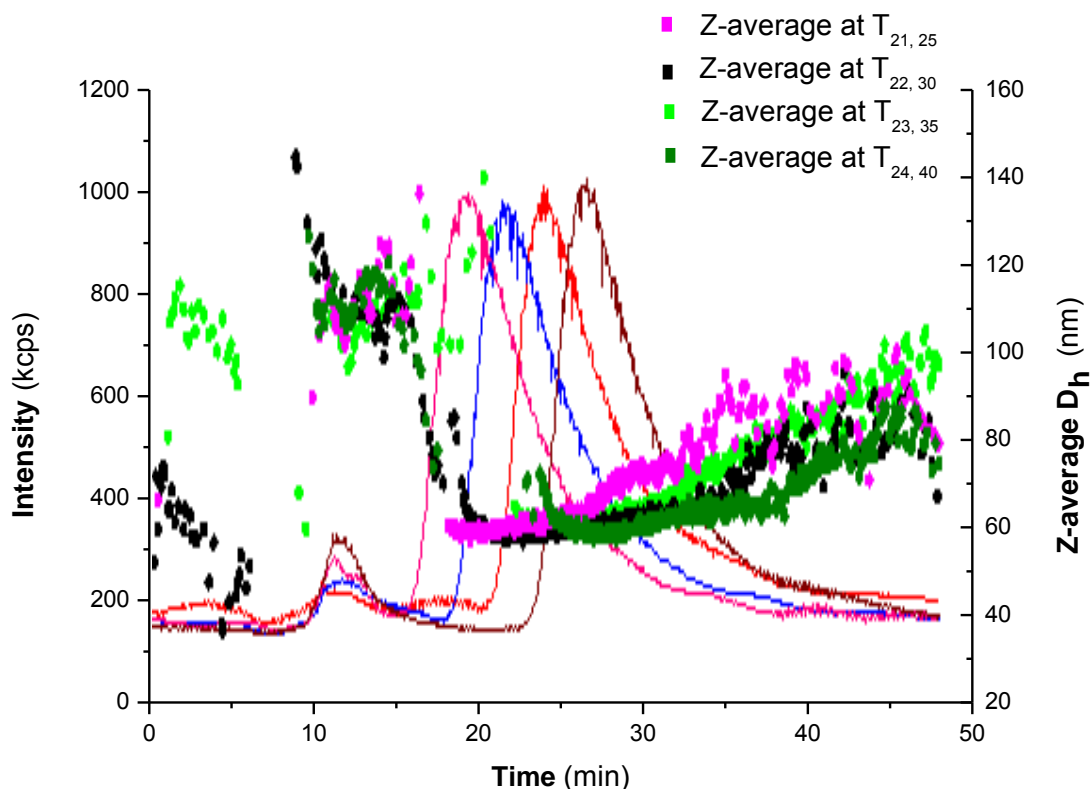

Figure 4.15.   Superimposed MALLS fractograms for PS_{385}-PEO_{636} micelles at various ΔT.
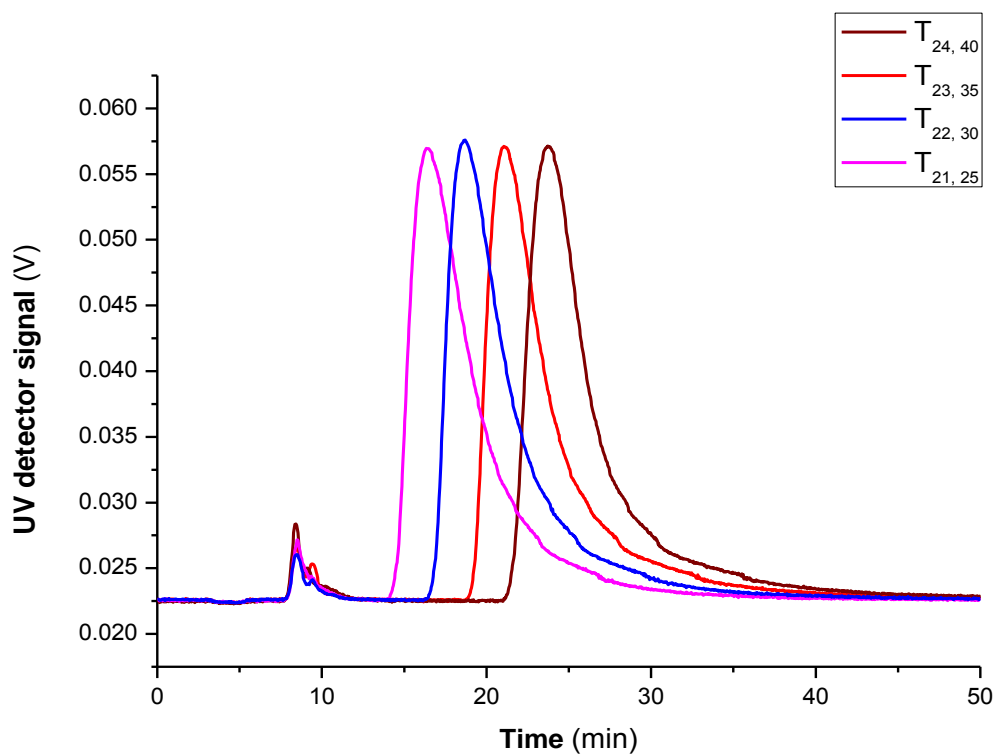
Figure 4.16.   Superimposed UV fractograms for PS_{385}-PEO_{636} micelles at various ΔT.
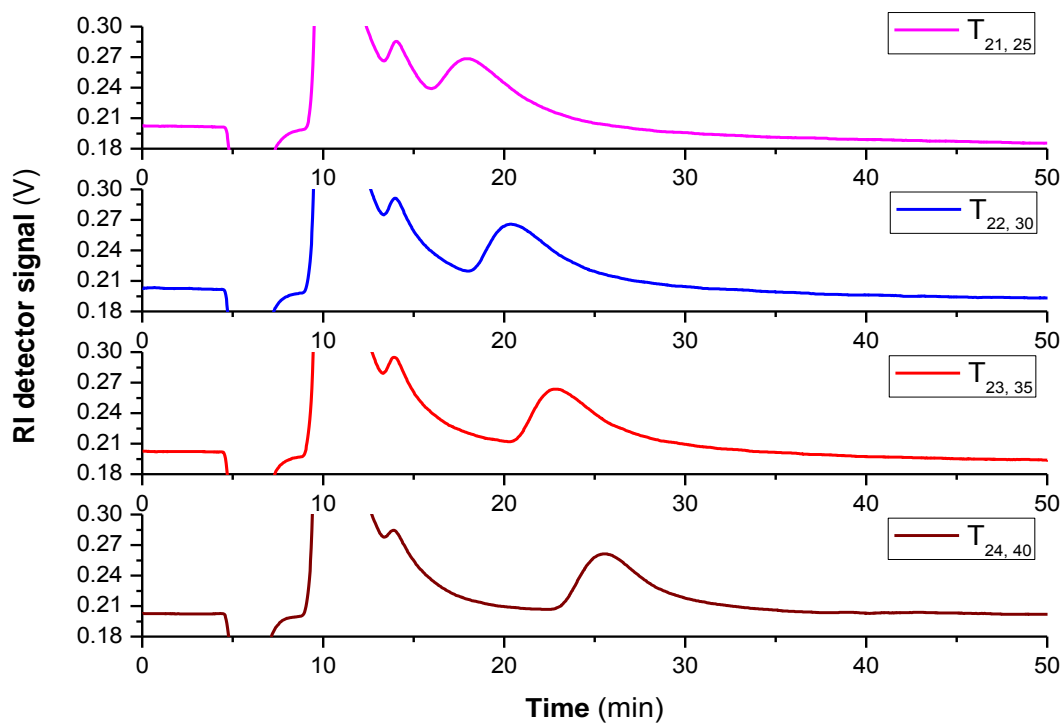
Figure 4.17.   Superimposed dRI fractograms for PS_{385}-PEO_{636} micelles at various ΔT.

Figure 4.18. Superimposed DLS fractograms for PS_{385}-PEO_{636} micelles at various ΔT.

In Table 4.5, D_T values are shown to increase with temperature gradients of ΔT 25-30 °C, although they are expected to remain constant. Such a deviation is due to the use of a simplified equation in calculating D_T.[13] The accuracy of the simplified equation improves at higher retention. This explains why D_T becomes constant for higher retentions involved with ΔT 35-40 °C.

Table 4.6 below summarises the ThFFF data collected for PS_{981}-PEO_{773} micelles, while the superimposed fractograms for the MALLS, UV, RI and DLS are shown in Figures 4.19-4.22. PS_{981}-PEO_{773} micelles show a similar ThFFF separation trend to PS_{385}-PEO_{636} micelles (see Figures 4.15-4.18), however, PS_{981}-PEO_{773} micelles show higher retention times under the same conditions. The increased retention can be attributed to the expected increase in Z owing to the larger core forming PS block.[14,15] As a result, PS_{981}-PEO_{773} micelles have approximately three times the Z value of PS_{385}-PEO_{636} micelles.

Table 4.6. Cold wall temperature (T_C), retention time (t_r), hydrodynamic diameter (D_h), diffusion coefficient (D), thermal diffusion coefficient (D_T), Soret coefficient (S), aggregation number (Z), and shape factor (R_g/R_h) for PS_{981}-PEO_{773} micelles determined by ThFFF at variable temperature gradients (ΔT).

| $T_{C,\Delta}$	t_r	Z	D_h	D x 10^{-7}	D_T x 10^{-8}	S x 10^{-1}	R_g/R_h
(°C)	(min)		(nm)	(cm^2/s)	(cm^2/s/K)	(1/K)	
22, 25	22.4 ±0.2	1011 ±12	67.9 ±0.2	1.87 ±0.03	0.86 ±0.01	0.46 ±0.01	0.86
22, 30	26.3 ±0.1	1010 ±10	67.8 ±0.8	1.87 ±0.02	1.00 ±0.01	0.53 ±0.01	0.84
23, 35	29.6 ±0.2	1006 ±11	67.8 ±0.6	1.87 ±0.02	1.10 ±0.01	0.59 ±0.01	0.83
24, 40	32.7 ±0.2	1015 ±16	67.7 ±0.6	1.87 ±0.01	1.20 ±0.01	0.64 ±0.01	0.83

In addition, the micelles clearly show larger D_h and lower D trends. Consequently, the micelles diffuse slower away from the cold plate and are subsequently restricted towards slower moving streamlines, thus the higher retention times. The calculated R_g/R_h values are similar and point to the existence of spherical micelles, which corroborates the STEM results. Furthermore, similar R_g/R_h values and size distributions show that no changes in morphology and size are stimulated by the ΔT, as seen with PS_{385}-PEO_{636} micelles.
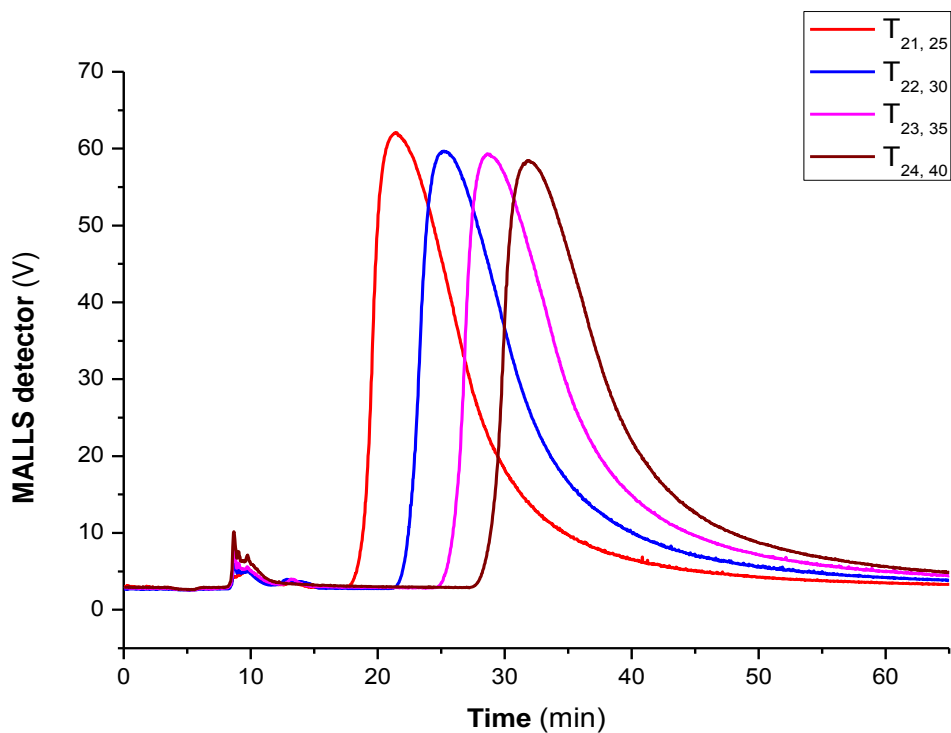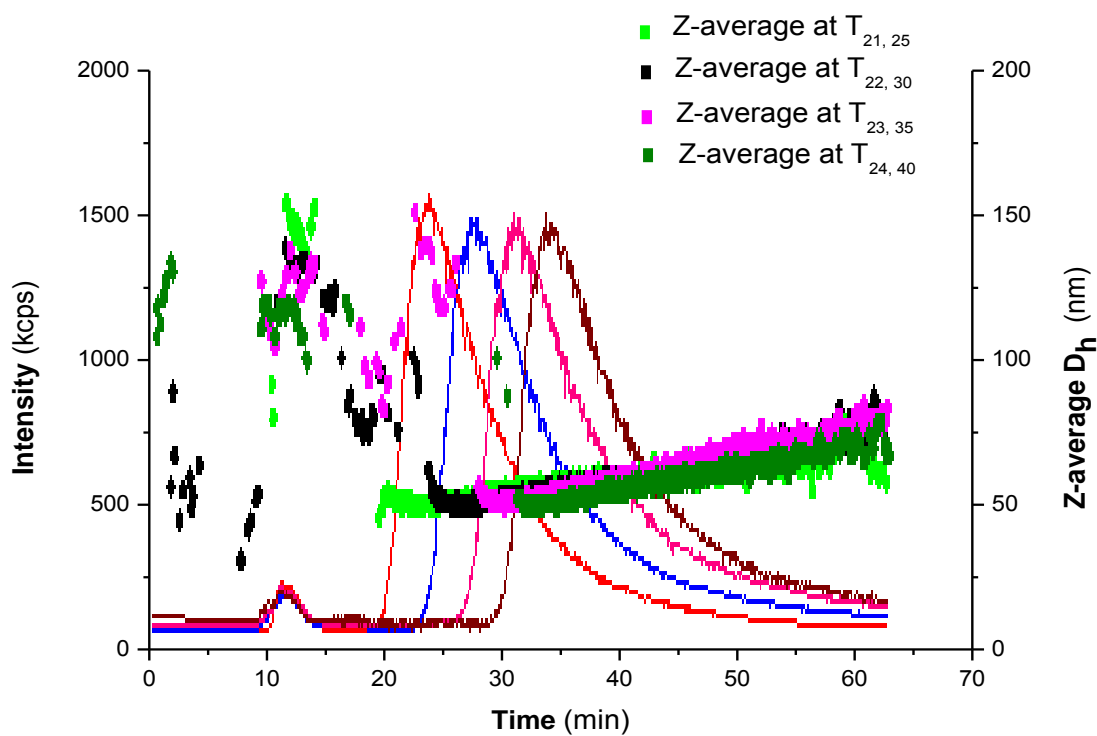
Figure 4.19. Superimposed MALLS fractograms for PS_{981}-PEO_{773} micelles at various ΔT.
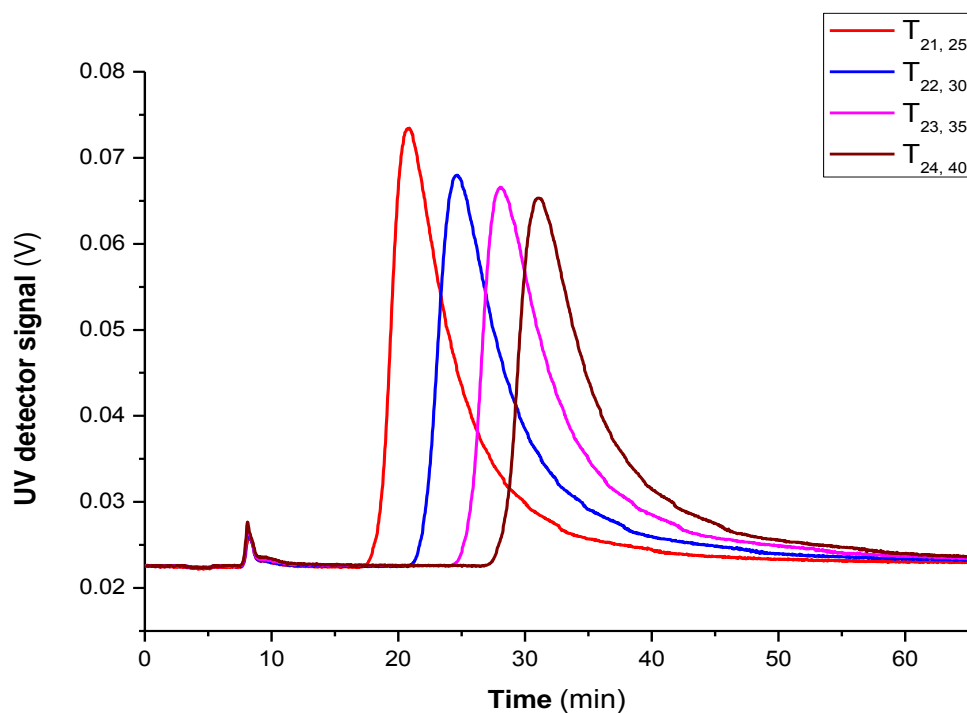
Figure 4.20. Superimposed UV fractograms for PS_{981}-PEO_{773} micelles at various ΔT.
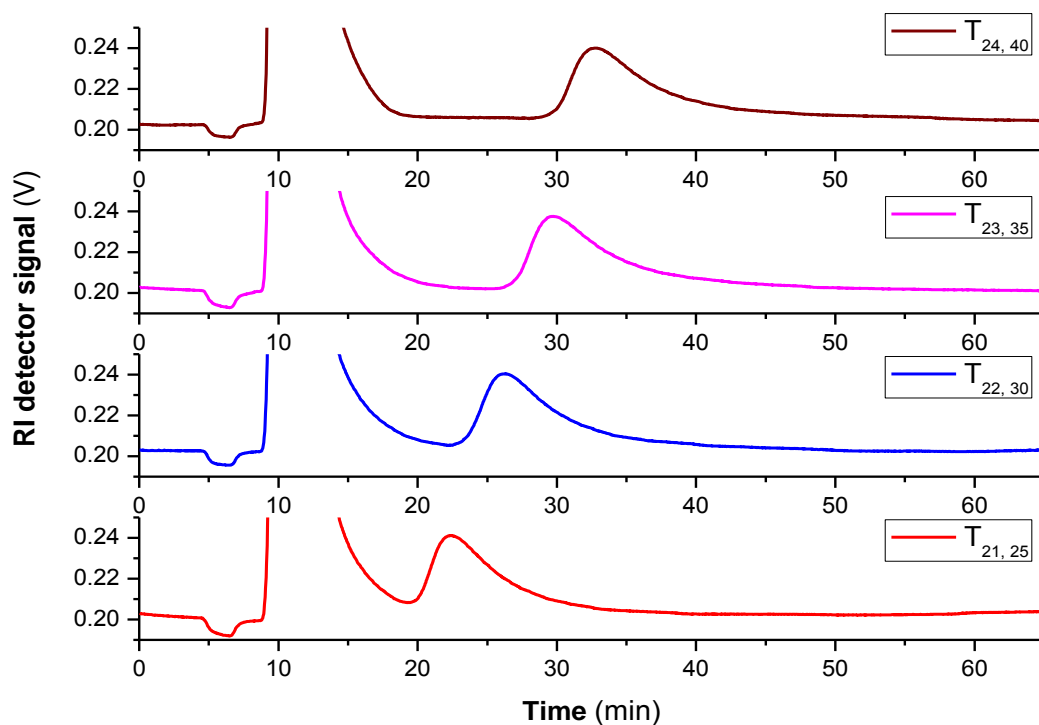
Figure 4.21. Superimposed dRI fractograms for PS_{981}-PEO_{773} micelles at various ΔT.

Figure 4.22. Superimposed DLS fractograms for PS_{981}-PEO_{773} micelles at various ΔT.

56

4.3.2 Mixed micelles

After successfully characterizing the pure micelles, the investigation shifted to the mixed micelles. Table 4.7 below shows the ThFFF data collected for the mixed micelles. The related MALLS, UV, dRI and DLS fractograms are shown in Figures 4.23-4.26 below. The calculated R_g/R_h values confirm the presence of spherical micelles as initially visualised from STEM imaging. Retention increases with mass % of the larger $PS_{981}-PEO_{773}$ BCP. S3M mixed micelles which have the lowest $PS_{981}-PEO_{773}$ mass % elute first, whilst S1M mixed micelles which have the highest $PS_{981}-PEO_{773}$ mass % elute last. SM mixed micelles which were prepared from equal mass % of $PS_{385}-PEO_{636}$ and $PS_{981}-PEO_{773}$, elute in between S1M and S3M mixed micelles.

Table 4.7. Mixed micelle (MM), retention time (t_r), aggregation number (Z), hydrodynamic diameter (D_h), diffusion coefficient (D), thermal diffusion coefficient (D_T), Soret coefficient (S), and shape factor (R_g/R_h) for various mixed micelles determined by ThFFF at temperature gradient of 30 °C.

| MM	t_r (min)	Z	D_h (nm)	$D \times 10^{-7}$ (cm^2/s)	$D_T \times 10^{-8}$ ($cm^2/s/K$)	$S \times 10^{-1}$ (1/K)	R_g/R_h
S3M	22.6 ± 0.1	720 ± 12	73.9 ± 0.1	1.72 ± 0.11	0.79 ± 0.10	0.46 ± 0.02	0.82
SM	23.6 ± 0.1	1278 ± 25	82.6 ± 0.2	1.54 ± 0.11	0.73 ± 0.10	0.48 ± 0.01	0.96
S1M	25.5 ± 0.1	1207 ± 17	77.7 ± 0.1	1.63 ± 0.10	0.84 ± 0.11	0.52 ± 0.01	0.86

From Table 4.7 it can be seen that SM mixed micelles have the largest Z and D_h followed by S1M and S3M in that order. S3M mixed micelles have the lowest Z, however, Z for SM and

S1M mixed micelles are similar. This is possibly due to a reduced influence of molar mass of the PS_{981}-PEO_{773} mass % above 50 % content in the mixed micelles. Overall, the retention trends cannot be explained by ordinary elution theories based on molar mass and size because the respective Z and D_h values do not follow a similar trend, and D_T is not similar.

Despite these trends, the Soret coefficient (S), which is a measure for the separation in ThFFF and is defined as D/D_T, shows an increase in retention with increasing PS_{981}-PEO_{773} mass %. Thus although D and D_T show unexpected trends, the interplay between D and D_T (and thus retention) shows an expected trend with PS_{981}-PEO_{773} %.
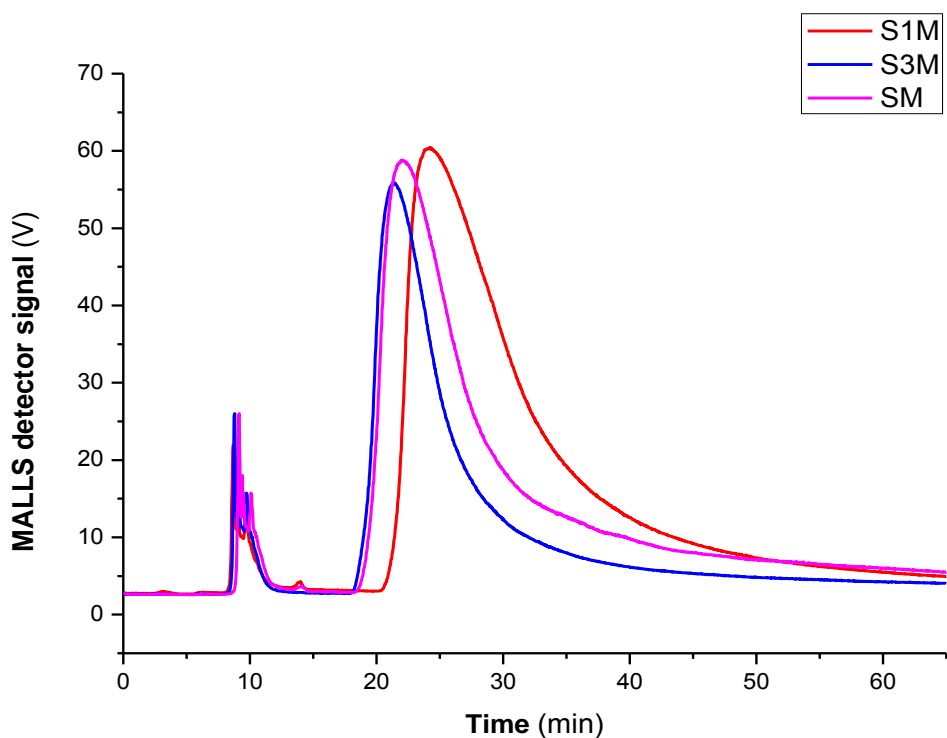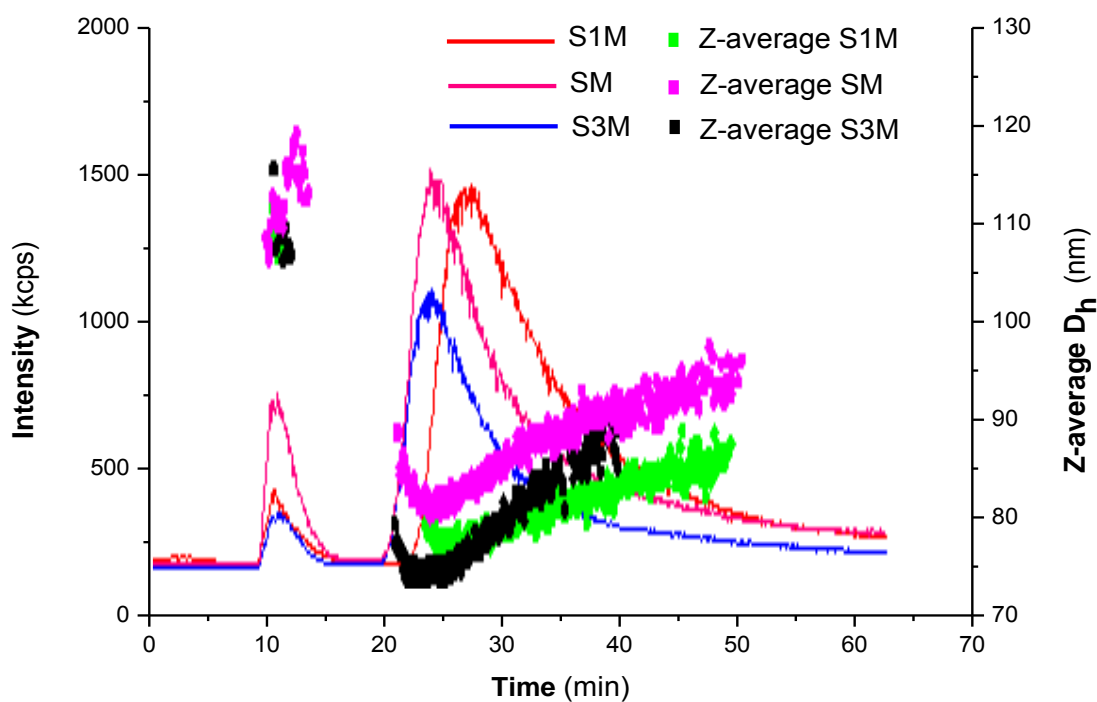

Figure 4.23.   Superimposed MALLS fractograms for S3M, SM and S1M at a ΔT of 30 °C.

58
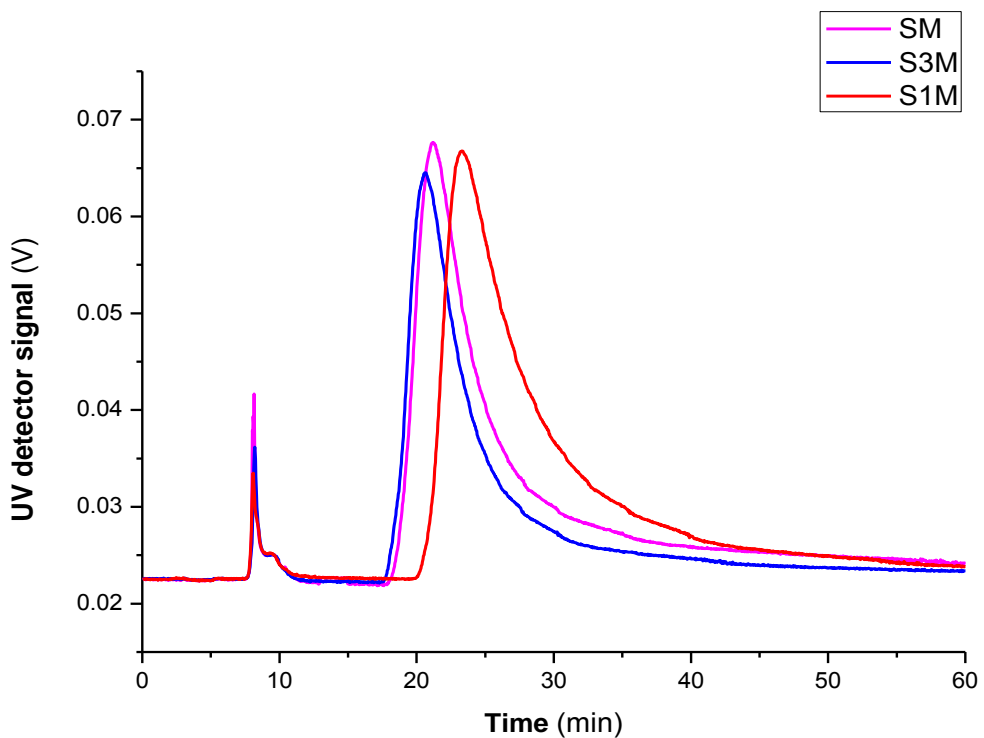
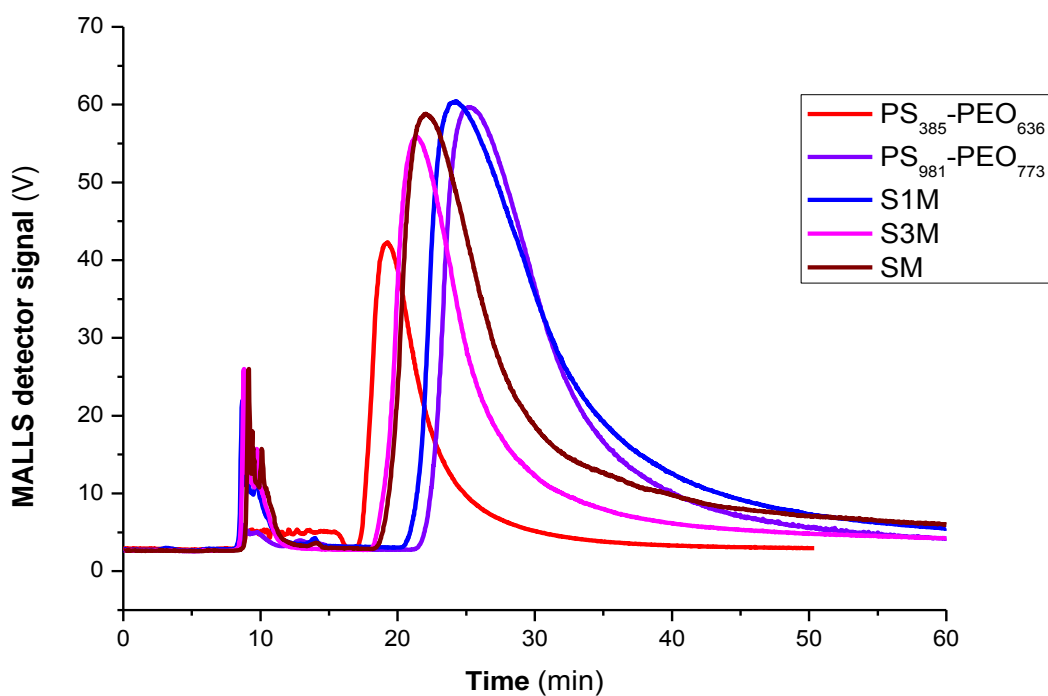**Figure 4.24.** Superimposed UV fractograms for S3M, SM and S1M at a ΔT of 30 °C.
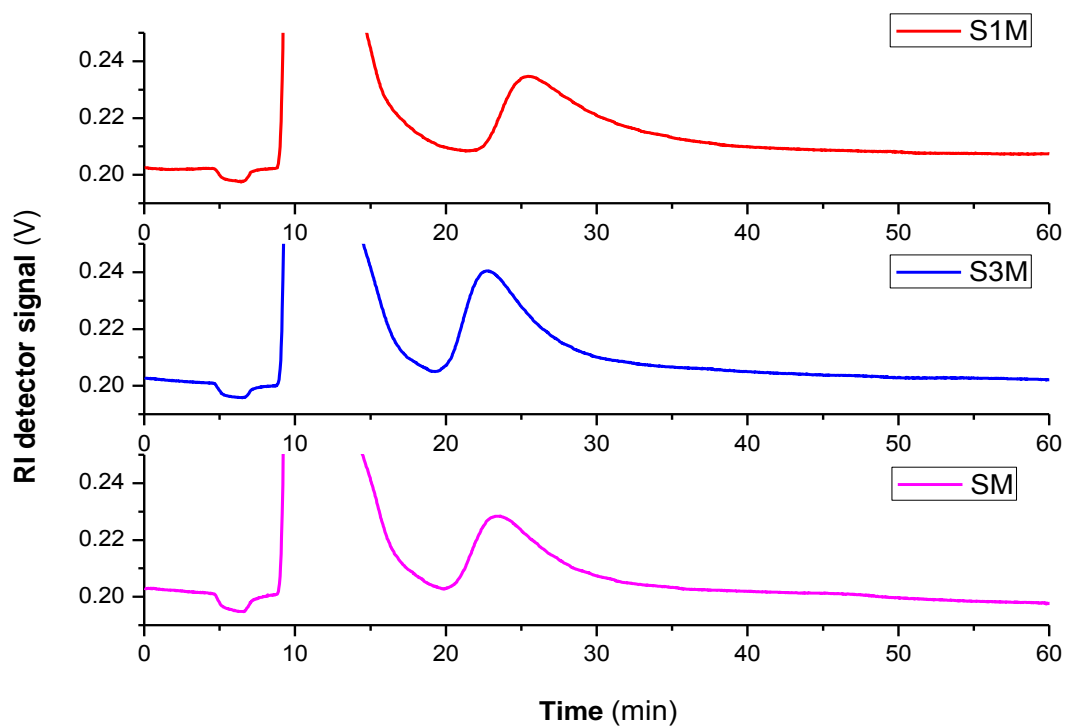
Figure 4.25. Superimposed dRI fractograms for S3M, SM and S1M at a ΔT of 30 °C.
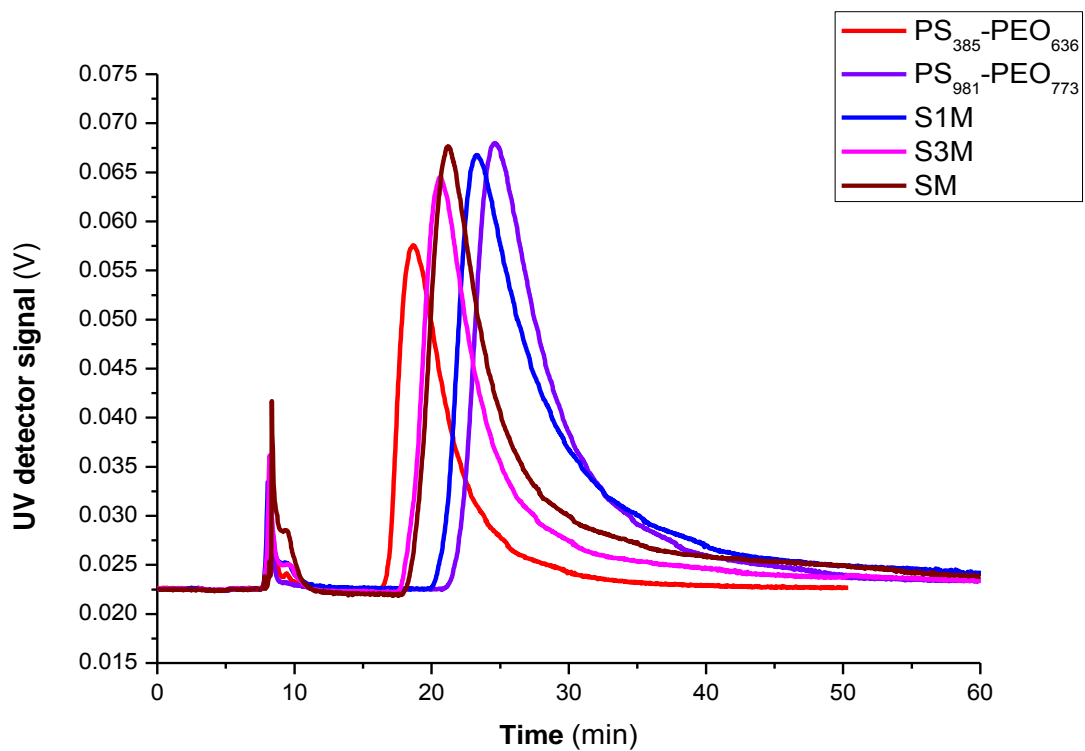
Figure 4.26.   Superimposed DLS fractograms for S3M, SM and S1M at a ΔT of 30 °C.

Figures 4.27-4.30 show that t_r values for all the mixed micelles is in between that of the two parent micelles despite the fact that the measured D_h and Z for the mixed micelles are larger (Table 4-6). Only the trends in the S values can explain the separation trends observed.

Figure 4.27. Superimposed MALLS fractograms for PS$_{385}$-PEO$_{636}$, PS$_{981}$-PEO$_{773}$, S3M, SM and S1M at a ΔT of 30 °C.

Figure 4.28. Superimposed UV fractograms for PS$_{385}$-PEO$_{636}$, PS$_{981}$-PEO$_{773}$, S3M, SM and S1M at a ΔT of 30 °C.

61
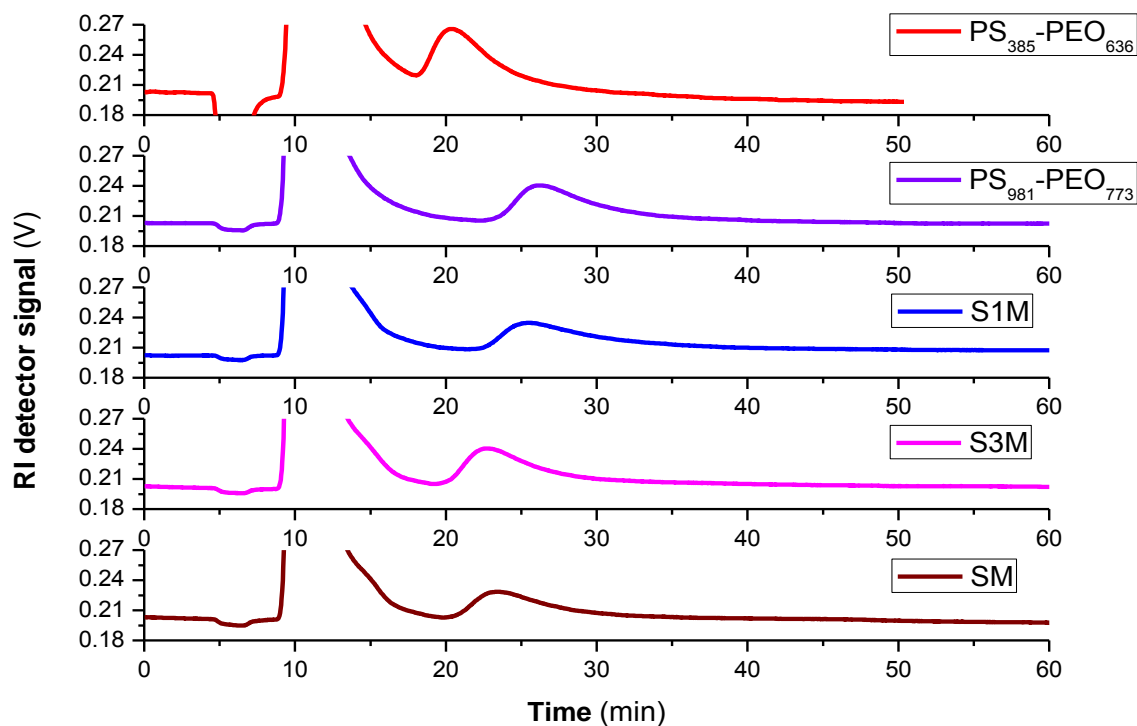
Figure 4.29. Superimposed RI fractograms for PS$_{385}$-PEO$_{636}$, PS$_{981}$-PEO$_{773}$, S3M, SM and S1M at ΔT of 30 °C.
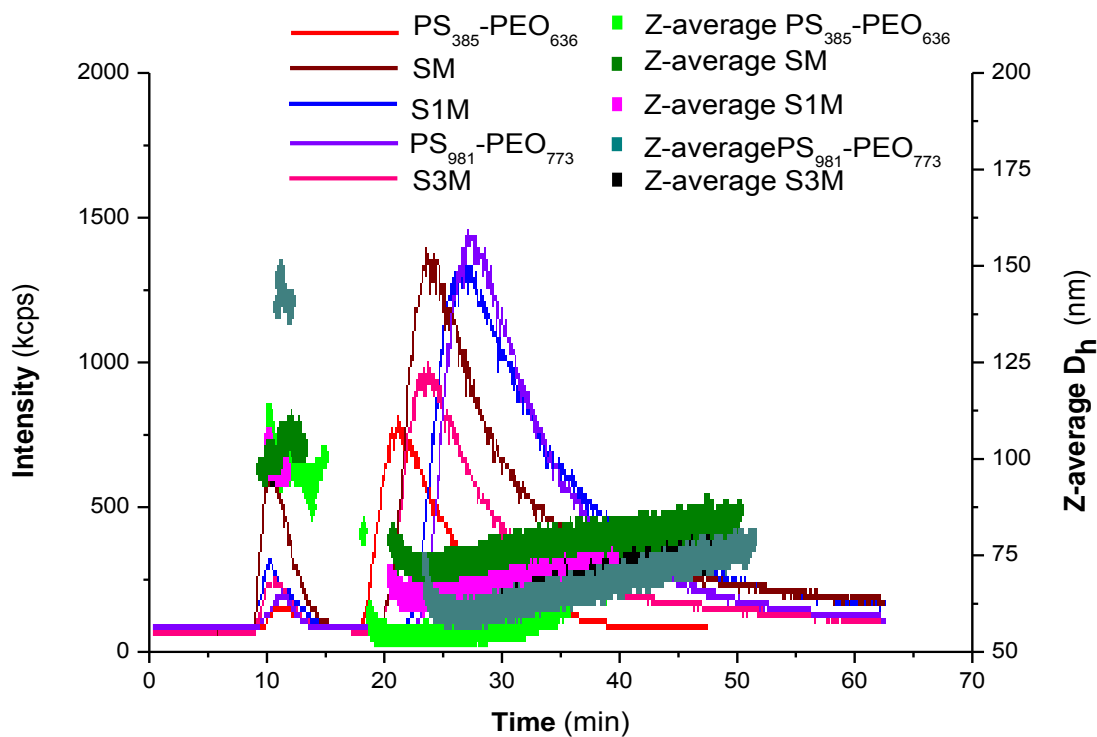
Figure 4.30. Superimposed DLS fractograms for PS$_{385}$-PEO$_{636}$, PS$_{981}$-PEO$_{773}$, S3M, SM and S1M at a ΔT of 30 °C.

Ultimately the formation of mixed micelles from various binary blends of PS_{385}-PEO_{636} and PS_{981}-PEO_{773} BCPs was shown to be thermodynamically feasible. Furthermore, unique size and molar mass properties were observed. In order to investigate the kinetics of formation of these mixed micelles, pure PS_{385}-PEO_{636} and PS_{981}-PEO_{773} micelles were mixed in a 1:1 ratio and the blend subsequently separated by ThFFF at hourly intervals. The micelle blend is referred to as SM_{pre}.

Table 4.8.   Equilibrium time (Time), retention time (t_r), aggregation number (Z), hydrodynamic diameter (D_h), diffusion coefficient (D), thermal diffusion coefficient (D_T), Soret coefficient (S), and shape factor (R_g/R_h) for SM_{pre} mixed micelles determined by ThFFF at a temperature gradient of 30 °C.

Time (hr)	t_r (min)	Z	D_h (nm)	D x 10^{-7} (cm^2/s)	D_T x 10^{-8} (cm^2/s/K)	S x 10^{-1} (1/K)	R_g/R_h
0	23.7 ± 0.1	709 ± 12	70.9 ± 0.1	1.79 ± 0.11	0.86 ± 0.01	0.48 ± 0.02	0.82
1	23.6 ± 0.1	705 ± 17	70.8 ± 0.1	1.79 ± 0.11	0.86 ± 0.01	0.48 ± 0.01	0.85
2	23.5 ± 0.1	698 ± 14	70.0 ± 0.3	1.81 ± 0.10	0.87 ± 0.01	0.48 ± 0.01	0.86

Table 4.8 above shows all the collected ThFFF data for the characterisation of the SM_{pre} micelle blend. The elution peaks for SM_{pre} mixed micelles are unimodal with a close overlay for both the respective time intervals investigated (see Figures 4.31-4.34). Furthermore, the measured Z and D_h values are also similar. This shows that the SM_{pre} mixed micelles attain dynamic equilibrium instantaneously, which is rather unexpected. Unlike with low molecular weight surfactants, unimer exchange is expected to be much slower for BCP micelles,[16] possibly due to their relatively larger size and molar mass, which constrains mobility. The

instantaneous formation is analogous to ordinary pure micelles, and might be triggered by the close similarity in size of the two component unimers. The size of the component unimers is expected to be comparable because the PEO blocks are similar and PS size is expected to be collapsed.

SM_{pre} mixed micelles have smaller Z and D_h values (hence higher D) in comparison to SM mixed micelles, prepared via similar mass % ratios (Table 4.7 and 4.8). However different preparation techniques were employed. These differences can thus be attributed to the use of different preparation techniques, which has been reported to happen.[1–3,14] However, both mixed micelles have similar t_r and S values and are therefore expected to co-elute. Thus, despite the size and molar mass differences, the interplay between D and D_T is similar for SM and SM_{pre} mixed micelles.
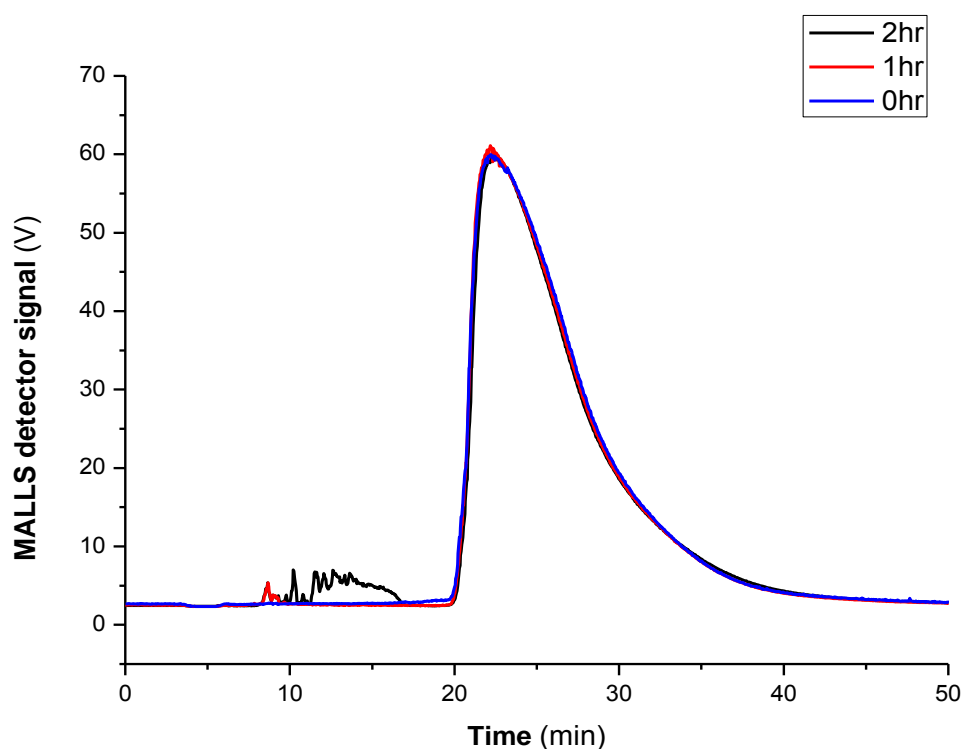
Figure 4.31. Superimposed MALLS fractograms for SM_{pre} mixed micelles at ΔT of 30 °C.
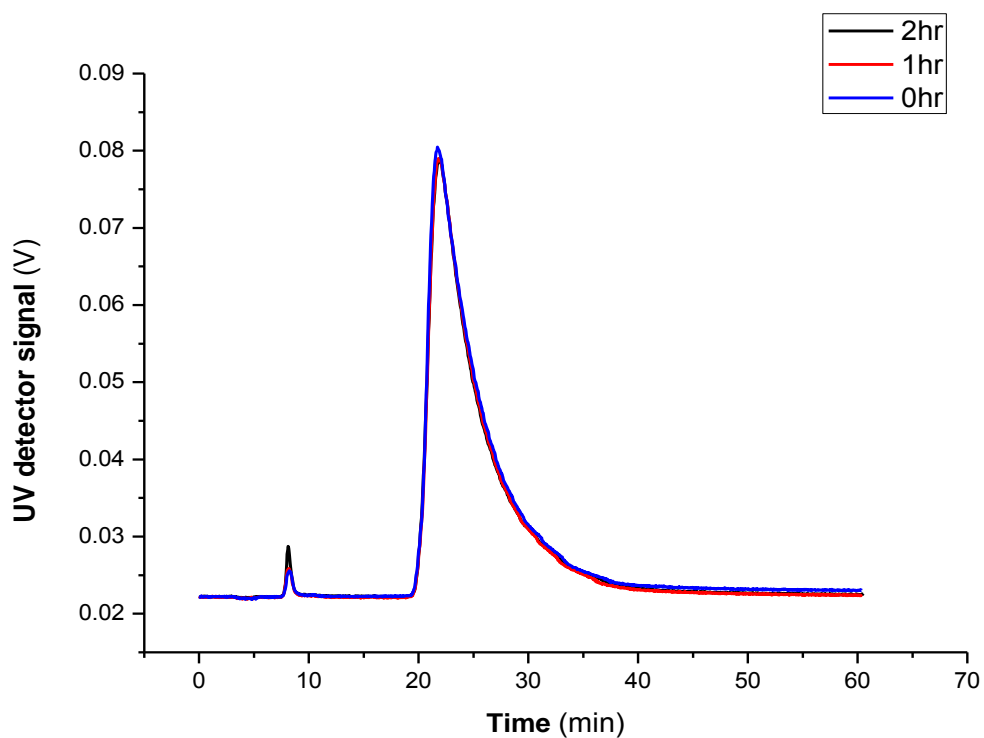
Figure 4.32. Superimposed UV fractograms for SM$_{pre}$ mixed micelles at a ΔT of 30 ℃.
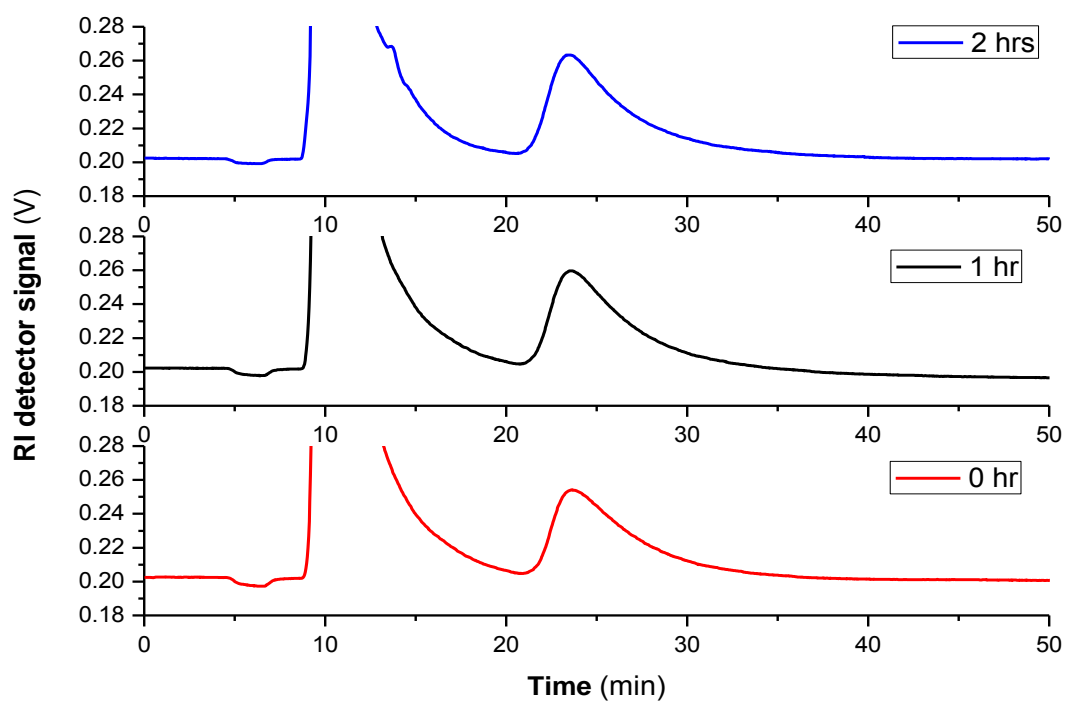
Figure 4.33. Superimposed dRI fractograms for SM$_{pre}$ mixed micelles at a ΔT of 30 ℃.

65

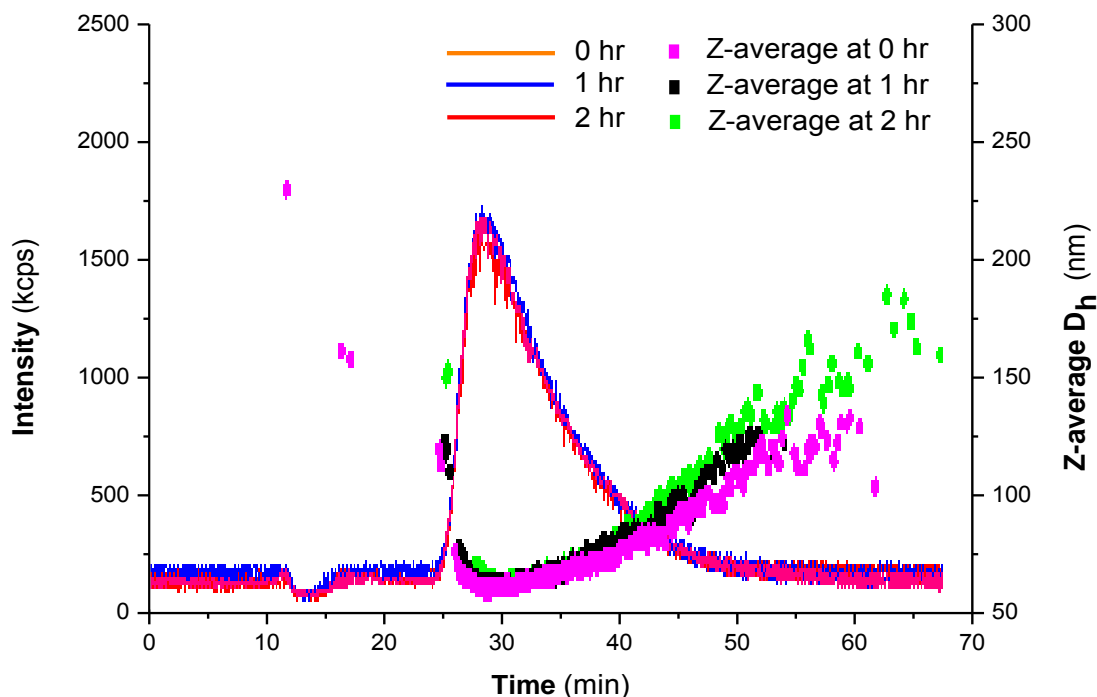**Figure 4.34.** Superimposed DLS fractograms for SM$_{pre}$ mixed micelles at a ΔT of 30 ^{o}C.

In order to further probe the dynamics of formation of SM$_{pre}$ mixed micelles, 1 mL of 1 mg/mL of PS$_{385}$-PEO$_{636}$ pure micelles was titrated with 1 mg/mL of PS$_{981}$-PEO$_{773}$ pure micelles. After every 0.25 mL of PS$_{981}$-PEO$_{773}$ micelle volume titrated, the mixed micelle solution was analysed by DLS. This titration enables a more gradual determination of the effect of the larger PS$_{981}$-PEO$_{773}$ micelles on the formation of the mixed micelles. It can be seen from Figure 4.35 that the size distribution of the mixed micelles remains unimodal for the entire titration. This corroborates with previous results that showed the instantaneous formation of the mixed micelles. Furthermore, there is an expected gradual increase in size of the mixed micelles as a function of PS$_{981}$-PEO$_{773}$ volume as illustrated in Figures 4.35 and 4.36. However, this size increase as a function of PS$_{981}$-PEO$_{773}$ volume eventually plateaus beyond 1.5mL, possibly due to PS$_{981}$-PEO$_{773}$ unimers having reached a point of excess whilst the PS$_{385}$-PEO$_{636}$ unimers have gradually become the limiting reagent with regards to size growth.

66
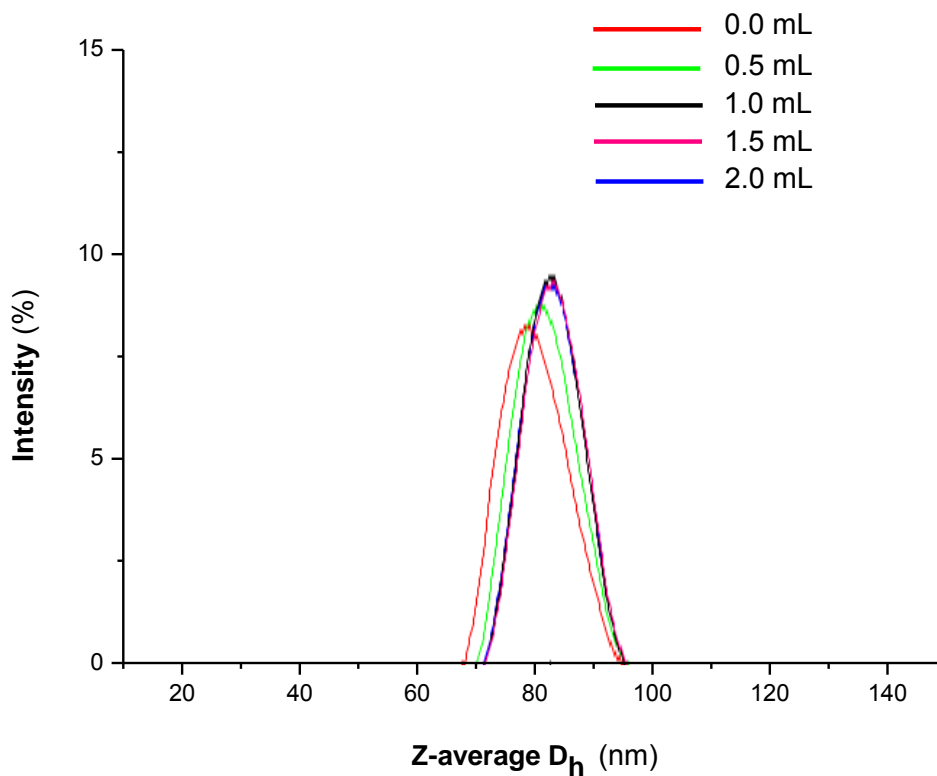
Figure 4.35. DLS fractograms for the titration of PS_{385}-PEO_{636} micelles with PS_{981}-PEO_{773} micelles.
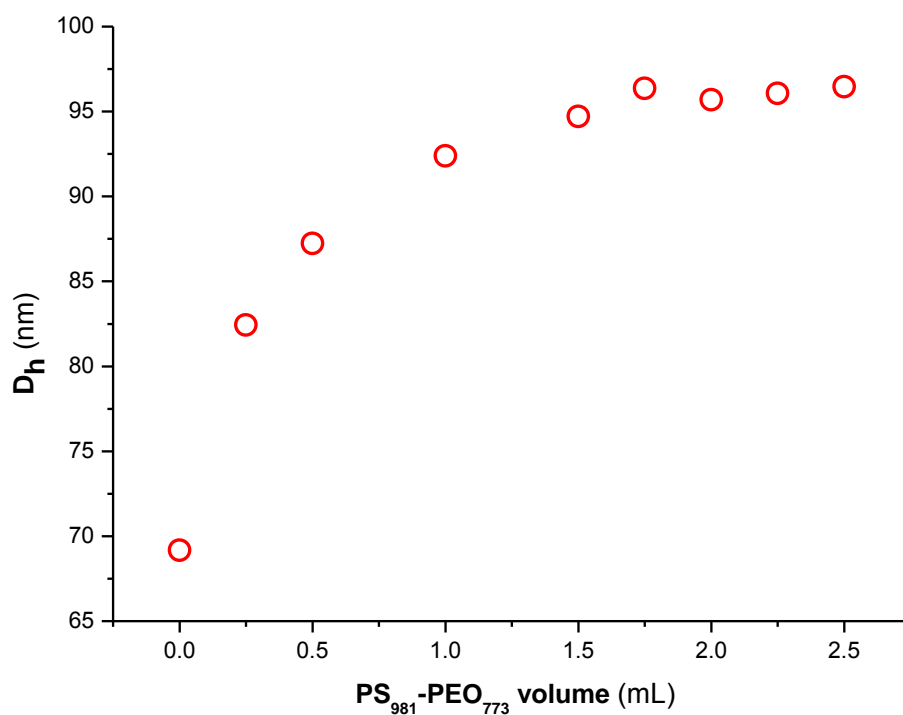
Figure 4.36. D_h of mixed micelles as a function of the titration volume of PS_{981}-PEO_{773} micelles.

67

4.3.3 PS$_{385}$-PEO$_{636}$ and PS$_{981}$-PEO$_{773}$ micelles modified with LiBr.

A stock solution of LiBr was prepared in ACN and diluted with the pure micelle solutions to give 1 mM LiBr micelle solutions. The introduction of LiBr induces morphological changes from spherical to cylindrical, vesicular, worm-like and a network of worm-like structures that look like jelly fish, as depicted by STEM micrographs in Figures 4.37 and 4.38.[17–19] The general description of how LiBr induces the morphological transformations is summarised in the following paragraph.

LiBr salt ions reduce the steric and electrostatic repulsion of the corona forming PEO chains, which promotes swelling and unimer-unimer interaction. Swelling results in three dimensional growth of the micelle, which is further enhanced by an increase in Z from the incorporation of additional unimers, and thus D$_h$ also increases. The swelling takes place only up to a certain limit which is imposed by concentration and molecular geometry, thereafter one-dimensional growth is permissible. One-dimensional growth gives rise to cylindrical, worm-like and ultimately jelly fish micelle structures. The specific morphological transformations induced by LiBr for PS$_{385}$-PEO$_{636}$ and PS$_{981}$-PEO$_{773}$ micelles shall be discussed in the next paragraph.

Figure 4.37 below shows micrographs of PS$_{385}$-PEO$_{636}$ micelles with an elaborate network of worm-like micelles which look like jelly fish. In contrast, PS$_{981}$-PEO$_{773}$ micelles have more short cylindrical morphologies as illustrated in Figure 4.38 below. These observed differences in morphological transformations can be attributed to dissimilar chain ratios of the two BCPs. In general, certain block ratios are more inclined towards certain morphological transformations than others.[1,19,20,10] Overall these morphological transitions are dependent on both ionic strength (salt) and block ratios. Similar salt induced morphologies have been reported in a number of studies, [17–19,21] however, no fractionations

were performed. Fractionation is essential to enable identification and quantification of these multiple morphologies as separate entities. The next paragraph will discuss ThFFF-based characterization of these multiple morphologies.
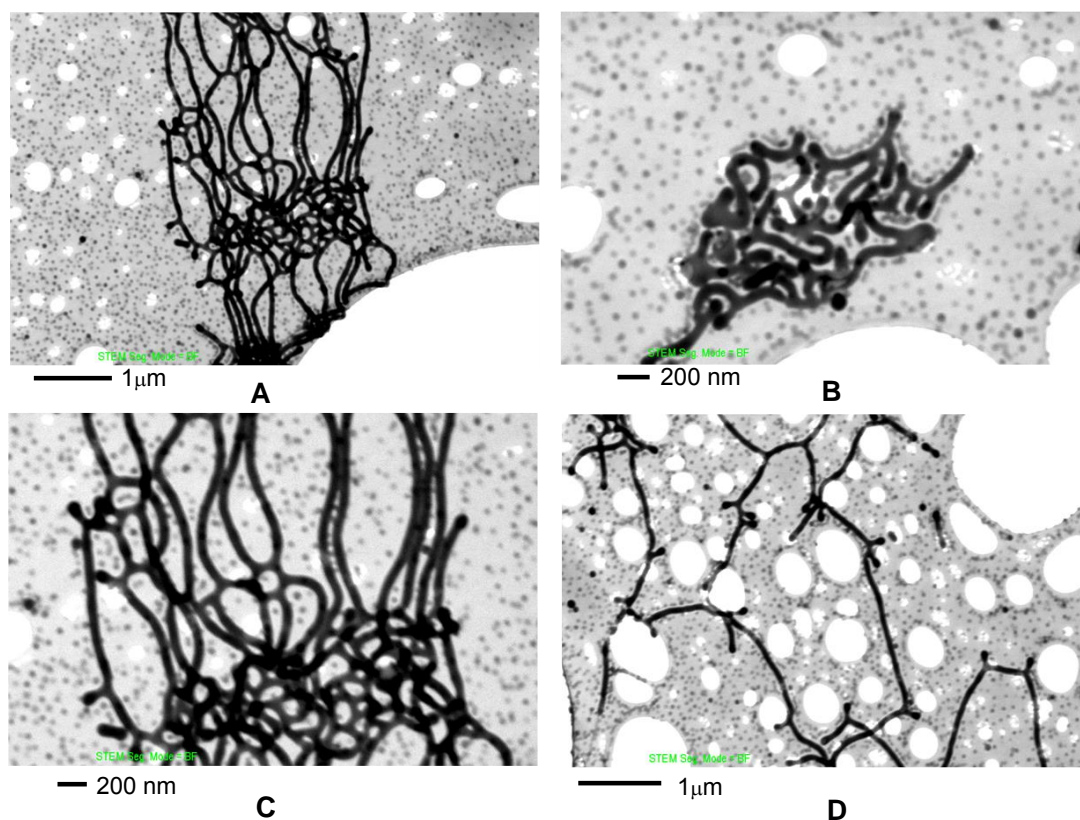
Figure 4.37. STEM images for PS_{385}-PEO_{636} micelles in 1 mM LiBr ACN solution; A-D indicate different positions of the sample at different magnifications.
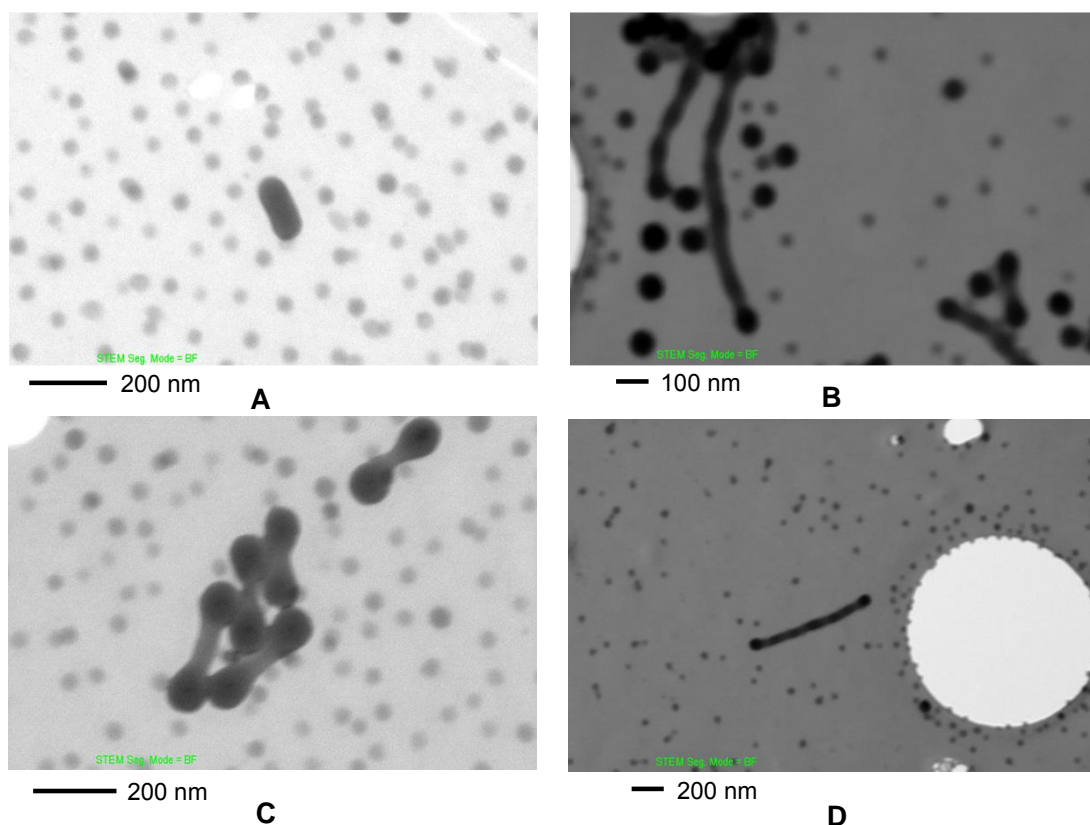
Figure 4.38. STEM images for PS_{981}-PEO_{773} micelles in 1 mM LiBr ACN solution; A-D indicate different positions on the sample at different magnifications.

1 mM LiBr was used as the carrier solvent and different PS_{385}-PEO_{636} micellar morphologies were separated by ThFFF. The ThFFF data are summarised in Table 4.9 below. Figures 4.39-4.42 show the relevant MALLS, UV, RI and DLS fractograms. Retention for all morphologies is shown to be a function of D and the associated D_h, therefore the separation can be classified as being size-based. Furthermore, similarities in D_T values are observed, which implies that the different PS_{385}-PEO_{636} morphologies have similar chemical composition of the corona, as expected. This validates the assertion that the separation is based on size.

The R_g/R_h values in Table 4.9 can be used to assign morphologies related to the respective peaks. R_g/R_h for Peak 1 has a value of 1.41 which points to the presence of vesicles, while Peak 2 and 3 have similar R_g/R_h values, which are 0.46 and 0.56, respectively. These two

70

values are relatively low and comparable to values for ordinary polymer chains. However, the respective D_h values are very large and typical of aggregate structures. By reference to the STEM micrographs and the very large D_h, Peaks 2 and 3 can be preliminarily assumed to be related to the jelly fish like structures. No reference R_g/R_h values are available in literature for further validation. However, studies show that the jelly fish micelles and ordinary polymer chains have similar viscoelastic, flexibility and rheological properties.[19,10,22–25] These similarities might explain why the measured R_g/R_h values for the jelly fish are analogous to ordinary polymer chains in solution.

Table 4.9.   Peak number (Peak), retention time (t_r), hydrodynamic diameter (D_h), diffusion coefficient (D), thermal diffusion coefficient (D_T), Soret coefficient (S), aggregation number (Z), and shape factor (R_g/R_h) for PS_{385}-PEO_{636} micelles in 1 mM LiBr determined by ThFFF at 25 ^{o}C temperature gradient (ΔT).

Peak	t_r (min)	Z	D_h (nm)	D x 10^{-7} (cm^2/s)	D_T x 10^{-8} (cm^2/s/K)	S x 10^{-1} (1/K)	R_g/R_h
1	23.6 ± 0.1	371 ± 10	65 ± 2	1.70 ± 0.01	1.10 ± 0.01	0.65 ± 0.01	1.41
2	32.1 ± 0.2	1750 ± 46	96 ± 2	1.15 ± 0.01	1.01 ± 0.01	0.88 ± 0.01	0.46
3	46.3 ± 0.1	4643 ± 125	132 ± 3	0.84 ± 0.02	1.06 ± 0.01	1.26 ± 0.01	0.56

Most importantly, the thermal gradient can stimulate temperature induced morphological transitions, in addition to being the fractionation force.[26] This may explain why one of the calculated R_g/R_h values (1.41) in Table 4.9 refers to vesicles, although these are not clearly identifiable from STEM micrographs, perhaps due to resolution limitations and the fact that STEM only shows a small portion of the entire sample.

The concentration based fractograms (UV and RI) show varying relative intensities for the three recorded peaks. Peak 1 (vesicles) has the highest intensity relative to Peak 2 and 3 (worm-like micelles), which implies that there are more vesicles in solution than jelly fish. It can be drawn from this observation that the smaller sized jelly fish (Peak 2) dominate the larger sized ones (Peak 3), since intensity for Peak 2 is higher than that for Peak 3. Salt modified PS_{981}-PEO_{773} micelles were separated thereafter, as explained in the next paragraph.
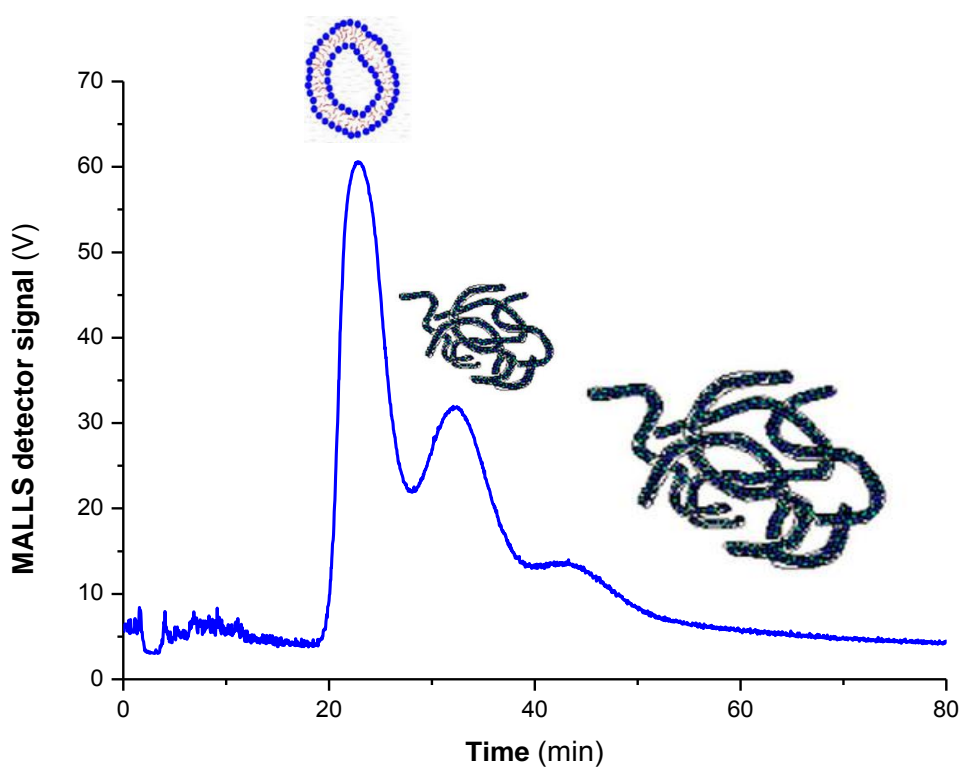
Figure 4.39.   MALLS fractogram for PS_{385}-PEO_{636} micelles in 1 mM LiBr solution at a ΔT of 25 ºC.
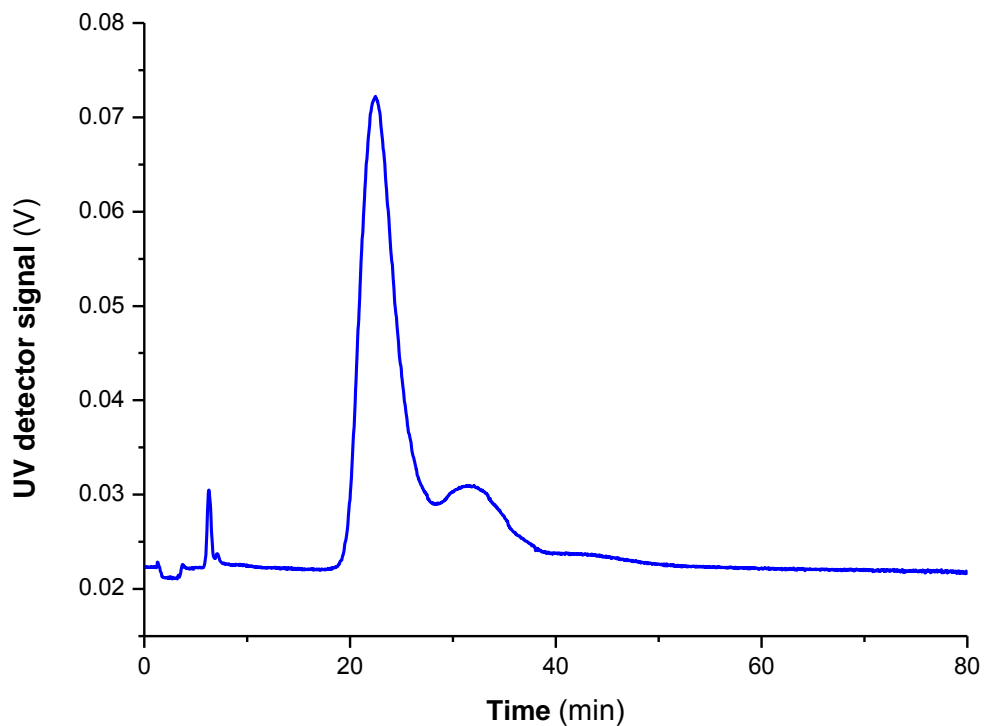
Figure 4.40. UV fractogram for PS$_{385}$-PEO$_{636}$ micelles in 1 mM LiBr solution at a ΔT of 25 °C.
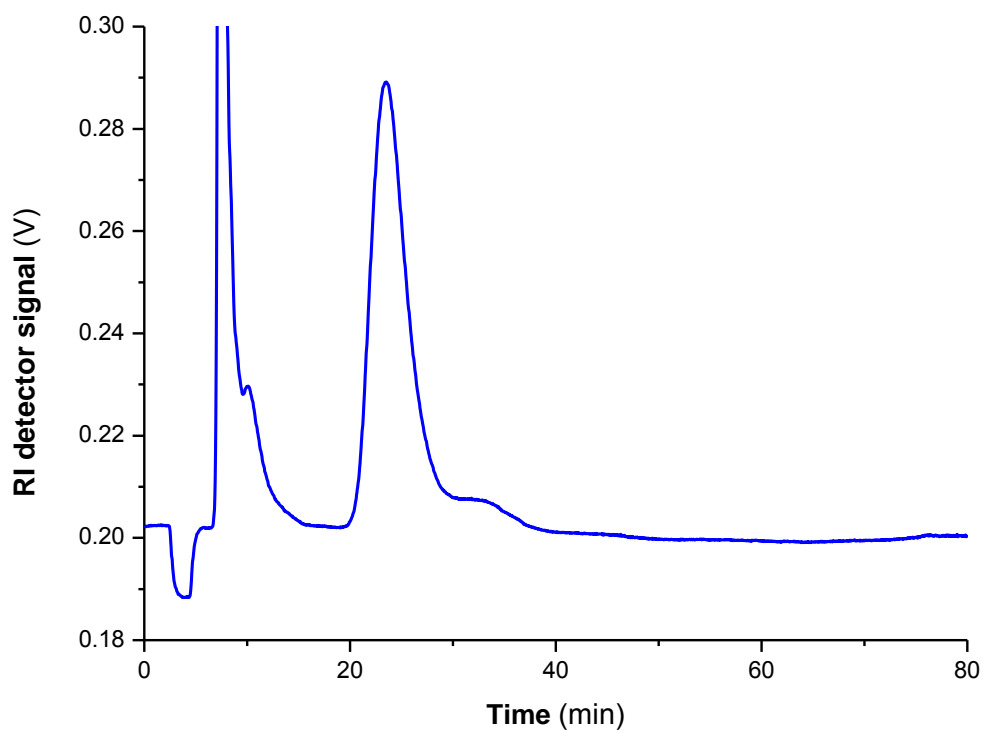
Figure 4.41. dRI fractogram for PS$_{385}$-PEO$_{636}$ micelles in 1 mM LiBr solution at a ΔT of 25 °C.
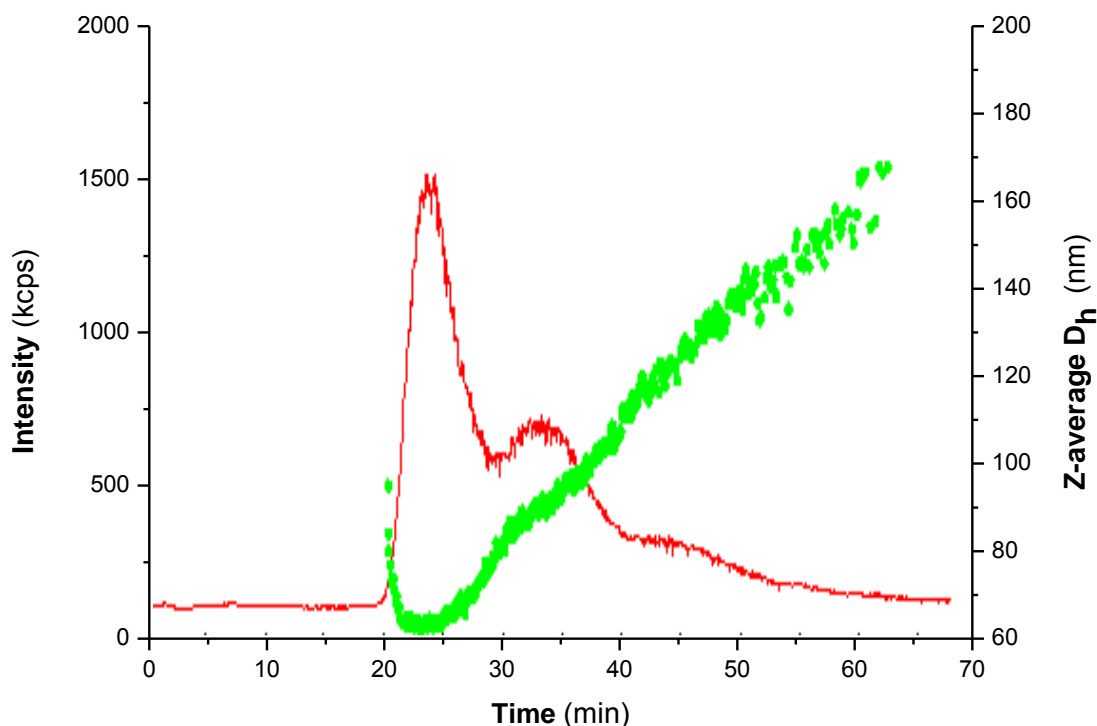
Figure 4.42. DLS fractogram for PS_{385}-PEO_{636} micelles in 1 mM LiBr solution at a ΔT of 25 ºC.

The characterisation of the multiple morphologies for PS_{981}-PEO_{773} micelles are summarised in Table 4.10 below. The relevant MALLS, UV and dRI fractograms are shown Figures 4.43-4.46. Salt modified PS_{981}-PEO_{773} micelles follow a similar size-based separation trend, where morphologies with smaller D_h elute first. D_T is comparable for all three peaks recorded and is notably similar to PS_{385}-PEO_{636}. This is because D_T is independent of M_w and both PS_{385}-PEO_{636} and PS_{981}-PEO_{773} micellar structures have similar surface chemistry. R_g/R_h for peak 1-3 relates to vesicular, spherical and worm-like micelles, respectively. This corroborates with the respective STEM images in Figure 4.38.

The signal intensities for both concentration detectors (UV and dRI) show that Peak 1 for vesicles has the highest intensity, followed by Peak 2 and 3 in that order, for spherical and worm-like micelles, respectively. This means that vesicles are the dominant morphology over spherical and worm-like morphologies, of which the latter has the lowest content.

74

Table 4.10. Peak number (Peak), retention time (t_r), hydrodynamic diameter (D_h), diffusion (D), thermal diffusion (D_T), Soret Coefficient (S), aggregation number (Z), and shape factor (R_g/R_h) for PS_{981}-PEO_{773} micelles in 1 mM LiBr determined by ThFFF at temperature gradient of 25 °C.

Peak	t_r (min)	Z	D_h (nm)	$D \times 10^{-7}$ (cm^2/s)	$D_T \times 10^{-8}$ ($cm^2/s/K$)	$S \times 10^{-1}$ (1/K)	R_g/R_h
1	26.6 ± 0.1	969 ± 18	76 ± 2	1.45 ± 0.02	1.06 ± 0.01	0.73 ± 0.02	1.32
2	50.8 ± 0.1	5455 ± 91	162 ± 3	0.68 ± 0.02	1.00 ± 0.01	1.40 ± 0.01	0.70
3	68.9 ± 0.1	14242 ± 500	199 ± 6	0.55 ± 0.02	1.05 ± 0.01	1.91 ± 0.01	1.11
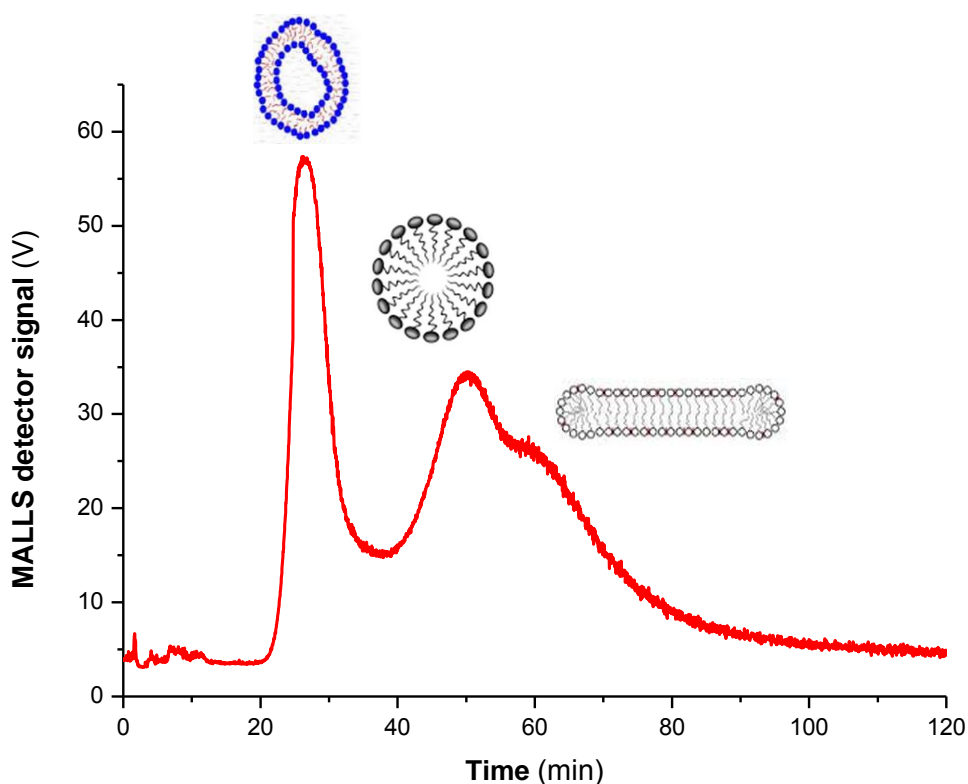
Figure 4.43. MALLS fractogram for PS_{981}-PEO_{773} micelles in 1 mM LiBr solution at a ΔT of 25 °C.

75
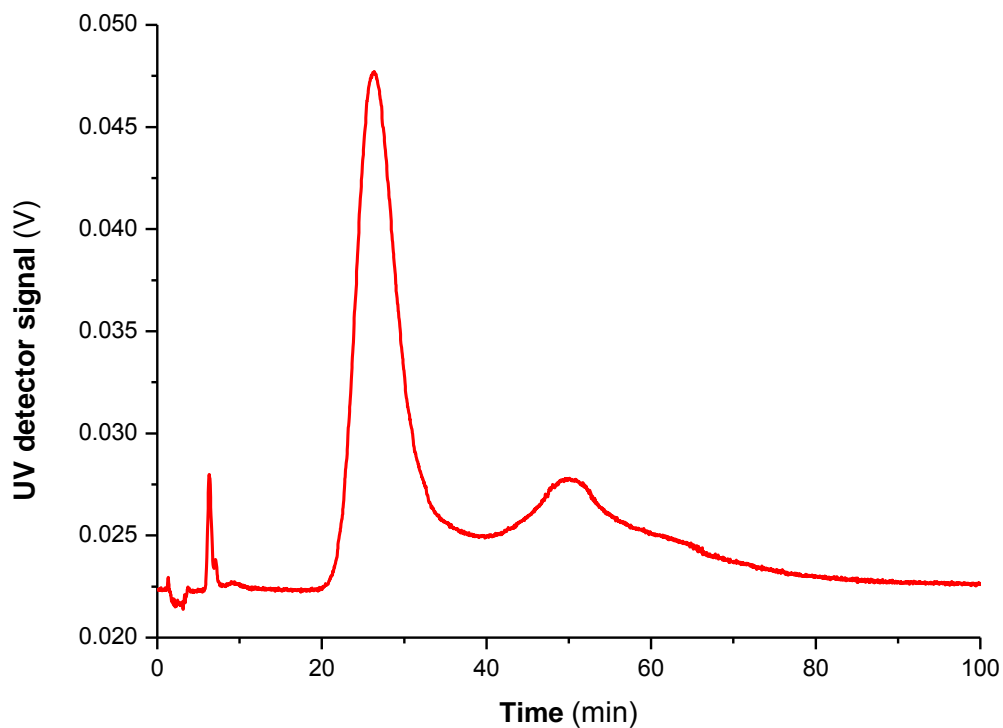
Figure 4.44. UV fractogram for PS$_{981}$-PEO$_{773}$ micelles in 1 Mm LiBr solution at a ΔT of 25 ºC.
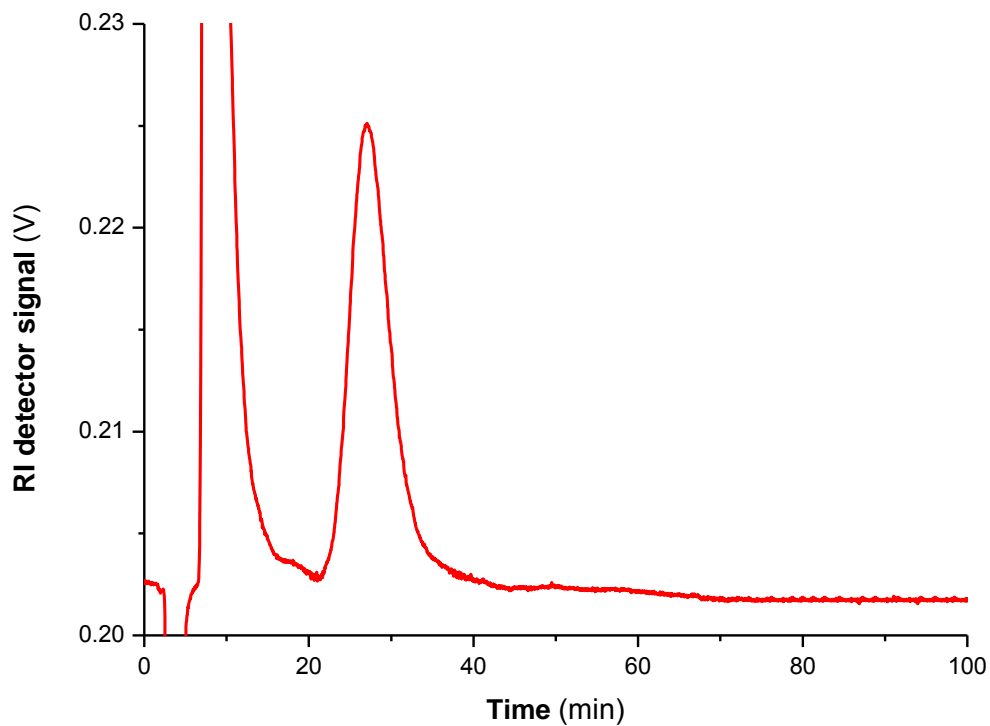
Figure 4.45. dRI fractogram for PS$_{981}$-PEO$_{773}$ micelles in 1 mM LiBr solution at a ΔT of 25 ºC.

Figure 4.46. DLS fractogram for PS_{981}-PEO_{773} micelles in 1 mM LiBr solution at a ΔT of 25 ºC.

4.4 References

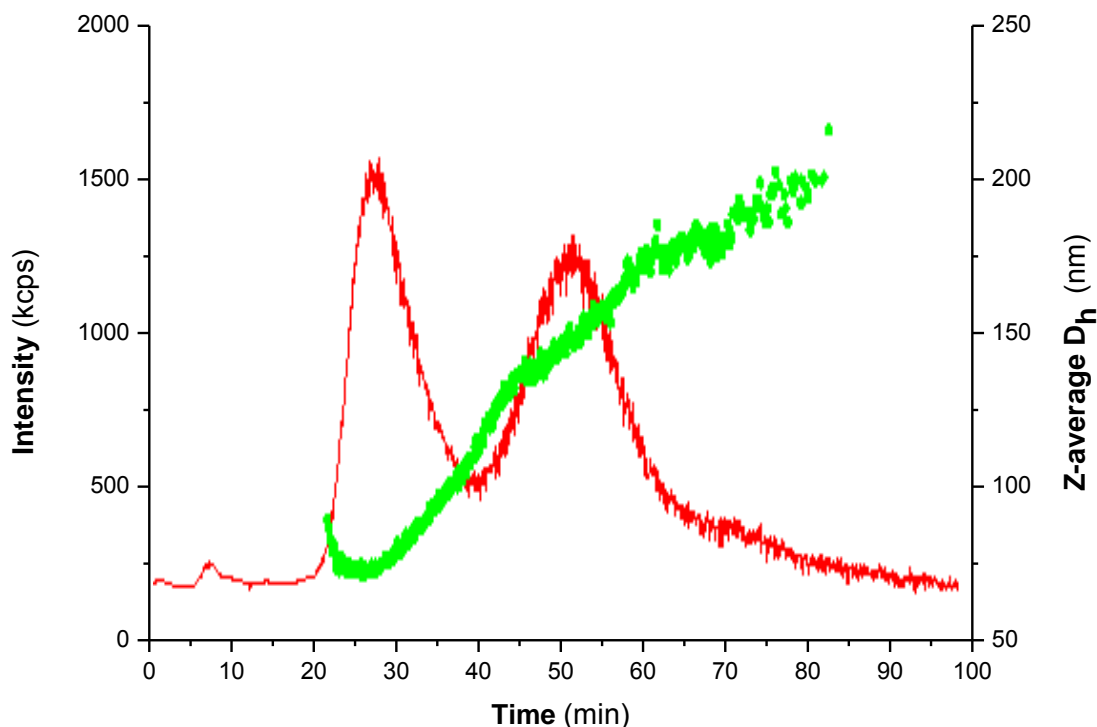(1)   Zhang, L.; Eisenberg, A. *Science* **1995**, *268*, 1728–1731.

(2)   Jain, S.; Bates, F. S. *Macromolecules* **2004**, *37* (4), 1511–1523.

(3)   Bates, F. S.; Jain, S. *Science* **2003**, *300* (April), 9–11.

(4)   Malvern Instruments Zetasizer Nano application note. Surfactant micelle characterization using dynamic light scattering www.malvern.com.

(5)   Horst, S.; Jurgen, K.; Rossmanith, P.; Frechen, T.; Gerst, M.; Feldthusen, J.; Muller, A. H. E. *J. Chromatogr.* **2000**, No. 33, 1734–1740.

(6)   Pioge, S.; Fontaine, L.; Gaillard, C.; Nicol, E.; Pascual, S. *Macromolecules* **2009**, *42* (12), 4262–4272.

(7)   Owen, S. C.; Chan, D. P. Y.; Shoichet, M. S. *Nano Today* **2012**, *7* (1), 53–65.

(8)   Riess, G. *Prog. Polym. Sci.* **2003**, *28* (7), 1107–1170.

(9)   Grubišic-Gallot, Z.; Sedláček, J.; Gallot, Y. *J. Liq. Chromatogr. Relat. Technol.* **1998**, *21* (16), 2459–2472.

(10)   Cai, S.; Vijayan, K.; Cheng, D.; Lima, E. M.; Discher, D. E. *Pharm. Res.* **2007**, *24* (11), 2099–2109.

(11)   Lambert, A. *Polymer (Guildf).* **1969**, *10*, 319–326.

(12)   Hitachi High-Tech Science Corporation. *DSC measurements of PS - MW vs Tg*; 1995.

(13)   Schimpf, M. E.; Caldwell, K.; Giddings, J. C. *Field-Flow Fractionation Handbook*; John Wiley & Sons: New York, USA, 2000; Vol. 4.

(14)   P. Alexandridis, B. L. *Amphiphilic Block Copolymers: Self-Assembly and Applications*; Elsevier: Amsterdam, 2000.

(15)   Liu, T.; Liu, L.-Z.; Chu, B. *Formation of Amphiphilic Block Copolymer Micelles in Nonaqueous Solution.*; Woodhead Publishing Limited: Cambridge, UK, 2000.

(16)   Creutz, S.; van Stam, J.; Antoun, S.; De Schryver, F. C.; Jérôme, R. *Macromolecules* **1997**, *30* (14), 4078–4083.

(17)   Aswal, V. K. *Chem. Phys. Lett.* **2003**, *371* (3–4), 371–377.

(18)   Hakem, I. F.; Lal, J. *Europhys. Lett.* **2007**, *64* (2), 204–210.

(19)   Shrestha, R. G.; Aramaki, K. *J. Nepal Chem. Soc.* **2009**, *23*, 65–73.

(20)   Zhang, Y.; Lam, Y. M. *J. Nanosci. Nanotechnol.* **2006**, *6* (12), 3877–3881.

(21)   Bronstein, L. M.; Chernyshov, D. M.; Timofeeva, G. I.; Dubrovina, L. V.; Valetsky, P. M.; Khokhlov, A. R. *Langmuir* **1999**, *15* (19), 6195–6200.

(22)   Bhargava, P.; Zheng, J. X.; Quirk, R. P.; Cheng, S. Z. D. *J. Polym. Sci. Part B Polym. Phys.* **2006**, *44* (24), 3605–3611.

(23)   Berret, J.-F. *Mol. Gels* **2005**, 235–275.

(24)   Das, N. C.; Cao, H.; Kaiser, H.; Warren, G. T.; Gladden, J. R.; Sokol, P. E. *Langmuir* **2012**, *28* (33), 11962–11968.

(25)   Yang, J. *Curr. Opin. Colloid Interface Sci.* **2002**, *7* (5–6), 276–281.

(26)   Yang, Y.; Liu, L.; Huang, X.; Tan, X.; Luo, T.; Li, W. *Soft Matter* **2015**, *11* (45), 8848–8855.

5   Conclusions and Future work

5.1   Summary

This study proved that multidetector ThFFF is capable of separating and characterising PS-PEO micelles having different core block sizes but similar corona block sizes. Multiple morphologies of the pure micelles and multiple mixed micelles (prepared from various binary blending protocols of the two micelles) were successfully separated and characterized. Information on molar mass, particle size, chemical composition and their respective distributions (MMD, CCD and PSD) as well as morphology was obtained in a single measurement. Furthermore CMC and CMT for all the micelles were determined via offline DLS.

5.2   Conclusions

The first part of the study showed that two types of PS-PEO micelles were successfully prepared from PS-PEO BCPs having different PS block sizes but similar PEO block sizes. Both micelles were shown to have spherical morphologies and similar D_T values. The micelles with the larger PS core block (PS_{981}-PEO_{773}) had larger D_h values than the micelles with the smaller PS block (PS_{385}-PEO_{636}), hence the two were separated as a function of size.

Multiple mixed micelles were prepared from various binary blending protocols of PS_{385}-PEO_{636} and PS_{981}-PEO_{773} block copolymers and successfully fractionated. Retention was shown to be the average of pure PS_{385}-PEO_{636} and PS_{981}-PEO_{773} micelles. Furthermore, retention was shown to linearly increase with increase of the larger PS_{981}-PEO_{773} component in the mixed micelles. However, the Z, and D_h values of the mixed micelles showed no linear trend and the 1:1 ratio of PS_{385}-PEO_{636} and PS_{981}-PEO_{773} components had the highest values.

Moreover, the mixed micelles had larger Z and D_h values relative to the pure micelles. The separations of the mixed micelles could not be explained via classical theories based only on size and M_w. However the separations could be explained by the Soret coefficient, as described by the interplay between D and D_T.

ThFFF was shown to be ideal for separating multiple morphologies of PS_{385}-PEO_{636} and PS_{981}-PEO_{773} micelles, namely spheres, vesicles, cylinders and worms. These morphologies were a result of the LiBr salt induced morphological evolution of the initial spherical micelles.

Ultimately ThFFF proved to be a suitable technique for monitoring the dynamics of formation of the mixed micelles, unlike most classical techniques which can only characterize mixed micelles before or after formation. The equilibrium time of formation for a 1:1 ratio of PS_{385}-PEO_{636} and PS_{981}-PEO_{773} mixed micelles was shown to be very short. The instantaneous formation of mixed micelles was not expected as unimer exchange between polymer micelles was expected to be slow, largely due to the large sizes of the chains.

Overall, multi-detector ThFFF demonstrates to have a high potential for the separation and characterization of multiple morphologies of complex self-assemblies of block copolymers, and for revealing information on molar mass, particle size, chemical composition and their respective distributions (MMD, CCD and PSD), in a single measurement.

5.3   Future work

Focus will be on hyphenating multidetector ThFFF with FTIR spectroscopy in order to reveal more information on chemical composition of block copolymers and their self-assemblies. ThFFF-FTIR can be a suitable technique for monitoring the dynamics of formation of more

complex mixed micelles prepared from pure micelles with different core and corona chemistries.

The evolution of multiple self-assembly morphologies has a dependency on salt concentration. This dependency can be investigated via ThFFF. Furthermore, the impact of different salts, both organic and inorganic, on micelle morphology can be investigated.